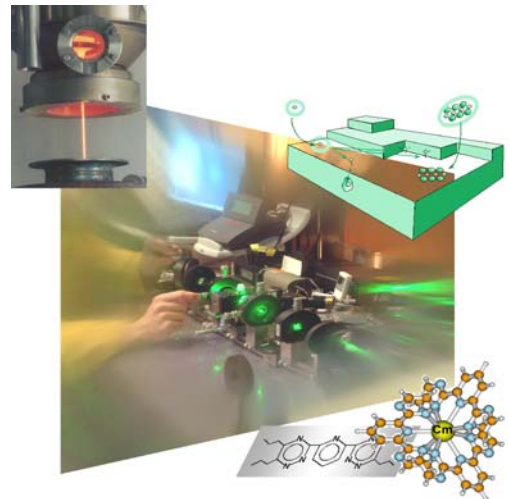




Forschungszentrum Karlsruhe
in der Helmholtz-Gemeinschaft



Annual Report 2006

Institute for Nuclear Waste Disposal
Institut für Nukleare Entsorgung

Forschungszentrum Karlsruhe

in der Helmholtz-Gemeinschaft

Wissenschaftliche Berichte

FZKA 7360

Institute for Nuclear Waste Disposal

Annual Report 2006

H. Geckeis; R. Klenze (Eds.)

Institut für Nukleare Entsorgung

Forschungszentrum Karlsruhe GmbH, Karlsruhe

2007

Publisher: Institut für Nukleare Entsorgung (INE), Forschungszentrum Karlsruhe GmbH (FZK)
Hermann-von-Helmholtz Platz 1, D-76344 Eggenstein-Leopoldshafen
FZK is a member of the Helmholtz Assoziation

Electronic version available from <http://www.fzk.de>
The INE Annual Report is available free of charge

Publication date: October, 5th 2007

Director of INE: Dr. Klaus Gompper (acting)

Table of contents

	page
1. Introduction of the Institut für Nukleare Entsorgung	1
2. Highlights	3
3. National and International Cooperations	5
4. Fundamental Studies: Process understanding on a molecular scale	7
4.1 Chemistry and thermodynamic of actinides in aqueous solution	7
4.2 Structural incorporation of actinides into calcite	11
4.3 Colloid formation and stability	16
5. Applied Studies: Radionuclide retention in the multibarrier system	22
5.1 Determination of key processes influencing the near field source term for spent nuclear fuel: Radiation induced UO ₂ (s) corrosion in presence of H ₂ and Br ⁻	22
5.2 Radionuclide retention in the Far Field	27
5.3 Influence of natural organics	34
5.4 TRANSAL: Development of a code for Coupled Transport and Reacting Modelling	40
6. Development of speciation methods: Speciation of actinides at trace concentrations	45
6.1 The INE-Beamline for Actinide Research at ANKA	45
6.2 Speciation of the functional groups at mineral/water interfaces probed by Vibrational Sum Frequency Spectroscopy and Quantum Chemistry	50
6.3 Direct observation of polynuclear Zr(IV) hydroxide complexes in solution by nano-electrospray MS and EXAFS	53
6.4 Computational Chemistry	57
7. Separation of long-lived minor actinides	60
7.1 Separation of Minor Actinides	60
8. Vitrification of High-level radioactive liquid waste	64
8.1 Commissioning of Process Systems of VEK	64
8.2 Application of vitrification technology	66
9. List of publications	69

1. Introduction of the Institut für Nukleare Entsorgung

Activities at the Institut für Nukleare Entsorgung (INE) are integrated into the research programme NUKLEAR of the Forschungszentrum Karlsruhe within the Hermann von Helmholtz Gemeinschaft Deutscher Forschungszentren (HGF). INE contributes to the German R&D on long-term safety assessment for final disposal of nuclear waste. Further activities deal with the separation of minor actinides from high-level waste (Partitioning) for subsequent transmutation and the immobilization of high-level liquid waste by vitrification.

Over 10.000 t spent fuel containing approximately 100 t plutonium, 8 t minor actinides (neptunium, americium and curium) and 400 t of fission products have been generated in Germany until 2005. About 7000 t were shipped to France and UK for reprocessing to recover plutonium and uranium. The safe disposal of high-level radioactive waste, i.e. spent fuel and heat producing waste arising from reprocessing, is in the responsibility of the federal government.

There is an international consensus that emplacement in deep geological formations is the safest way to dispose of highly radioactive waste. It ensures the effective protection of the population and the biosphere against radiation exposure arising from the waste over very long periods of time. The isolation and immobilization of nuclear waste in a repository is accomplished by the appropriate combination of redundant barriers (multi barrier system). INE research focuses on the geochemical aspects of nuclear waste disposal. Special emphasis is laid on actinides and long-lived fission products because of their significant contribution to the radiotoxicity for long periods of time.

Relevant scenarios for the geological long-term behaviour of nuclear waste disposal in general assume radionuclide transport via the groundwater pathway. Thermomechanical studies are performed at INE in order to describe the evolution of the repository after closure. The possible groundwater access to emplacement caverns is assumed to cause waste form corrosion. Radionuclide mobility is then determined by the various geochemical reactions in the complex aquatic systems: dissolution of the nuclear waste form (high level waste glass, spent fuel), radiolysis phenomena, redox reactions, complexation with inorganic and organic ligands, colloid

formation, surface sorption reactions at mineral surfaces, precipitation of pure solid phases and solid solutions. Characterisation and quantification of all those processes requires the availability of thermodynamic data and a comprehensive understanding on all processes at a molecular scale. Relevant radionuclide concentrations in natural groundwater lie in the nano-molar range which is infinitesimal small in relation to the main components of the groundwater. Quantification of the chemical reactions occurring in those systems calls for the application and the development of innovative methods and experimental approaches, which provide insight into the chemical speciation of radionuclides. Laser and X-ray spectroscopic techniques are developed and applied at INE. Quantum chemical calculations are currently being applied as an additional tool to confirm the experimental results and to estimate data, which are difficult to derive experimentally.

The long term safety assessment of a repository for nuclear waste has to be demonstrated by application of modeling tools being applicable to geological time scales. The experimental research programme at INE aims to acquire fundamental knowledge on model subsystems and to derive model parameters. Geochemical models and thermodynamic databases are developed as a basis for the description of geochemical behaviour of radionuclides in complex natural aquatic systems. The radionuclide migration behaviour in the geosphere becomes predictable by coupling geochemistry to transport. Transferability and applicability of model predictions are examined by designing dedicated laboratory experiments, field studies in underground laboratories and by studying natural analogue systems. This strategy allows to identify and to analyse key uncertainties related to the accuracy and the relevance of the developed models.

The Partitioning & Transmutation (P&T) strategy is pursued in many international programmes in order to achieve a significant reduction of nuclear waste radiotoxicity. P&T is considered as an alternative to final disposal of long-lived fission products and actinides. The aim of R&D at INE is to separate and isolate long-lived minor actinides from high-level nuclear waste for the subsequent transmutation into short-lived or stable fission products, thus reducing the time horizon for waste storage from more than 100000 to less

than 1000 years. INE develops highly selective extracting agents and performs extraction experiments to derive kinetic and thermodynamic data for the extraction reaction. The continuous extraction by means of hollow-fibre modules is investigated as a separation technique alternative to classical mixer-settler, pulsed column or centrifugal extractors.

Beside research for the long-term safety assessment of nuclear waste disposal and reduction of nuclear waste radiotoxicity by partitioning, INE contributes to the decommissioning of nuclear facilities. The core process technology for the Karlsruhe vitrification plant (VEK) at the WAK site located at the area of Forschungszentrum Karlsruhe has been essentially developed at INE. This work comprises design of process components including the glass melting furnace and the off-gas cleaning installation. The VEK facility is now in the commissioning phase and hot operation is scheduled for early 2008. INE is involved in functional testing of major process systems, the preparation of qualification records and the certification of product quality. The basis of the tests are detailed functional test programs and test instructions for each system which have been approved by the licensing authority.

Promotion of young scientists is of fundamental importance to ensure a high level of competence and to maintain a leading international position in the field of nuclear - and radiochemistry. Therefore, close cooperation with universities is indispensable. INE scientists are strongly involved in teaching at the Universities of Heidelberg, Karlsruhe, Mainz, Jena and Berlin. Radiochemistry lectures at the University of Heidelberg are supplemented by practical training courses at FZK and INE laboratories. By this combination, students are educated in the field of nuclear and actinide chemistry, which most universities are not any more able to offer. Hence INE makes a vital contribution to the medium and long-term perspective of maintaining nuclear technology competence. On the European level the Network of Excellence ACTINET has been established to educate young scientists in actinide sciences by opening the main facilities in Europe, where handling of

transuranium elements is possible, to universities and other national institutions. INE/FZK is one of the core institutions of this network.

INE laboratories are equipped with all facilities necessary to perform radionuclide/actinide research. Alpha glove boxes, shielded boxes with remote control devices and controlled atmosphere boxes are available. Classical α , β , γ spectroscopy instruments exist for the sensitive detection and analysis of radionuclides. Trace element and isotope analysis is made by instrumental analytical techniques such as X-ray fluorescence spectrometry (XRF), atomic absorption spectrometry (AAS), ICP-atomic emission spectrometry (ICP-AES) and ICP-mass spectrometry (ICP-MS). Surface sensitive analysis and characterisation of solid samples is done by X-ray diffraction (XRD), photoelectron spectroscopy (XPS) and atomic force microscopy (AFM). Sensitive laser spectroscopic techniques are developed and applied to the sensitive speciation analysis of actinides such as the laser time-resolved laser fluorescence spectroscopy (TRLFS), the laser photoacoustic spectroscopy (LPAS), the sum frequency infrared spectroscopy, and the laser-induced breakdown detection (LIBD). Structural insight into actinide species is obtained by Extended X-ray fine structure (EXAFS) spectroscopy at the INE-beamline at the Karlsruhe synchrotron source (ANKA). The new INE-Beamline in the direct vicinity of INE actinide laboratories and analytic methods represents a world-wide unique experimental and analytic infrastructure, which profits from INE's expertise in the field of chemistry and spectroscopy of the actinides.

A non-radioactive vitrification test facility (1:1 mock-up of the VEK plant) is available at INE in order to investigate and to simulate vitrification processes for hot plants. INE is furthermore equipped with CAD workstations enabling construction and planning of hardware components, process layout and flowsheets.

2. Highlights

Contributions collected in the present report provide a representative overview on the scientific outcome of INE research activities in 2006. The structure of the report follows widely the organisation of the institute according to research topics: Basic understanding of geochemical reactions of radionuclides on a molecular scale with a direct link to application to the description of the 'real' repository situation. In order to obtain detailed chemical information on radionuclide speciation and structures, INE consequently develops speciation methods and analytical techniques. Beside spectroscopic methods, quantum chemical calculations are increasingly implemented as an additional tool to gain insight into the molecular structure of radionuclide species. Speciation techniques are not only applied to geochemical studies but also to answer questions towards mechanisms underlying the partitioning of minor actinides by solvent extraction using new types of extractants. Research dedicated to the immobilisation of high-level radioactive liquid waste is much more technically oriented. In this field, the long time experience of INE engineers has led to the realization of a vitrification plant on the WAK (Karlsruhe reprocessing pilot plant) site using INE technology.

A selection of milestones and highlights out of the research activities in 2006 are listed below:

One of the most important geochemical reactions of tetravalent actinide ions such as Pu(IV) is colloid formation. **Generation of tetravalent element oxide/hydroxide oligomers** is for the first time studied by **electrospray mass spectrometry (ESI-MS)**. In first experiments Zr(IV) is investigated as a chemical homologue to tetravalent actinides. From the mass of individual clusters the number of metal ions, anions, OH-ligands and water molecules, including their natural isotopic composition can be determined. As the generation of ionized clusters is performed under soft conditions reliable information on the speciation in aqueous solution under the given chemical conditions may be derived. ESI-MS data are complemented with EXAFS experiments and the Zr(IV) speciation is established as a function of pH and can be taken as a basis for the validation and derivation of a thermodynamic dataset. Those first ESI-MS experiments demonstrate the capacity of the method, which will in turn be

applied to study colloid formation of Th(IV) and Pu(IV).

Aquatic actinide chemistry appears still to have surprises in store. The consistent description of Pu redox chemistry under consideration of polymeric species has been a highlight of the annual report 2005. This report contains experimental results on unexpected actinide behaviour under repository relevant conditions. **For the first time the formation of positively charged ternary Ca-metal hydroxo complexes has been observed** and confirmed by spectroscopy. This may lead to an increase in solubility of tri- and tetravalent actinides by more than four orders of magnitude in Ca containing alkaline solution such as cementitious environments.

The exact structure of trivalent actinide ion aqua complexes has been studied for the first time for the nonhydrates of the transplutonium ions Am(III) and Cm(III). Structural data are obtained by growing the well defined trifluoromethanesulfonate crystals and characterisation by X-Ray diffraction and optical spectroscopy. The now available comprehensive molecular scale information on those species is the basis for the improvement of our understanding on trivalent actinide behaviour in aqueous solution and to further develop fluorescence spectroscopic techniques for the elucidation of their speciation in aquatic solution. Those studies have partly been performed in cooperation with the Institute for Transuranium Elements (ITU).

Co-precipitation and subsequent solid solution formation represent a key retention mechanism for many radionuclides. In particular trivalent actinides and lanthanides have a high affinity for calcite, which is an omnipresent mineral in many waste repository concepts. **For the first time the actual substitution mechanism: $2 \text{Ca}^{2+} \leftrightarrow \text{Na}^+ + \text{An}^{3+}/\text{Ln}^{3+}$ could be unambiguously identified** based on site selective TRLFS and EXAFS measurements.

Radionuclide retention by sorption in the barrier system of a nuclear waste repository is widely determined by their interaction of radionuclide species with surface hydroxyl groups. The chemical nature and structure of the functional groups at the mineral surface/solution interface is now characterised by application of non-linear optical **vibrational sum frequency spectroscopy**. Spectra are interpreted to show different surface OH-

groups at the $\alpha\text{-Al}_2\text{O}_3$ with variant tilt angles with respect to the (001) crystal plane. Quantum chemical calculations performed for various Al/O clusters reveal excellent agreement for experimentally obtained spectra and calculated vibrations. The independent proof by theoretical considerations thus confirms the assignment of measured spectral bands to different surface hydroxyl group structures.

The preferential extraction of trivalent actinides over trivalent lanthanides by alkylated 2,6-ditriazinylpyridines can now be explained by combining spectroscopic and theoretical evidences. Trivalent lanthanides form under certain conditions and notably at low ligand to metal ratio a 1:1 complex which is only weakly extracted. Am(III) and Cm(III) exclusively form the efficiently extracted 1:3 complex. This hitherto lacking understanding on the extraction mechanism can now be used to design and further optimise a **minor actinide partitioning process**.

The **Karlsruhe Vitrification plant (VEK)** has been set into commissioning procedure. As part of the extensive functional testing the melter has been heated up and fed with glass frit and deionized water. In the scope of integral plant test operation vitrification of simulated non-radioactive waste solution will be performed in spring 2007. Concept and technology of the facility has been developed and designed by the INE process engineering group, which also plays a major role in facility operation. As main hardware equipment, the waste glass melter has been constructed and installed in the VEK hot cell by INE personnel.

3. National and International cooperation

INE research is involved in a number of national and international cooperations and projects.

INE coordinates the **Virtual Institute Functional Properties of Aquatic Interfaces** supported by the HGF and comprising research groups at the Universities of Heidelberg, Karlsruhe and Münster. Aim of research performed at the virtual institute is the characterisation of the mineral surface/solution interface. Laser spectroscopy, X-ray spectroscopy, acoustic sensors and various microscopic techniques are being developed and applied to investigate solid/liquid interface reactions relevant to the understanding of actinide reactions in the geosphere.

"Fundamental processes of radionuclide migration" (**FUNMIG**) is an Integrated Project within the European Commission's 6th Framework Program. It started Jan. 2005, with a duration of four years. With respect to the number of partners and geographical distribution it is the largest such project within the EURATOM program. There are 51 Contractors from 15 European countries. There are also 20 Associated Groups from an additional three European countries, Korea and Canada. All types of key players are well represented, i.e. research organizations, universities, SME's, national waste management organizations and national regulatory bodies. The project is coordinated by INE with EnviroS S.L. as the coordination secretariat. The research program builds around five research and technological development components (RTDC's). Two of these deal with well established and less established processes, applicable to all host-rock types. Three of them deal with processes specific to the three host-rock types under investigation in Europe, i.e. clay, crystalline and salt. Another RTDC deals with integration of the scientific progress towards application to long-term safety assessment of a nuclear repository. An important part of the project is management and dissemination of knowledge, including training.

The "Network of Excellence for actinide sciences" (**ACTINET**) is a consortium gathering more than twenty-five European research institutions. The consortium is supported by the European Commission under a four year contract established in March 2004 as an European Network of Excellence for actinide sciences. The objective of ACTINET is

to take steps in order to bring both research infrastructures and human expertise in Europe to an enhanced performance level, thereby contributing to the development of the European Research Area in the fields of physics and chemistry of actinides. INE acts as one of the core members of the ACTINET consortium together with the coordinating institution Commissariat à l'Energie Atomique (CEA, France), the Institute for Transuranium Elements (ITU, European Joint Research Center), and the Studiecentrum voor Kernenergie - Centre d'Etude de l'Energie Nucléaire (SCK•CEN, Belgium). A first priority objective within ACTINET is to pool selected parts of the major facilities for actinide research of some large European institutes (CEA, ITU, INE, SCK-CEN, Forschungszentrum Dresden (FZD), and Paul Scherrer Institut (PSI)) and to operate this pool as a multi-site user facility, in order to make it accessible to all members through a competitive selection of joint projects. Further objectives are to support training and education in actinide research fields and dissemination of the achieved knowledge in actinide sciences.

INE is partner in the Integrated Project **EUROPART**. The research within this project concerns the separation (Partitioning) of minor actinides that are contained in the nuclear wastes from reprocessing of nuclear spent fuels. After separation, the actinides will be either destroyed into short-lived or stable nuclides by nuclear means (Partitioning & Transmutation, P&T strategy) or conditioned into stable dedicated solid matrices (Partitioning & Conditioning, P&C strategy). INE's R&D is focused on the extraction of actinides over lanthanides. This includes spectroscopic investigations to understand the high selectivity of extraction reagents for trivalent actinides as well as kinetic studies of the extraction process.

INE participates in a further European Integrated Project entitled **NF-PRO**: Understanding and physical and numerical modelling of key processes in the near-field, and their coupling, for different host rocks and repository strategies. NF-PRO is a four-year Integrated Project (2004-2007) that investigates key processes affecting the barrier performance of the near-field environment of geological repositories for the disposal of high-level radioactive waste and spent nuclear fuel. The near-field is an

important component of the geological disposal system as it plays an essential role in ensuring the overall safety of geological disposal. In particular, the near-field is made of engineered barriers that enclose the disposed waste and contain and minimise the release of radionuclides over extended periods of time.

Two international projects focus onto the influence of colloids on radionuclide migration in crystalline host rock: The Colloid Formation and Migration (**CFM**) experiment is coordinated by NAGRA (National Cooperative for the Disposal of Radioactive Waste, Switzerland) at the Grimsel Test Site and the **Colloid Project** has been initiated by SKB (Swedish Nuclear Fuel and Waste Management Co., Sweden) and includes field experiments at the Äspö Hard Rock laboratory. INE plays a decisive role in the laboratory programmes of both projects and is also involved in the field activities.

INE is furthermore involved in various bi- and multilateral cooperations with national universities on different topics. Scientific cooperation with various universities within Germany is partly supported by the German ministry for Economy and Technology (BmWi). Those research programs are dedicated to actinide geochemistry and specifically the impact of colloidal and natural organic matter.

Among the 15 Helmholtz University Young Scientist Groups (**HHNG**) supported in 2006, INE was successful with its research project on "Elucidation of Geochemical Reaction Mechanisms at the Water/Mineral Phases Interface." Its partner is the Faculty of Chemistry and Geosciences of the University of Heidelberg. The project will run for five years with funds totaling 1.25 million Euro, out of which the position of the working group leader, scientific or technical staff members, and non-personnel items are covered. The leader of the working group also has teaching functions at the university.

4. Fundamental Studies: Process understanding on a molecular scale

The studies reported in this section deal with the aquatic chemistry of actinides, the formation of actinide containing solid solution phases and finally actinide colloid formation processes. The groundbreaking studies on the fundamental understanding of plutonium redox in aqueous solution have been completed in 2006. Furthermore, the non-expected formation of Ca-An(III, IV)-OH species is reported for the first time and their actinide solubility increasing effect under alkaline conditions is described. Further systematic investigations in actinide solution chemistry resulted in new insights into the aqua ion structure of trivalent transplutonium elements Am and Cm. This insight is of relevance for understanding their solution chemistry but also their spectroscopic properties. Mineralisation by solid-solution formation is considered an efficient retention mechanism for actinides in a repository system but up to now not considered in nuclear waste disposal safety analysis. Comprehensive molecular scale information is now available on Am(III), Eu(III) and Np(V) interaction with calcite and notably the structure of those metal ions when incorporated in the calcite crystal structure. Incorporation of actinides into the structure of aluminosilicate colloids is another topic of interest. Here, the incorporation is considered as a relevant reaction mechanism for actinide mobilisation. In order to assess colloid mobility as a function of geochemical boundary conditions, studies on colloid stability and the interaction of colloids with mineral surfaces complement this chapter.

4.1 Chemistry and thermodynamic of actinides in aqueous solution

M. Altmaier, H.R Cho, R. Klenze, P. Lindqvist-Reis, C.M. Marquardt, V. Neck, P. Panak, A. Seibert, C. Walther, J.I. Yun, Th. Fanghänel

Introduction

The objectives were to fill in the gaps of thermodynamic data on solubility and complexation reactions of actinides. The focus in this report is Pu-redox chemistry and actinide speciation and solubility in Ca rich solutions. The second part deals with the structure of trivalent actinide aqua ions.

Redox reactions and hydrolysis of Pu(IV) in acidic solution

The redox behaviour, hydrolysis and colloid formation of 10^{-5} - 10^{-3} M Pu(IV) solutions in 0.5 M HCl-NaCl ($pH_c = 0.3 - 2.1$) was studied by UV/Vis/NIR absorption spectroscopy with a 1 m liquid core waveguide capillary and LIBD measurements. It could be shown that the spectra of the mononuclear hydroxide complexes $Pu(OH)_n^{4-n}$ with $n = 1, 2,$ and 3 do not differ from that of the $Pu^{4+}(aq)$ ion [1]. The decrease of the Pu(IV) absorption with increasing pH and/or Pu concentration was unequivocally identified as an effect of polymer formation. The combination of spectroscopy and redox potential measurements was used to determine the formation constants of the first three mononuclear hydroxide complexes from the measured Eh values and the spectroscopically determined Pu(III) and the Pu(IV) concentrations. The values extrapolated to $I = 0$ with the SIT are: $\log \beta^{\circ}_{11} = 14.0 \pm 0.2$, $\log \beta^{\circ}_{12} = 26.8 \pm 0.6$, and $\log \beta^{\circ}_{13} = 38.9 \pm 0.9$ [2].

Another important conclusion from these studies concerns the reaction mechanism leading to the observed oxidation state distributions in initially pure Pu(IV) solutions at $pH_c = 0.3 - 2.5$. The redox potentials measured in the steady state, after 10 - 20 days, were consistent with Eh calculated from the spectroscopic data and known equilibrium constants for the redox couples Pu(V)/Pu(VI) and $PuO_2(am,hyd)/Pu(V)$ if solid or colloidal Pu(IV) particles are present. The equilibrium state between the different Pu oxidation states is usually ascribed to the "disproportionation" of Pu(IV) into Pu(III) and Pu(V) or Pu(VI). However, a closer look at the oxidation state distributions, in particular after short reaction times, shows that the underlying mechanism is a two-step process. The initial step is the formation of PuO_2^+ , either by the redox equilibrium with colloidal $PuO_2(am,hyd)$ or by the oxidation of colloids or smaller polynuclear Pu(IV) species by dissolved O_2 . The second step is the simultaneous equilibration of the redox couples Pu(V)/Pu(VI) and Pu(III)/Pu(IV) which are related by pe (and pH because of Pu(IV) hydrolysis equilibria) [3].

Trivalent and tetravalent actinides: Formation of ternary Ca-An-OH complexes in alkaline $CaCl_2$ solution

An hitherto unknown type of aqueous complexes, ternary Ca-M(IV)-OH complexes causes unexpectedly high solubilities of Zr(IV) and Th(IV) hydrous oxides in alkaline $CaCl_2$ solutions (for Zr(IV) at $pH_c = 10 - 12$ and $CaCl_2$ concentrations > 0.05 M (Fig.1), and for Th(IV)

at $\text{pH}_c = 11 - 12$ and CaCl_2 concentrations $> 0.5 \text{ M}$ (Fig. 2)).

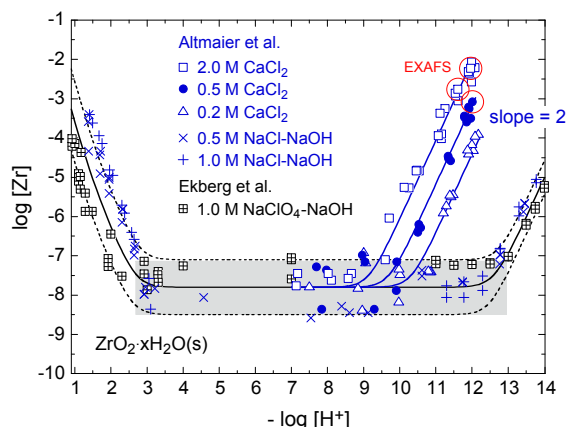


Fig.1 Solubility of $\text{ZrO}_2 \cdot x\text{H}_2\text{O}(\text{s})$ in NaClO_4 , NaCl , and CaCl_2 solutions at $20\text{-}25^\circ\text{C}$ (from Ekberg et al. [4] and Altmaier et al. (INE)). The solid lines for the solubility in alkaline CaCl_2 solutions are calculated with the SIT and $\log K^\circ_{\text{s},6-3} = 0.7 \pm 0.3$.

Partly the Zr(IV) and Th(IV) concentrations are sufficient for aqueous speciation by EXAFS as a complementary spectroscopic method (cf. section 6.1 of this report). The number of OH^- ligands in the first coordination sphere was found to be $N_{\text{O}} = 6$ (6.6 ± 1.2) for Zr and $N_{\text{O}} = 8$ (8.6 ± 1.2) for Th and the number of neighbouring Ca^{2+} ions in the second shell around the $[\text{Zr}(\text{OH})_6]^{2-}$ and $[\text{Th}(\text{OH})_8]^{4-}$ units was determined to be $N_{\text{Ca}} = 3$ (2.7 ± 0.6) at a distance of $R_{\text{Zr-Ca}} = 3.38 \pm 0.02 \text{ \AA}$ and $N_{\text{Ca}} = 4$ (3.8 ± 0.5) at a distance of $R_{\text{Th-Ca}} = 3.98 \pm 0.02 \text{ \AA}$. The EXAFS results are consistent with the dissolution equilibria

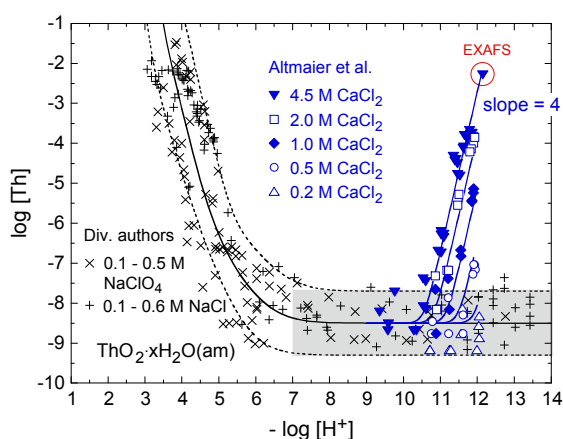
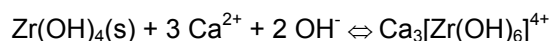


Fig. 2 Solubility of $\text{ThO}_2 \cdot x\text{H}_2\text{O}(\text{s})$ in NaClO_4 , NaCl , and CaCl_2 solutions at $17\text{-}25^\circ\text{C}$. The experimental data in NaClO_4 and NaCl media are taken from [5] and references therein, the data in CaCl_2 solution are from Altmaier et al. (INE). The solid lines for the solubility in alkaline CaCl_2 solutions are calculated with the SIT and $\log K^\circ_{\text{s},8-4} = 1.8 \pm 0.5$.

derived from the dependence of the Zr(IV) and Th(IV) solubilities on pH_c (slopes of 2 and 4 in the solubility curves of $\log [M]_{\text{tot}}$ versus pH_c) and the CaCl_2 concentration:



The presence of polynuclear hydrolysis species and the formation of complexes with chloride ligands can be excluded. The $[\text{Zr}(\text{OH})_6]^{2-}$ octahedrons and $[\text{Th}(\text{OH})_8]^{4-}$ cubes with an extraordinary large number of OH^- ligands are stabilized by the formation of associates or ion pairs with Ca^{2+} ions. In analogous studies with Pu(IV) hydrous oxide, the solubility increasing effect of ternary complexes with Ca^{2+} ions is less pronounced and only observed at CaCl_2 concentrations above 2 M.

Similar observations were made for Nd(III) and Cm(III). In CaCl_2 solutions above 1 M, the solubility of Nd(III) hydroxide clearly increases at $\text{pH}_c = 11 - 12$. This is consistent with a TRLFS study with $2 \cdot 10^{-7} \text{ M}$ Cm(III) in alkaline CaCl_2 solutions. The fluorescence spectra at $\text{pH}_c 11.7$ in 0.1 - 1.0 M CaCl_2 and at $\text{pH}_c 10.7 - 11.3$ in 1.0 M CaCl_2 show Cm(III) emission bands with peak maxima in the range 607 - 612 nm. At CaCl_2 concentrations above 1.0 M and $\text{pH}_c > 11.5$ a further band appears at 615 nm. Increasing the CaCl_2 concentration strongly enhances the formation of the observed complexes. In alkaline NaCl solutions the major fraction of the Cm(III) is present as $\text{Cm}(\text{OH})_3$ colloids which do not show fluorescence emission bands. The curium hydroxide complexes formed in alkaline CaCl_2 solutions are obviously stabilized by the association of Ca^{2+} ions. Peak deconvolution and the evaluation of the pH dependence of the spectroscopic data indicate that the observed fluorescence emission bands come from the ternary complexes $\text{Ca}_x[\text{Cm}(\text{OH})_3]^{2-x}$, $\text{Ca}_y[\text{Cm}(\text{OH})_4]^{2y-1}$ and $\text{Ca}_z[\text{Cm}(\text{OH})_6]^{2z-3}$, the latter complex being formed at higher CaCl_2 and OH^- concentrations.

The only type of similar complexes reported in the literature are ternary calcium-uranyl(VI)-carbonate complexes, $\text{Ca}[\text{UO}_2(\text{CO}_3)_3]^{2-}$ and $\text{Ca}_2[\text{UO}_2(\text{CO}_3)_3]^\circ$, observed in NaClO_4 solutions containing 10^{-3} to 10^{-2} M Ca^{2+} [6-8]. Possibly, the stabilization of anionic hydroxide and carbonate complexes by Ca^{2+} ions is a more general phenomenon that deserves further investigation. These species might have a significant impact on the solubility and aqueous speciation of actinide ions.

Transplutonium Hydrates

Apart from a relatively large number of papers reporting XRD structures of actinyl containing compounds, there are only few reports on trivalent actinide compounds, especially on hydrated/solvated complexes. This is largely due to the redox instability of the lighter actinides and the short half-lives of the heavier actinides. Nevertheless, basic coordination chemistry of these elements are essential, for example, for prediction of actinide migration in the aquatic systems of a nuclear repository as well as for separation chemistry. Up to now the only published structure containing a fully hydrated An(III) ion was Pu(III) trifluoromethanesulfonate (triflate), $[\text{Pu}(\text{H}_2\text{O})_9](\text{CF}_3\text{SO}_3)_3$ [9]. To provide structural data across the series of An(III) hydrates we determined the corresponding structures of Am(III) and Cm(III) [10].

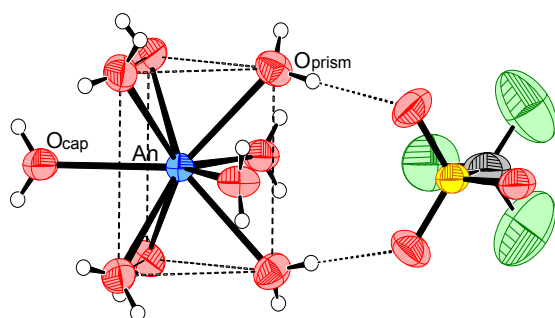


Fig. 3 Molecular structure of the $[\text{An}(\text{H}_2\text{O})_9]^{3+}$ entity hydrogen bonded to a CF_3SO_3^- ion in $[\text{An}(\text{H}_2\text{O})_9](\text{CF}_3\text{SO}_3)_3$ (An = Am, Cm). The TTP geometry and the hydrogen bonding are indicated with dashed lines. Selected bond An–O bond distances (in Å) to the prismatic (p) and capping (c) waters: Am–O_p 6 × 2.466(4); Am–O_c 3 × 2.578(6); Cm–O_p 6 × 2.454(6); Cm–O_c 3 × 2.565(8).

In these triflate salts the An (or Ln) ions are surrounded by nine water molecules in a tricapped trigonal prismatic (TTP) fashion. Owing to the hydrogen bonding between the water ligands and the triflate ions and the steric crowding between the former, the An–O bond distances to the prismatic waters become ~ 0.1 Å shorter than to the capping waters (Fig. 3). This steric crowding becomes increasingly important with decreasing ionic radii. This explains why the Ln–O distances to the capping waters, in contrast to the prismatic ones, do not follow the lanthanide contraction (Fig. 4a). With this in mind, it is not surprising that the heavier Ln³⁺ ions are octahydrated in aqueous solution [10], and, hence, we expect the actinides beyond Cf³⁺ to also be octahydrated (Figs. 4a and b).

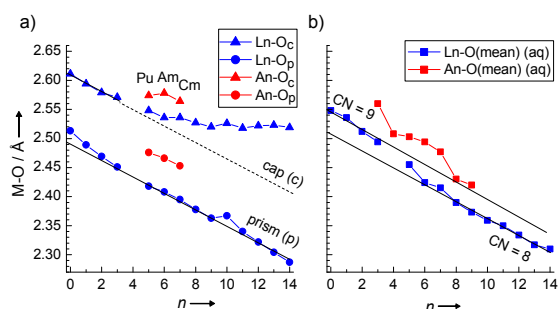


Fig. 4 a) M–O bond lengths in the isotypic $[\text{M}(\text{H}_2\text{O})_9](\text{CF}_3\text{SO}_3)_3$ (M = Ln, An) compounds. The straight lines show the predicted M–O distances assuming (linear) Ln and An contractions of about 0.20 Å. b) Mean M–O distances for Ln³⁺(aq) and An³⁺(aq) determined by EXAFS quoted by ref [10] and refs therein.

The derived An–O mean bond distance for Pu³⁺(aq), 2.51 Å, and Am³⁺(aq), 2.48–2.51 Å, are similar to those of their triflate salts, 2.51 Å and 2.50 Å, respectively, while the distances reported for Cm³⁺(aq), 2.45–2.47 Å, are slightly shorter than the Cm–O mean distance for the solid, 2.49 Å. Our recent Cm³⁺(aq) EXAFS data revealed an asymmetric distribution of 8.5(8) waters at the mean Cm–O distance 2.477(5) Å [10,11]. This asymmetry is consistent with a TTP coordination geometry with two Cm–O back-scattering contributions from waters in the prismatic and capping positions, while the shorter Cm–O mean bond distance compared to the solid is explained by the presence of ~10 % octahydrated ions [12].

A deeper insight into the local structures of these aqua ions was gained from their optical spectra [10]. The striking similarities between the electronic absorption spectra of Am³⁺(aq) and $[\text{Am}(\text{H}_2\text{O})_9](\text{CF}_3\text{SO}_3)_3$ indicate a similar TTP coordination geometry for the Am³⁺ aqua ion as that for the solid (Fig. 5). The same conclusion is derived by the comparison of fluorescence spectra on Cm³⁺(aq) and $[\text{Cm}:\text{Y}(\text{H}_2\text{O})_9](\text{CF}_3\text{SO}_3)_3$.

In summary, the crystal structures of transplutonium nonahydrates and their 5f optical spectra are reported for the first time: The presented structures, $[\text{An}(\text{H}_2\text{O})_9](\text{CF}_3\text{SO}_3)_3$ (An = Am, Cm), add new and important information to the isotypic An(III) and Ln(III) series. Comparisons of these compounds with the Am³⁺(aq) and Cm³⁺(aq) EXAFS together with their respective 5f optical spectra, indicate prevailing TTP coordination for these aqua ions.

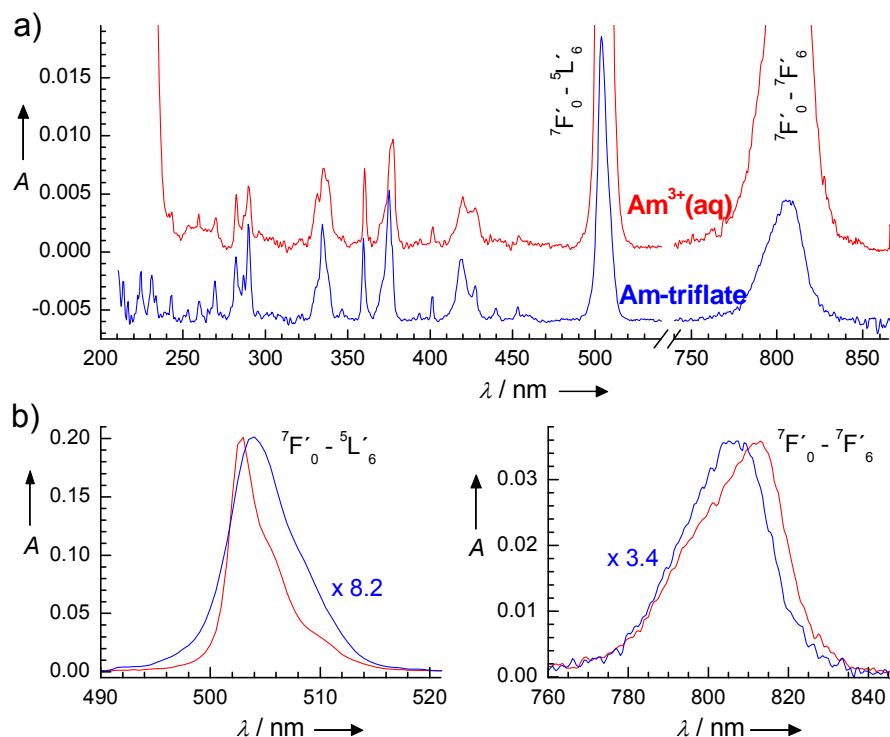


Fig. 5 UV-Vis electronic absorption spectra of $[\text{Am}(\text{H}_2\text{O})_9](\text{CF}_3\text{SO}_3)_3$ and $\text{Am}^{3+}(\text{aq})$ (4.9 mM $\text{Am}(\text{CF}_3\text{SO}_3)_3$ in 1.4 M HCF_3SO_3 ; optical path = 1.0 mm) at room temperature: a) the region 200–860 nm; b) the bands near 503 and 810 nm (ref. [10]).

References

- [1] Walther, C., Cho, H.R., Marquardt, C.M., Neck, V., Seibert, A., Yun, J.I., Fanghänel, Th., *Radiochim. Acta* 95, 7-16 (2007).
- [2] Yun, J.I., Cho, H.R., Neck, V., Altmaier, M., Seibert, A., Marquardt, C.M., Walther, C., Fanghänel, Th., *Radiochim. Acta* 95, 89-95 (2007).
- [3] Cho, H.R., Marquardt, C.M., Neck, V., Seibert, A., Walther, C., Yun, J.I., Fanghänel, Th., *Proc. of the conf. Actinides 2005*, Manchester, UK, July 4-8, 2005, in: *Recent Advances in Actinide Science* (Eds: I. May, R. Alvarez, N. Bryan), pp. 602-604, The Royal Society of Chemistry, Spec. Publ. No. 305, RCS Publishing, Cambridge, UK, 2006.
- [4] Ekberg, C., Källvenius, G., Albinsson, Y., Brown, P.L., *J. Solution Chem.* 33, 47-79 (2004)
- [5] Neck, V., Müller, R., Bouby, M., Altmaier, M., Rothe J., Denecke, M.A., Kim, J.I., *Radiochim. Acta* 90, 485 - 494 (2002).
- [6] Bernhard, G., Geipel, G., Brendler, V., Nitsche, H., *Radiochim. Acta* 74, 87-91 (1996).
- [7] Bernhard, G., Geipel, G., Reich, T., Brendler, V., Amayri, S., Nitsche, H., *Radiochim. Acta* 89, 511-518 (2001).
- [8] Kalmykov, S.N., Choppin, G.R., *Radiochim. Acta* 88, 603-606 (2000).
- [9] J. H. Matonic, B. L. Scott, M. P. Neu, *Inorg. Chem.*, 40, 2638-2639 (2001).
- [10] P. Lindqvist-Reis, C. Apostolidis, J. Rebizant, A. Morgenstern, R. Klenze, O. Walter, T. Fanghänel, R.G. Haire, *Angew. Chem.*, 119, 937-940 (2007); *Angew. Chem. Int. Ed.* 46, 919-922 (2007).
- [11] P. Lindqvist-Reis, B. Brendebach, K. Dardenne, J. Rothe, R. Klenze, R. Haire, *ANKA/FZK Annual Report 2006*, p. 141-143 (2006).
- [12] P. Lindqvist-Reis, R. Klenze, G. Schubert, T. Fanghänel, *J. Phys. Chem. B*, 109, 3077-3083 (2005).

4.2 Structural incorporation of actinides into calcite

Th. Stumpf, D. Bosbach, M. Schmidt, F. Heberling, M. Marques-Fernandes, C. Walther, K. Dardenne, M.A. Denecke, Th. Fanghänel

Introduction

The geochemical behavior of radionuclides in the environment is to a large extent governed by heterogeneous reactions like adsorption, ion exchange and structural incorporation reactions. Especially the structural incorporation of actinides into secondary phases via coprecipitation and the formation of solid solutions can play a key role which controls their migration in the geosphere.

The interaction of actinides with calcite (CaCO_3) is of interest with respect to long-term safety of a nuclear waste repository system over extended periods of time. Calcite is omnipresent in many potential nuclear waste repository host rock formations such as granite or clay rock. Furthermore, many waste repository designs include cement based components. Taking geological timescales into account, calcite is one of the major secondary alteration products which are formed during the degradation process of cement.

Here, we have studied structural incorporation of pentavalent (Np) and trivalent (Cm) actinides as well as lanthanides (Eu, Gd) (as non-radioactive chemically homologous elements) into calcite via coprecipitation with spectroscopic techniques. Time resolved laser fluorescence spectroscopy (TRLFS) and extended x-ray absorption fine structure spectroscopy (EXAFS) provided a molecular level picture of the incorporated species within the calcite host structure as baseline information for further thermodynamic aqueous – solid solution (AqSS) models.

Coprecipitation experiments

Actinide containing calcite crystals were synthesized by using a Mixed Flow Reactor (MFR). Surface reaction controlled (as opposed to transport/diffusion controlled) coprecipitation experiments were performed under steady conditions by feeding a calcite suspension from independent Ca, carbonate and actinide reservoirs. As a result, calcite seed crystals are coated with an actinide containing calcite layer. The actinide concentration within the doped layer is homogeneous without any concentration gradient.

Two Cm(III) containing calcite samples were synthesized at pH 8.1. In a first experiment, the Cm(III) concentration in solution was about 3×10^{-10} M Cm(III): sample LCMpH8.1 with 0.7 ppm Cm. In a second experiment, the total tri-

valent metal ion concentration M^{3+} in the input solution was significantly increased to 4×10^{-7} M by adding non-fluorescent gadolinium (3×10^{-10} M Cm^{3+} and 4×10^{-7} M Gd^{3+}): sample HCMpH8.1 with 750 ppm M^{3+} .

Four Np(V) containing calcite samples were synthesized in a mixed-flow-reactor under varying conditions, two at a pH of about 10.3, one at pH 12.8, and one at pH 8.2 to check if the aqueous speciation has an influence on the incorporation. At the chosen solution compositions the pure NpO_2^+ -ion dominates the aqueous speciation at pH 8.2, at pH 10.3 the neptunyl monocarbonate complex dominates, and at pH 12.8 the neptunyl dihydroxo complex. The saturation index $\text{SI}(\text{calcite})$ of the input solutions is chosen to be between 1 and 1.3 in order to avoid homogeneous nucleation ($\text{SI} = \log_{10}(\text{IAP}/\text{K}_{\text{sp}})$, with the Ion Activity Product, IAP, and the Solubility Product, K_{sp}). All the experiments are conducted with a Np concentration of $1 \mu\text{mol/L}$ and a background electrolyte concentration of 0.01M NaCl. The input solution is undersaturated with respect to all known solid Np(V) phases. The reactive surface in the reactor is $\sim 0.2 \text{m}^2$ (measured by BET). Three stock solutions, the first containing NaCl and Na_2CO_3 (+ NaHCO_3 or NaOH, to adjust the pH), the second NaCl and NpO_2^+ (taken from a 0.073 mol/L pH 3 perchloric acid stock solution) and the third NaCl and CaCl_2 , are pumped continuously into the reactor.

Trivalent f-elements, Cm(III), Eu(III), Gd(III)

TRLFS -The fluorescence emission of the Cm^{3+} aquo ion shows a peak maximum at 593.8 nm. Spectral shifts and splitting of emission bands are the main sources for the speciation of the actinide ion.

Selected fluorescence emission spectra of the Cm(III) aquo ion, LCMpH8.1 and HCMpH8.1 are presented in Fig.1. Both fluorescence spectra of LCMpH8.1 and HCMpH8.1 show two emission bands at 606.2 nm (1) and 620.3 nm (2). The two emission bands can clearly be assigned to different Cm(III) species. The peak positions are identical to the peak positions of the Cm(III) species identified by Stumpf and Fanghänel [1]. Cm(III) species (1) has a peak maximum at 606.2 nm. This red shift is in the range of the shift observed for Cm(III) sorption onto mineral phases. The extraordinary red shift of the fluorescence emission spectrum of the Cm(III) species (2) to a peak maximum at

620.3 nm is a clear indication for a strong change in the ligand field of Cm(III).

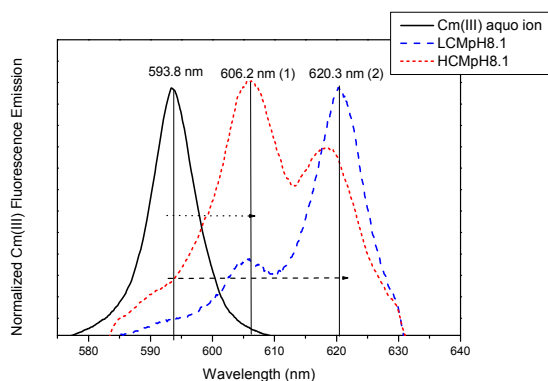


Fig. 1 Fluorescence emission spectra of the Cm(III) aquo ion (solid line), Cm(III) in LCMpH8.1 and HCMpH8.1 (red dashed and blue dotted line).

Complementary to the energy of the fluorescence emission band, the lifetime of excited state contains supplemental information about the complexation state. In principle, the fluorescence lifetime is controlled by quenching due to high-frequency oscillating molecules in the first coordination sphere, such as H₂O [2]. Without OH-quencher in the first coordination sphere of Cm(III), the calculated decay rate is 770 s⁻¹ [3], this corresponds to a radiative lifetime (reciprocal decay rate) of 1.3 ms. This value is verified for Cm³⁺ lifetime measurements in D₂O. In contrast to that, the Cm(III) aquo ion (in H₂O) has a lifetime of 68 μs [4]. A correlation between inner-sphere water molecules and lifetime of the excited state can be used to determine the hydration state of Cm(III). We applied the linear relationship developed by Kimura et al. and recalculated by Stumpf (unpublished results), to calculate the number of associated hydration waters for Cm(III) species.

$$n(\text{H}_2\text{O}) = 0.642k_{\text{obs}} - 0.45$$

$n(\text{H}_2\text{O})$: the number of coordinated water molecules, k_{obs} : observed decay rate (reciprocal lifetime) of the excited state (ms⁻¹).

Fig.2a and 2b show the Cm(III) fluorescence emission spectra of HCMpH8.1 and LCMpH8.1 at different delay times. By changing the delay time the ratio of the two Cm(III) species changes. This indicates that Cm(III) species (1) and (2) have different fluorescence emission lifetimes and that the shorter one can be attributed to Cm(III) species (1). The decay rate for the Cm(III) fluorescence emission of LCMpH8.1 and HCMpH8.1 show a bi-exponential decay which confirms the presence of two Cm(III) species.

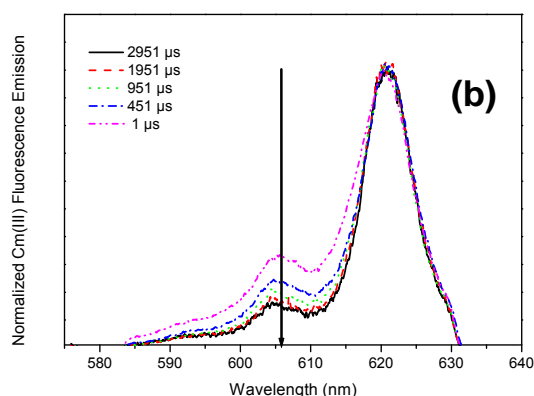
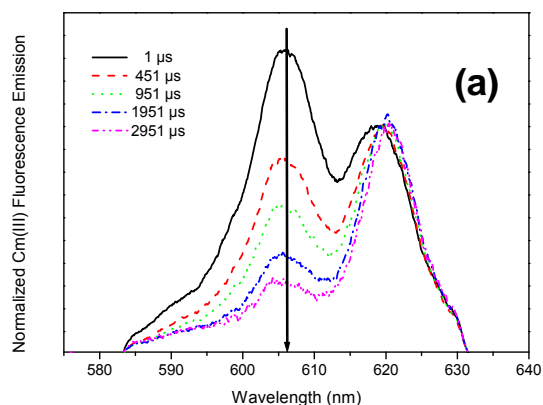


Fig. 2 Fluorescence emission spectra of Cm(III) in calcite at different delay times. a) HCMpH8.1 and b) LCMpH8.

Applying the correlation between inner-sphere water molecules and lifetime of the excited state, it follows that Cm(III) species (1) contains approximately one H₂O molecule in the first coordination sphere, whereas Cm(III) species (2) has lost his complete hydration sphere. This is a clear indication for the incorporation of Cm(III) in the calcite bulk structure. The hydration state of both species is in good agreement with the hydration state determined by Stumpf and Fanghänel in their Cm(III)/calcite batch experiment.

EXAFS - To get additional information about the structural parameters of this incorporated species, EXAFS measurements with Am(III) doped calcite were done. The Fourier transform (FT) of the k^2 - weighted EXAFS function is shown in Fig. 3.

The FT spectrum exhibits a single low-R peak at $R-\Delta$ near 1.8 Å, which can be modeled as a single oxygen shell ($N = 6.3 \pm 0.6$ O at 2.40 \pm 0.01 Å). This coordination number is much lower than the N which is found for the Am³⁺ aquo ion (8-9 oxygen atoms) and for Am sorbed onto mineral surfaces. In the case of

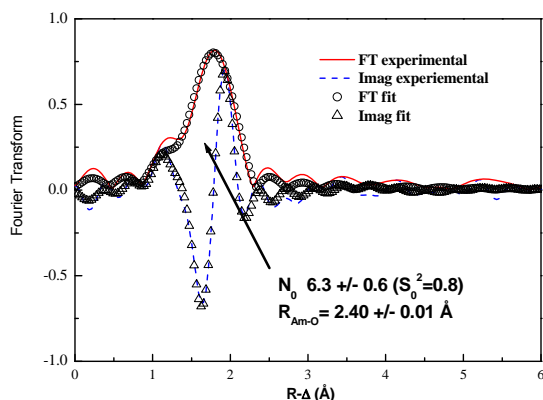


Fig. 3 Fourier transform (FT) of the k^2 -weighted EXAFS function of Am(III) in doped calcite (solid line - experiment; dotted line - theoretical fit results from fits to $\chi(k)$)

Am(III) sorbed onto clay minerals like smectite and kaolinite the coordination number is found to be between 7 and 9. Furthermore the Am-O distance measured for Am in calcite is significant shorter than the distance which is found for $\text{Am}(\text{H}_2\text{O})_{8-9}$ (2.49 Å) and which was detected for the Am/clay sorption species (2.47-2.49 Å). No shell splitting, as might be expected from the different TRLFS species, is observed. As known from the TRLFS data, the incorporated Am/calcite species is the predominant component in the system. We suggest that the signal of the Am/calcite sorption species is covered by the EXAFS signal of the dominating Am/calcite incorporation species. Furthermore, there is no Am-Am interaction, excluding the presence of separate Am mineral phases. The Am-O distance differs slightly from the Ca-O distance (2.36 Å) in calcite but is in good agreement with structural parameters obtained in EXAFS studies on rare-earth element doped calcite. In summary, Am(III) TRLFS and EXAFS measurements of an actinide doped calcite show that americium is incorporated into the calcite bulk structure. A solid solution is formed and the structural parameters indicate that Am(III) replaces Ca(II) in the calcite lattice.

Site-selective Eu(III) TRLFS - An important question for any heterovalent substitution is the charge compensation mechanism in the near field of the substituting cation, to maintain electroneutrality. To answer this question the optical properties of Eu^{3+} (as an analogue for trivalent actinides) was used to investigate the nature of the different sites (different chemical environments or crystal fields) induced by the substitution of Ca^{2+} by Eu^{3+} in the calcite lattice and the potential influence of sodium (Na^+) as charge compensating cation. For this reason site selective TRLFS was performed on Eu(III)

doped calcite samples synthesized in the presence of Na^+ (Eu/calcite 1) and samples synthesized in the presence of K^+ (Eu/calcite 2). Since K^+ has a larger ionic radius (138 pm in the sixfold coordination) than Na^+ (102 pm) and Ca^{2+} (100 pm), it is presumed that the incorporation of K^+ or the vacancy site induced because K^+ is not incorporated, will modify the crystal field around the incorporated Eu(III) ion. Because the $^5\text{D}_0 \rightarrow ^7\text{F}_0$ transition is non degenerate, the excitation spectra of the $^5\text{D}_0 \rightarrow ^7\text{F}_0$ transition allow to determine the number of different sites which are occupied by Eu(III) in the calcite lattice. Furthermore, the analysis of the lifted degeneracy of the $^5\text{D}_0 \rightarrow ^7\text{F}_j$ transitions (obtained after selectively exciting the $^5\text{D}_0 \rightarrow ^7\text{F}_0$ transitions) in terms of the group theory provides information on the symmetry of the sites occupied by Eu^{3+} in the investigated system [5]. The maximum splitting of the F_j levels for a given site is $2J+1$. In highly symmetric sites, the $^5\text{D}_0 \rightarrow ^7\text{F}_0$ and $^5\text{D}_0 \rightarrow ^7\text{F}_2$ transitions are forbidden or weak. The higher the splitting magnitude of the $^5\text{D}_0 \rightarrow ^7\text{F}_{1,2,3,4}$ transitions of one Eu(III) site, the lower is the symmetry of the site.

Site-selective TRLFS measurements at low temperature (< 18 K) of europium doped samples allowed to discriminate three different sites (sites A, B, and C) occupied by Eu(III) in calcite. Site A: The position of the F_0 transition, the magnitude of the splitting of F_1 and F_2 transitions as well as the short fluorescence lifetime correlates with a Eu(III) ion incorporated at the calcite surface with 1-2 H_2O molecules in the first coordination sphere. Site A is equivalent with Cm species (1) in the Cm/calcite system.

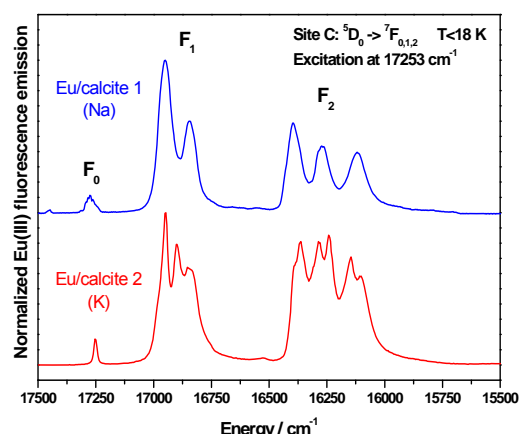


Fig. 4 Emission spectra of the $^5\text{D}_0 \rightarrow ^7\text{F}_{0,1,2}$ transitions of the Eu/calcite incorporation site at 17 K in Eu/calcite 1 and 2 when exciting resonantly at 17253 cm^{-1} .

The long fluorescence lifetimes measured for site B and site C indicate that Eu(III) which occupies these sites is without water

molecules in the inner coordination sphere. Therefore, we conclude that Eu(III) that is located at sites B and C is incorporated in the calcite bulk structure. These two sites which are discriminated by site-selective Eu TRIFS correspond to Cm species (2) in the Cm/calcite system.

The emission spectrum of Eu(III) in site B is typical for a low symmetry site, whereas, the emission spectrum of site C exhibits a twofold splitting of the 7F_1 transition and a threefold splitting of the hypersensitive 7F_2 level. The magnitude of the splitting of the F_1 and F_2 transitions correlate with a trigonal site symmetry, indicating that at this site Eu(III) replaces Ca(II) in the calcite frame work.

The total splitting of the F_1 and F_2 transition in the emission spectrum of site C in Eu:calcite II (synthesized in presence of K^+ ions) shown in Fig.4, indicates a strong distortion of this site compared to site C in Eu/calcite I (synthesized in presence of Na^+). Indeed, the magnitude of splitting is typical of Eu(III) occupying a low symmetry site in calcite. Two explanations are possible. The incorporation of the larger K^+ (138 pm) in the neighborhood of Eu^{3+} instead of smaller Na^+ (102 pm) would lower the symmetry of the site considerably. A similar effect would be induced by a vacancy site in the neighborhood of Eu^{3+} since K^+ is too large for the Ca^{2+} site. Both mechanisms proof the charge-compensating role of Na^+ during the incorporation of Eu^{3+} into calcite.

Pentavalent actinides, Np(V)

EXAFS - The four synthesized samples are examined by EXAFS measurements at the Np L3 edge (17.608keV). The measurements are performed at the INE-Beamline at ANKA in fluorescence-mode. As monochromator crystals we use Ge(422). The energy calibration is done by parallel measurement of a Zr-foil, defining the first inflection point as 17.998keV. We record seven to ten spectra for each sample from about 150eV beneath the absorption edge up to 700eV-1100eV above the edge and analyze the resulting averaged spectra using backscattering amplitude and phase shift functions calculated with Feff 8 [3] and the FEFFIT 2.54 software. Background removal is done with WinXAS 3.1 [8].

Np L3 k-weighted EXAFS for all four samples and their corresponding fit curves are displayed in Fig. 5. The model spectra fit the data very well. The relative shift in ionisation energy ($\Delta\epsilon_0$) and the amplitude reduction factor (S_0^2) are held constant at their initial first and second shell fit values (6.1, 5.6, 9.2, and 9.8 and 0.92, 0.87, 0.89, and 0.87 for the samples 1, 2, 3, and 4, respectively) and then repeating the fit.

All samples show within the uncertainties the same result, i.e. the same nearest neighbour ordering of atoms surrounding Np. The degeneracy of the scattering paths corresponding to the carbonate ions in the first coordination sphere around the central neptunyl-ion (i.e. coordination number for O-carb1, C-carb, and O-carb2) is about four. Therefore we conclude that the neptunyl-ions occupy calcium sites in the calcite lattice with the oxygens of the linear neptunyl molecule substituting two carbonate-ions in the first coordination sphere. Consequently the neptunyl is coordinated by four carbonates only. The interatomic distances indicate structural relaxation of the remaining four carbonate groups from their ideal sites ($r(O-carb1) = 2.39\text{\AA}$ to 2.41\AA instead of 2.35\AA [5], $r(C-Carb) = 3.26\text{\AA}$ - 3.41\AA instead of 3.20\AA [5], and $r(O-carb2) = 3.52\text{\AA}$ instead of 3.44\AA [5]). This relaxation causing structural strain indicates a positive enthalpy of mixing. Therefore a complete solid solution series of mixing at room temperature cannot be expected. The small Debye-Waller Factors (σ^2) are evidence for the high order in this structure. A picture of the suggested near-ordered structure for neptunyl incorporated into the calcite host at a calcium site is shown in Fig. 6. A similar structural model was reported for U(VI) incorporated into natural calcite [6].

This structure leaves a charge excess of +3 in the calcite lattice (loss of two carbonate molecules and replacement of divalent calcium with single charged neptunyl cation). There is not yet evidence how this charge is balanced. Possible charge balancing mechanisms would be substitution of Ca^{2+} by Na^+ or vacant Ca^{2+} sites. The critical scattering path to obtain information about coupled substitution mechanisms would be the calcium shell surrounding the incorporated neptunyl. Fits to this shell are only possible for the spectrum of sample 4. The best fit result is however achieved with a model using six Ca^{2+} ions near 4Å. This distance is to within the uncertainty of the EXAFS analysis equal to the calcium-calcium distance in the calcite lattice (4.03\AA [7]). The next distant calcium coordination sphere (4.97\AA [9]) where the charge could also be balanced is too far away to be measured in the room temperature EXAFS data.

The charge excess of the observed structure gives us one possible reason for the apparent higher affinity of Np(V) for calcite compared to U(VI). Incorporation of the pentavalent neptunium leads to a charge excess of only +3, while for the hexavalent uranium as doubly charged uranyl cation this charge excess is +4.

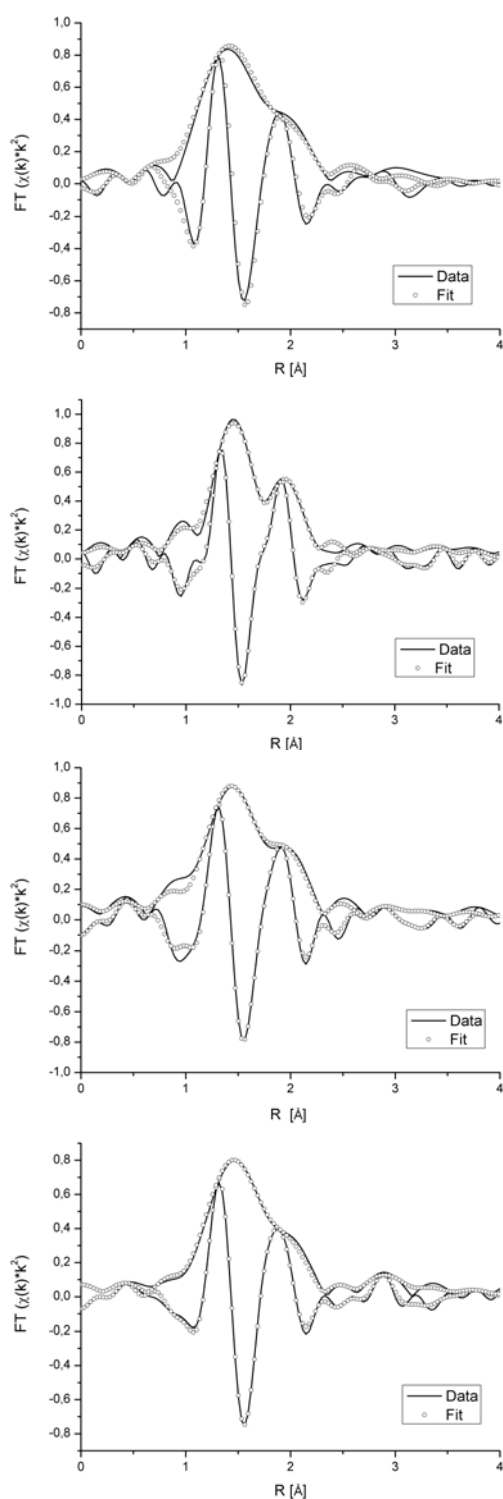


Fig. 5 EXAFS spectra of the samples 1 to 4 and the corresponding fits in K-space. (Spectra and fits are shifted along the y-axis for clarity.)

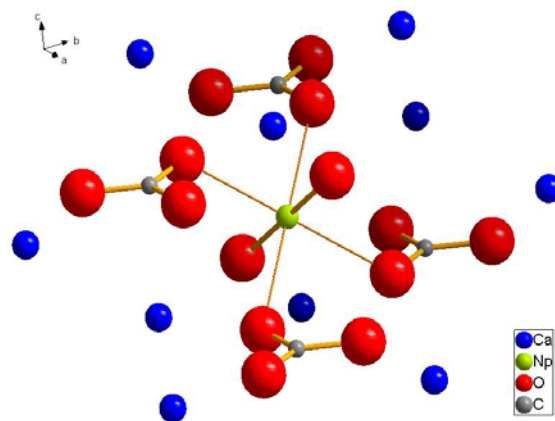


Fig. 6 Structural model of neptunyl incorporated into the calcite host.

Conclusions

Combining well defined coprecipitation experiments with spectroscopic techniques have provided a complex picture of structural incorporation / uptake of trivalent and pentavalent actinides in calcite. Macroscopic sorption reactions of trivalent f-elements with calcite involve several molecular level reactions. The actual structural incorporation is related to complex substitution schemes of M^{3+} for Ca^{2+} . Coprecipitation of Np(V) with calcite seems to result in structural substitution for Ca^{2+} despite, the size and charge of the neptunium dioxo cation.

References

- [1] T. Stumpf, Th. Fanghänel (2002), *J. Coll. Int. Sci.* 249, 119.
- [2] T. Kimura, G. R. Choppin (1994), *J. Alloys Comp.* 213/214, 313.
- [3] W. T. Carnall, H. M. Crosswhite (1995), Report ANL, 84.
- [4] J. V. Beitz, D. L. Bowers, M. M. Doxtader, V. A. Maroni, D. T. Reed (1988), *Radiochim. Acta* 44-45, 87.
- [5] C. Görller-Walrand, K. Binnemans (1996) *Handbook on the Physics and Chemistry of Rare Earths*, 121–244, North Holland Publishing, Amsterdam, , Editors: K. A. Gschneider, L. Eyring.
- [6] S.D. Kelly, M.G. Newville, L. Cheng, K.M. Kemner, S.R. Sutton, P. Fenter, N.C. Sturchio and C. Spötl (2003), *Environmental Science and Technology* 37, 1284-1287.
- [7] J.J. Rehr, J. Mustre de Leon, S.I. Zabinsky and R.C. Albers (1991), *Journal of the American Chemical Society* 113, 5135
- [8] T. Ressler (1997), *Journal of Physics*, IV 7 (C2), 267-270.
- [9] (7) R. Warchtow (1989), *Zeitschrift für Kristallographie* 186, 300-302.

4.3 Colloid formation and stability

D. Breban^{1,2}, H. Seher¹, A. Filby¹, J. Rothe¹, K. Dardenne¹, M. A. Denecke¹, M.A. Kim², J.I. Kim¹, P.J. Panak¹, M. Bouby¹, H. Geckeis¹, Th. Schäfer¹

¹Forschungszentrum Karlsruhe, Institut für Nukleare Entsorgung, Germany

²Technische Universität München, Institut für Radiochemie, Garching, Germany

Introduction

Aquatic colloids are known to be ubiquitous in natural ground water and have been frequently discussed as potential carriers for radionuclides [1, 2]. Colloidal matter may be generated by (co)precipitation phenomena or by erosion from sediments or rock. The focus of the reported work is on actinide-colloid interaction mechanisms notably under conditions where aquatic colloids are generated due to oversaturation. The stability of clay colloids which may be potentially released from bentonite barriers into groundwater of different composition is studied in the second part of this section. Finally experiments on colloid interaction with mineral surfaces are reported. Such processes have to be understood in order to quantify colloid retention processes in a given aquifer.

Interactions of actinides with hydroxy-aluminosilicate colloids (HAS) in “*statu nascendi*”

Hydroxyaluminosilicate colloids (HAS) are omnipresent in all natural systems and are assumed to be precursors of natural aluminosilicates. HAS colloids form by coprecipitation of silicic acid and/or oligomeric ($\text{Si}_x\text{O}_z(\text{OH}_{4x+y-2z})^y$) species with dissolved aluminum ions and/or aluminum hydroxo species. The average size is generally smaller than 50 nm and their number density ranges from 10^8 to 10^{14} particles per liter of water [3]. Actinide (An) ions of higher charge ($z \geq 3+$) can interact with HAS colloids, generating colloid-borne actinide species. Our research focuses on the interaction of An(III, IV, V, VI) with aluminosilicate colloids during the process of colloid formation. For studying their interaction with actinides of different oxidation states, coprecipitation is performed in the presence of trace amount of Cm(III), Am(III), Eu(III), Th(IV), Np(V), and U(VI). The colloid-borne actinide species are characterized by spectroscopic methods, i.e. time-resolved laser fluorescence spectroscopy (TRLFS) [4-6] and extended X-ray fine structure (EXAFS) spectroscopy [7-9].

Results and discussion

To quantify the formation of stable actinide-HAS colloids, radiometric screening experiments are performed as a function of pH, Si- and Al concentration. Three fractions are separated by filtration/ultrafiltration after the coprecipitation process (solution, colloidal fraction, and precipitate), and the actinide concentration in each fraction is determined by LSC. Fig. 1 shows the activity in the colloidal fraction at various pH and Al-concentrations by using polysilicic acid ($[\text{Si}] = 10^{-2}$ M [3]) for copolymerization. As shown in the contour diagram, tri-, tetra-, and hexavalent actinides form stable colloidal actinide-HAS-species after 35 d conditioning time. Np(V) does not interact with HAS colloids under these conditions (data not shown). Np(V) is observed to associate with the colloidal phase only at pH values > 12.

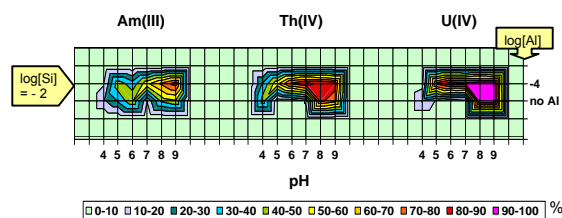


Fig. 1 Activity in colloidal fraction of Am(III), Th(IV), and U(VI) ($[\text{Si}] = 10^{-2}$ M).

For speciation of colloid-borne actinide(III), the nucleation process is investigated by TRLFS using Cm(III) as a trivalent actinide with excellent spectroscopic properties [4-6]. TRLFS results show that three different colloid-borne species are formed, with two types of actinide-colloid interaction: surface bound species and an incorporated species. Two surface-bound Cm(III) species are identified, Cm-HAS(I) and Cm-HAS(II). The third colloidal Cm(III) species formed, (Cm-HAS(III)), is found to have Cm(III) embedded into the colloid molecular structure [6].

Speciation studies of colloidal An(III,IV,V,VI)-HAS species are performed by EXAFS spectroscopy, using Eu(III) as a non-radioactive homologue for trivalent actinides, Th(IV), Np(V), and U(VI). The experimental conditions for the EXAFS investigations are

selected where maximum interaction of actinides with the aluminosilicate colloids is observed in Fig. 1. The EXAFS sample of colloidal Np(V) is prepared at pH 12. Fig. 2 shows the Fourier transforms of the k^n -weighted L_3 -edge EXAFS spectra of the HAS solutions investigated.

The FT of the Eu- L_3 EXAFS exhibits two significant peaks corresponding to backscattering from oxygen and silicon / aluminum atoms in the first and second Eu coordination sphere. Fits to the data show that Eu (Fig. 2a) is surrounded by 8 O atoms at a distance of 2.40 Å and 5 Si/Al atoms at a distance of 3.70 Å [7]. Differentiation between Si and Al in the second coordination shell of the Eu-HAS sample is not possible, as they are Z+1 elements. Calculation of the Eu-O-Si/Al bond angle using tabulated Si/Al-O distances [9] yields a bond angle of approximately 130° indicating that each $\text{SiO}_4(\text{AlO}_6)$ polyhedron links to Eu by one O atom (corner sharing link). An edge-sharing link to SiO_4 tetrahedron or AlO_6 octahedron via two O-atoms would lead to significantly shorter Eu-Si/Al distances (approximately 3.1 and 3.3 Å, respectively), and can be excluded [9]. Comparison with literature data shows that the Eu-Si/Al coordination number in the HAS system is significantly larger than for Eu-species sorbed onto silica or aluminosilicate surfaces [9]. These results are in good agreement with our TRILFS results [6], confirming the incorporation of trivalent f-element cations into the structure of HAS colloids.

In case of Th(IV) we obtain approximately 6 O atoms at an average distance of 2.41 Å from the EXAFS fits. The large asymmetry of the O coordination shell, reflected by a σ^2 value of 0.013 Å², indicates large variation in the Th-O bond lengths. The second coordination shell is comprised of 3-4 Si or Al atoms located at an average distance of 3.79 Å. The Si/Al-O-Th bond angles are in the range of 130-140° indicating also a corner-sharing link of Th. Similar to the results for Eu(III) we can exclude an edge-sharing link to SiO_4 tetrahedrons or AlO_6 octahedrons because this would lead to significantly shorter Th-Si/Al distances of 3.1 and 3.4 Å, respectively. The Si/Al coordination number (3-4 atoms) is larger for our coprecipitated aluminosilicates than for surface-sorbed Th(IV) species described in [9]. No contribution of any Th-Th distance is detected indicating that no polynuclear Th-complexes and/or surface precipitates are formed. This fact combined with observation of a Si/Al coordination still proves the incorporation of Th(IV) into the aluminosilicate bulk. We conclude that the copolymerization reaction between Th and the aluminosilicate

units is favoured over the self-condensation reaction of hydrolyzed Th complexes otherwise expected under these conditions.

The FT spectra of U(VI) exhibit two significant peaks. The first peak has a significant shoulder and results from backscattering from O_{axial} (2 O-atoms at 1.73 Å) and $\text{O}_{\text{equatorial}}$ (~ 5 O-atoms at 2.40 Å). The second peak corresponds to Si/Al-atoms at longer distance. The best fit to the data is obtained using a model of a coordination shell split into two distances Si/Al(1) and Si/Al(2) yielding interatomic distances of 3.2 and 3.4 Å. The splitting of the Si/Al shell indicates that the U(VI) exists in different coordination environments. The short 3.20 Å U-Si/Al distance is associated with Si/Al-O-U bond angles of 100° and 110°, suggesting an edge-sharing link of U(VI) to AlO_6 octahedrons. The longer U/Si(Al) distance with a bond angle in the range 110-120° indicates a corner sharing link with Si/Al polyhedrons. The coordination number of 3-4 Si and/or Al atoms again suggests incorporation of the uranyl into the aluminosilicate structure. In comparison, no more than one Si/Al atom has been found for uranyl surface complexes with aluminosilicate minerals [9].

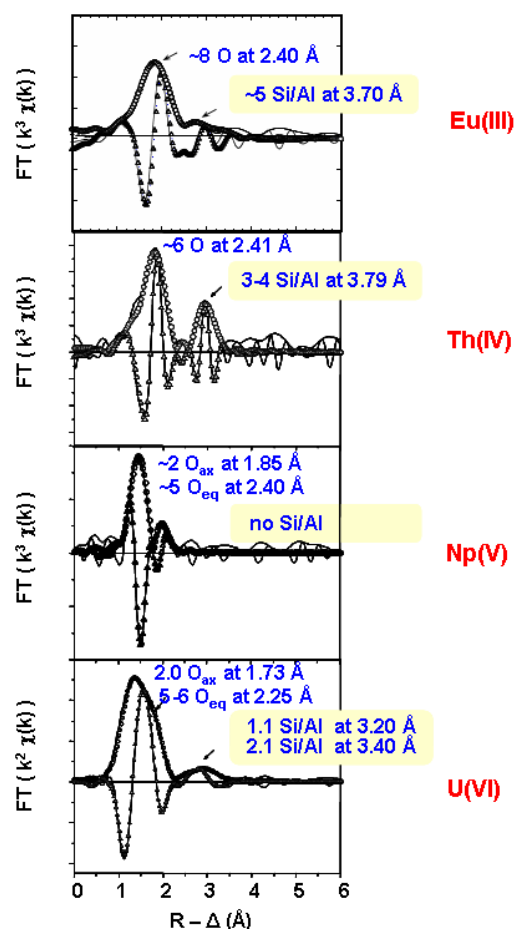


Fig. 2 Fourier transforms of the k^n -weighted An L_3 -edge EXAFS spectra of actinides in HAS solutions

We do not detect a Si/Al coordination shell for Np(V) (Fig. 2c), which would suggest inner sphere complexation with the HAS colloids. Nevertheless, these results do not necessarily exclude the presence of an electrostatic and/or inner-sphere interaction between Np(V) and the aluminosilicates. Several monodentate surface species do not exhibit a Si/Al peak in the EXAFS spectrum [9].

Conclusions

With the exception of Np(V), actinides of different oxidation states are shown to be structurally incorporated into aluminosilicate colloids forming in solution. The formation of colloidal actinide species, and in particular incorporation of actinides into the structure of aquatic colloids, may have an important impact on actinide transport in natural systems.

Structural information obtained by EXAFS gives new insight into the formation and stability of An-HAS colloids under natural conditions, which can be used for reliable assessment of the transport behaviour of colloid-borne actinide species in the near and/or far field of a given nuclear waste repository.

Clay colloid stability in groundwater

Concepts for high-level nuclear waste disposal in crystalline rock foresee bentonite as appropriate barrier material both to inhibit ground water access to the waste canister and to retard radionuclide transport away from the repository near field. Smectite colloids have been observed to detach from the bentonite barrier by erosion phenomena when contacted with ground water [10]. The relevance of colloids for radionuclide migration is strongly controlled by their agglomeration, sedimentation, surface attachment and filtration behavior in a given aquifer system. Only under conditions where colloids are sufficiently stable, they may be able to transport sorbed radionuclides [11-13].

The present work describes first experimental results on bentonite colloid stability over a wide pH and ionic strength range, relevant to natural ground water conditions. Colloids have been prepared from a natural bentonite (FEBEX bentonite, Spain). NaCl, CaCl₂ and MgCl₂ are taken as electrolytes in order to compare the influence of 1:1 and 2:1 electrolytes on bentonite colloid stability.

Results and discussion

The PCS determined mean bentonite colloid size used throughout the stability investigations was 185 nm with a half width of 90 nm recalculated from the polydispersivity index of 0.24. The rather broad size distribution determined by PCS is in accordance with literature data [14]. The calculation of the stability ratio *W* from the coagulation rate is described in [15]. The stability ratio is calculated based on the following equation:

$$W = \frac{\left[\left(\frac{d r_h / dt}{C} \right)_{t \rightarrow 0} \right]^f}{\left[\left(\frac{d r_h / dt}{C} \right)_{t \rightarrow 0} \right]}$$

whereas *W* is the stability ratio, *r_h* is the hydrodynamic radius, *C* the colloid concentration and the superscript (*f*) refers to measurements in the regime of fast (diffusion limited) coagulation. Coagulation experiments are performed under different conditions: pH 6-10; ionic strength 0.001M-0.5M; electrolyte types NaCl, MgCl₂, CaCl₂; colloid concentration of 3.7 mg/L.

Fig. 3a shows the stability ratio (*W*) for different ionic strengths in the MgCl₂ system as a function of pH. Initially, *W* increases with increasing pH value starting from pH 6 until a maximum value of *W* = 3.5 · 10² at pH 7.2 for an ionic strength of 0.001M is reached. At pH > 8 the stability ratio decreases again. Increasing the ionic strength from 1mM to 0.5M decreases the stability ratio to values around one showing diffusion controlled aggregation for the pH range investigated. Comparable results were obtained for the CaCl₂ system (Fig. 3b). The highest stability ratio of 1.7 · 10³ is found at pH 7.9 for an ionic strength of 0.001M and appears to be slightly higher than that found in the MgCl₂ system under similar conditions. The variations of *W* as a function of pH and ionic strength are comparable in the two bivalent systems investigated, namely CaCl₂ and MgCl₂. The highest stability ratios have been measured in the NaCl system (Fig. 3c). At all ionic strengths an increase of *W* with increasing pH is observed and no decrease under alkaline conditions could be detected. Stability ratios larger than 5 · 10² are detected for solution with ionic strengths < 0.003 M in the full pH range investigated. Under alkaline conditions (pH > 9) bentonite colloids are even stable within the observation period in 0.01 M solutions.

The low stability ratio at pH values ≤ 6 in all systems investigated can be explained by edge-face interactions of the colloids leading to card house type structures.

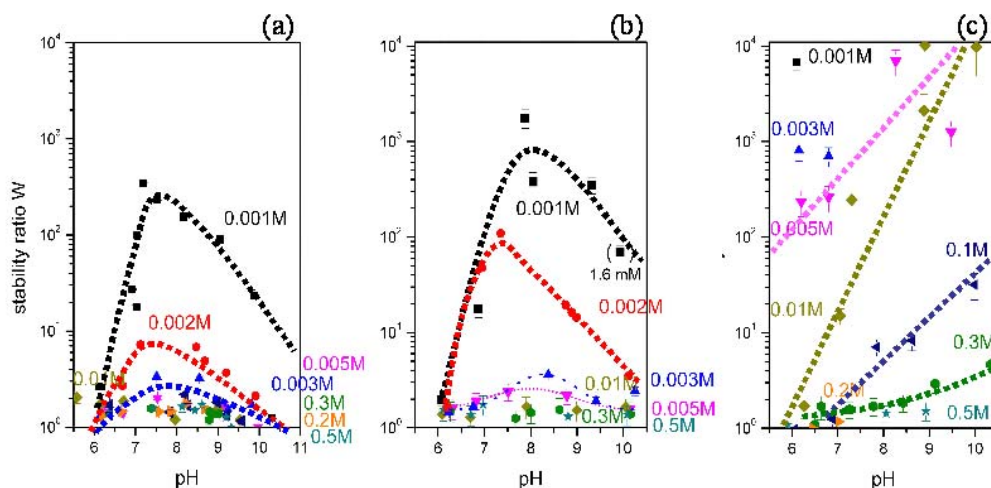


Fig. 3 Measured stability ratios W as a function of ionic strength and pH for $MgCl_2$ (a), $CaCl_2$ (b) and $NaCl$ (c) solutions; electrolyte concentrations are given in terms of ionic strength.

Taking into account the pH dependent edge charge with a point of zero charge (pH_{PZC}) around pH 6-7 neutral or positive charged clay edges due to protonation of Al-OH edge groups are expected [16]. Below the pH_{PZC} clay colloid edges are positively charged and thus interaction with permanently negative charged basal planes induced by isomorphous substitutions in the bentonite structure can be expected. At pH values above the pH_{PZC} both the edge and basal planes are negatively charged and therefore bentonite colloids are electrostatically stabilized due to repulsive forces. Higher ionic strengths decrease the electrical double layer thickness and coagulation is again initiated [16].

The observed decrease of the stability ratio in the $MgCl_2$ and $CaCl_2$ systems at $pH > 8$ cannot be explained taking simple electrostatic interactions into account. The observed destabilization might be attributed to the precipitation of $MgCO_3$ and $CaCO_3$, thus scavenging the bentonite colloids. $MgCO_3$ and $CaCO_3$ precipitation due to oversaturation of electrolyte solutions under atmospheric pCO_2 cannot be ruled out and are focus of further investigations.

For stability ratios $> 5 \cdot 10^2$ or in other words coagulation rates $< 10 \text{ nm/hour}$ we operationally defined colloids as stable. Looking at the actual ionic strengths found in Äspö ground water it can be clearly shown that bentonite colloids derived from backfill material are not expected to be stable and therefore mobile. Under Grimsel ground water conditions showing much lower ionic strength colloids appear to be stable according to our stability criterion. Our operationally defined stability criterion does however not represent a straightforward limit. Colloid agglomeration might still be relevant on longer time scales.

Conclusions

Bentonite colloid stability increases as expected with increasing pH due to increasing charge repulsion by deprotonated surficial OH groups. Increase in ionic strength screens the surface charge and thus causes a clear stability decrease. Measurable coagulation is found for all electrolyte concentrations starting from $3.3 \cdot 10^{-4} \text{ M}$ for $MgCl_2$ and $CaCl_2$ (corresponding to an ionic strength of $1 \cdot 10^{-3} \text{ M}$). For $NaCl$ solutions W exceeds a value of 10^3 indicating high colloid stability at ionic strength < 0.01 and $pH > 8$. The faster colloid agglomeration rates observed in $MgCl_2$ and $CaCl_2$ solutions as compared to $NaCl$ solutions of identical ionic strength follows the known Schulze-Hardy rule [17]. Edge-face interaction delimits colloid stability at low pH. Depending on the composition of a given natural ground water it is thus possible to predict bentonite colloid behavior. Further studies will focus on the influence of low DOC (i.e. fulvic acid) concentration in the range of 1-10 mg/L as usually found in fractured rock systems and their effect on bentonite stability.

Interaction of colloids with mineral surfaces

Beside agglomeration and sedimentation, colloids can also be retarded or retained by interaction with mineral surfaces. The interaction of colloids as nanoscopic radionuclide carriers with natural mineral surfaces is complex and only insufficiently understood. A complete understanding of the processes involved is complicated, for example, by the chemical heterogeneity and roughness of the surfaces, discrete surface charges and by surface contamination.

The present work describes first experimental results on sorption experiments with carboxylated polystyrene colloids and natural rock surfaces. In these experiments, the pH is varied over a wide range while the ionic strength of the colloidal suspension is maintained constant. Sorption of the colloids on the mineral surfaces is made visible by means of fluorescence microscopy and the observed fluorescence is assigned to specific mineral phases. Using different analytical techniques, such as Scanning Electron Microscopy (SEM), energy-dispersive X-Ray spectroscopy (EDX) and Raman-Microscopy those mineral phases are to be identified on which a predominant colloid sorption takes place.

Results and Discussion

For the sorption experiments carboxylated polystyrene colloids (Postnova Analytics; Landsberg/Lech, Germany) with a diameter of 25 nm are used. The colloids have a polydispersity index of < 0.1 and a density of COOH groups of 120 nmol/mg. The natural rock samples (Grimsel granodiorite) used are from a water-bearing fracture in the underground Grimsel rock laboratory. For the experiments these rock samples were cut into small cubes and contacted with the colloid suspension. In the initial experiments fluorescein-doped colloids with an excitation wavelength of 475 nm and an emission wavelength of 510 nm were used. After contacting the rock samples for 15 minutes with the colloid suspension, the rock samples are rinsed with MQ-water and dried in an oven. After this procedure, fluorescence can be observed by means of fluorescence microscopy. pH was varied from 2 – 9.5 and the ionic strength was kept constant at 0.01 M with NaCl. The colloid concentration was set to 0.05 g/l. For ease of handling, the initial experiments were carried out with polished rock surfaces. Experiments with natural surfaces were also carried out; these surfaces were only treated with isopropanol and MQ-water to remove organic impurities which also may contribute to the fluorescence signal.

Fig. 4a shows an example of an interesting region on the granodiorite surface viewed with the light microscope. Clearly distinguishable is the Apatite grain in the centre of the image. The same region is shown in Fig. 4b viewed with the fluorescence microscope. It is noticeable that the fluorescein-doped colloids are sorbed solely on the Apatite grain. Increased fluorescence, indicated by increased brightness is found on the Apatite surface and especially on the Apatite edges, whereas the

surrounding area is free of adsorption, indicated by the darkness of the image.

Only weak fluorescence intensities were observed at natural surfaces under neutral and alkaline pH conditions (6 – 9.5; $I = 0.01$ M NaCl). Colloids are mainly found at mineral edges. At $pH < 4$ colloids adsorb preferentially to apatite, titanite, illite and feldspars. Sorption always takes place on the natural (unpolished) surfaces. High pH should prevent the sorption of colloids, since at high pH there are repulsive conditions for the relevant minerals (Quartz, Feldspars, Mica, Biotite, Illite, Apatite). Especially in regions with high surface roughness, considerable sorption is observed regardless of pH. Since on polished surfaces there are only very few mineral edges available, there is far less adsorption observed.

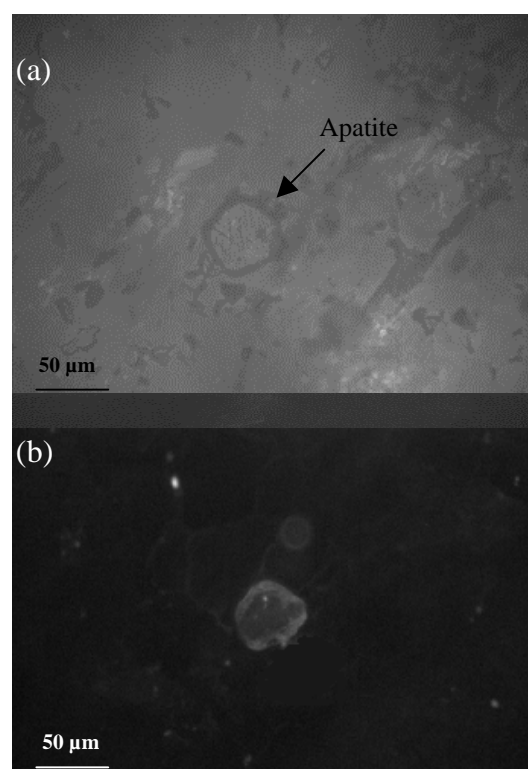


Fig. 4 Granodiorite surface viewed with the light optical microscope (a). In (b) the same region is viewed with the fluorescence microscope. Sorption of fluorescing colloids on the Apatite mineral can be clearly seen; (colloid concentration = 0.05 g/l; $pH = 2$; $I = 0.01$ M NaCl).

Further experiments have been carried out with some of the individual minerals occurring in the Grimsel granodiorite, such as Quartz, Chlorite, Biotite and Mica. Until now, their sorption behaviour has been observed at $pH = 4$ and an ionic strength of 0.01 M NaCl. Colloids do not sorb onto quartz, while

adsorption to edges of biotite, chlorite and mica could be identified. Since the point of zero charge of quartz is around 2 [18] the findings of this experiment are explained by the dominating repulsive conditions. For the phyllosilicates (Biotite, Chlorite, Mica) the edges are assumed to be positively charged (attracting conditions), whereas the basal planes are negatively charged.

Conclusions

Adsorption of carboxylated polystyrene colloids increases with decreasing pH, both on natural (rough) and polished surfaces. On the polished surfaces, no adsorption is observed at higher pH-values (> 6), whereas on the natural surface adsorption is observed over the whole pH range, although at higher pH-values repulsive conditions are expected.

Future sorption experiments will be carried out with variations in ionic strength and background electrolyte (e.g. CaCl₂). The influence of 10⁻⁶ M Eu³⁺ will also be investigated.

Recently, initial experiments using atomic force microscopy (AFM) were carried out in order to obtain force-distance curves between mica and a Si₃N₄ cantilever tip. It is planned to obtain such curves with several relevant mineral phases identified in the sorption experiments in order to distinguish the forces responsible for the differing modes of interaction of colloids with the various mineral phases. In these experiments the so-called colloid-probe technique will be applied in which the forces between spherical colloids (attached on AFM cantilevers) and mineral surfaces will be recorded.

References

[1] Kim, J.I., (1991) Actinide colloid generation in groundwater. *Radiochimica Acta*, 52/53 71-81.
 [2] Ryan, J.N., Elimelech, M., (1996) Colloid mobilization and transport in groundwater. *Coll. Surfaces*, 107, 1-65.
 [3] Kim, M. A., Panak, P.J., Yun, J.I., Kim, J.I., Klenze, R., Koehler, K., *Colloids and Surfaces A* 216, 97-108 (2003).
 [4] Panak, P. J., Kim, M. A., Yun, J. I., Kim, J. I., *Colloids and Surfaces A* 227, 93-103 (2003).

[5] Kim, M. A., Panak, P. J., Yun, J. I., Kim, J. I., Priemyshev, A., Köhler, K., *Einfluss von Kolloiden auf die Migration von Actiniden*, RCM-Bericht 012004, Institut für Radiochemie, Technische Universität München, Garching, 2004.
 [6] Kim, M. A., Panak, P. J., Yun, J. I., Priemyshev, A., Kim, J. I., *Colloids and Surfaces A* 254, 137-145 (2005).
 [7] Panak, P. J., Loiseau, P., Dardenne, K., Rothe, J., Denecke, M. A., Klenze, R., Kim, M. A., Kim, J. I., Fanghänel, Th., ANKA/FZK Annual Report 2003, 51-52 (2003).
 [8] Panak, P. J., Breban, D., Dardenne, K., Rothe, J., Denecke, M. A., Kim, M. A., Kim, J. I., Fanghänel, Th., ANKA/FZK Annual Report 2005, 92-93, (2005).
 [9] Breban, D., *Provenance and Characterization of Aquatic Actinide Colloids: Interaction of Aminosilicate and Humate Colloids with Actinides*, Ruprecht-Karls-Universität Heidelberg, 2007.
 [10] Missana T., Alonso T., Turrero M. J. S. (2003), *J. Contam. Hydrol.* 61(1-4), 17-31.
 [11] Geckeis H., Schäfer T., Hauser W., Rabung T., Missana T., Degueldre C., Möri A., Eikenberg J., Fierz T., Alexander W. R. (2004) *Radiochim. Acta* 92 (9-11), 765-774.
 [12] Möri A., Alexander W. R., Geckeis H., Hauser W., Schäfer T., Eikenberg J., Fierz T., Degueldre C., and Missana T. (2003), *Coll. & Surfaces A*, 217(1-3), 33-47.
 [13] Schäfer T., Geckeis H., Bouby M., Fanghänel T. (2004), *Radiochim. Acta* 92, 731-737.
 [14] Plaschke M., Schäfer T., Bundschuh T., Manh T. N., Knopp R., Geckeis H., and Kim J. I. (2001), *Anal. Chem.* 73(17), 4338-4347.
 [15] Kretzschmar R., Holthoff H., Sticher H. (1998), *J. Colloid and Interface Science* 202, 95-103.
 [16] Schäfer T., Geckeis H., Bouby M., Mihai S., Delos A., Alonso U., and Missana T. (2006) Bentonite colloid stability in natural and simulated granite groundwater. In *1st annual workshop proceedings of integrated project fundamental processes of radionuclide migration IP FUNMIG, Vol. CEA-R-6122* (ed. P. Reiller, G. Buckau, B. Kienzler, L. Duro, and M. Martell), pp. 248. CEA
 [17] Bastos D., de las Neves F.J. (1994), *Colloid & Polymer Science* 272, 592-597.
 [18] Stumm, W., (1992) *Chemistry of the Solid-Water Interface*, John Wiley and Sons, New York, 19-20.

5. Applied Studies: Radionuclide retention in the multibarrier system

Investigations reported in this section aim to the understanding of processes determining mobilization and retention of radionuclides within the individual components of the multi-barrier system. A major impact on behaviour of the nuclear waste form is given by radiolytic effects. The complex redox reactions in a given system can only be assessed if all on-going reactions are quantified. The influence of H_2 generated by container corrosion as an inhibitor of spent fuel corrosion is studied in presence of trace concentrations of Br^- being present as groundwater component. The description of near field processes is also aim of the last part: The in-house developed code TRANSAL which couples chemistry to transport is presented and first applications to the radionuclide redox reactions in the presence of a corroding container are discussed. First results on Pu diffusion in natural clay rock are reported in the section dealing with radionuclide reactions in the far-field. Another issue in far-field studies is the impact of clay colloids on radionuclide speciation in a natural granite groundwater (Äspö, Sweden) of relatively high salinity. These studies have been initiated within a collaborative project with SKB and KTH, Sweden. Natural organic matter is beside inorganic colloids known to influence radionuclide geochemistry due to its redox properties, formation of stable complexates and its tendency towards colloid formation. Latest findings on that issue are discussed.

5.1 Determination of key processes influencing the near field source term for spent nuclear fuel: Radiation induced $UO_2(s)$ corrosion in presence of H_2 and Br^-

E. Bohnert, B. Kienzler, A. Loida, V. Metz and N. Müller

Introduction

For disposal of spent nuclear fuel, SNF, in a deep geological repository the geo-technical barrier system prevents to some extent groundwater contacting the waste product. Since intrusion of solutions into disposal caverns has to be considered on a long term, chemical reactions between the waste forms and intruding solutions must be taken into account within the safety case of a SNF repository. The fate of spent nuclear fuel and the associated release of radionuclides depends both on SNF corrosion kinetics and on thermodynamic constraints. The corrosion rate of SNF is influenced by a variety of factors such as the radiation field, dose rate, groundwater composition and the apparent redox potential. Our studies focus on the effect of the geochemical environment on the radiation induced corrosion of the $UO_2(s)$ matrix of SNF as well as on the consecutive radionuclide release and retention processes.

Basic description of the protective “hydrogen effect”

Radiolysis of aqueous solutions is accompanied by formation of oxidants (O_2 , H_2O_2 , OH and HO_2) and reductants (H_2 , H and e^-_{aq}). As long as concentrations of inhibitors such as H_2 are sufficiently low, aqueous solution in contact with spent nuclear fuel could radiolytically produce oxidants to convert the relatively stable $UO_2(s)$ matrix of SNF into much more soluble U(VI) and thus promotes radionuclide release.

In the near field of spent nuclear fuel, an oxygen free environment will be achieved within few years after closure of the repository. Corrosion of Fe-based waste containers will result in strongly reducing conditions (relative high Fe^{2+}/Fe^{3+} ratios) and high hydrogen concentrations. Hydrogen remains dissolved as long as the pressure built-up in the disposal site does not exceed the minimal principal stress. For instance at a depth of about 500 m, in granite a gas pressure of $P_{H_2} = 5$ MPa corresponding to $[H_2] = 4 \cdot 10^{-2}$ mol (kg H_2O)⁻¹ and in rock salt a gas pressure of $P_{H_2} = 12$ MPa corresponding to $[H_2] = 1 \cdot 10^{-1}$ mol (kg H_2O)⁻¹ may be reached. Radiolysis experiments and SNF leaching tests indicated that hydrogen both considerably inhibits corrosion of the $UO_2(s)$ matrix and radionuclide release and suppresses radiolytic decomposition of the used synthetic groundwater samples [1-6].

Radiation induced $UO_2(s)$ corrosion in presence of hydrogen and bromide

Though bromide is a minor constituent in groundwater of deep geological formations, it is present in a concentration range relevant for radiolytic processes, i.e. up to 10^{-3} mol (kg H_2O)⁻¹ in granitic groundwater samples [7-8], up to 10^{-4} mol (kg H_2O)⁻¹ in argillaceous porewater samples [9] and up to 10^{-1} mol (kg H_2O)⁻¹ in Zechstein salt brine samples [10-12]. It is known from radiolysis of water that even low concentrations of bromide compete with hydrogen for oxidative radiolytic products and consequently reduces the inhibition effect of

hydrogen on radiolytic decomposition [13-14]. Results of γ -radiolysis experiments in NaCl brine demonstrate that Br^- concentrations of 10^{-4} to 10^{-3} mol (kg H_2O) $^{-1}$ considerably promote radiolytic decomposition, even at $[\text{H}_2] = 10^{-2}$ mol (kg H_2O) $^{-1}$ [5, 14].



Fig. 1 Corrosion experiment using high pressure autoclave with spent nuclear fuel pellets in NaCl brine containing hydrogen and bromide.

We studied $\text{UO}_2(\text{s})$ corrosion in NaCl brine comprising H_2 and Br^- . Two types of experiments were conducted:

- 1 α -, β -, γ -radiation induced $\text{UO}_2(\text{s})$ corrosion: SNF pellets (50 MWd / kgU burnup) with cladding were immersed in 5.3 mol (kg H_2O) $^{-1}$ NaCl solution, containing 10^{-4} to 10^{-3} mol (kg H_2O) $^{-1}$ Br^- under external H_2 overpressure of 3.2 bar (Fig. 1). Details of the SNF corrosion experiments are given in [15]
- 2 γ -radiation induced $\text{UO}_2(\text{s})$ corrosion: Pellets of depleted $\text{UO}_2(\text{s})$ ($4 \cdot 10^3$ Bq / pellet) were γ -irradiated in 6 mol (kg H_2O) $^{-1}$ NaCl solution at the GB77 ^{60}Co -source (IOM, Leipzig). Both experiments contained initially 10^{-2} mol (kg H_2O) $^{-1}$ H_2 . One of the experiments was conducted without bromide, the other contained 10^{-4} mol (kg H_2O) $^{-1}$ Br^- . The radiolysis experiments are described in detail in [14].

In the first type of experiments (cf. 1), the release of strontium from corroding spent nuclear fuel in the presence of bromide was found to be enhanced by two orders of magnitude in comparison to bromide-free conditions. Fig. 2 shows the variation of Sr release rates (in terms of *fraction in aqueous phase*, FIAP, per day) as function of $p(\text{H}_2)$ in bromide-free NaCl brine [16] and in NaCl brine, containing 10^{-4} to 10^{-3} mol (kg H_2O) $^{-1}$ Br^- [15]. It is obvious that bromide drastically affects the release of Sr from corroding spent nuclear fuel.

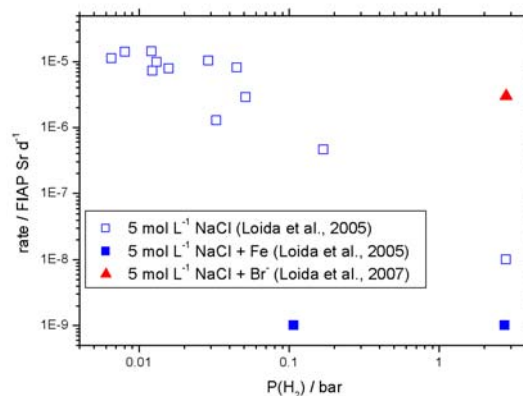


Fig. 2 Sr release rates (FIAP d^{-1}) as a function of partial hydrogen pressure observed in bromide-free SNF corrosion experiments [16] and in SNF corrosion experiments in presence of bromide [15].

Since most of the Sr inventory is distributed homogeneously in the $\text{UO}_2(\text{s})$ matrix of SNF and Sr is scarcely involved in retention processes, the time dependent release of Sr is used as a proxy for the SNF matrix dissolution rate [17, 18]. Thus, the effect of bromide on Sr release reflects a significant influence of dissolved bromide on the corrosion of spent nuclear fuel. The release of cesium from highly reactive surface sites of SNF is considerably enhanced in the presence of bromide, too. However, preliminary results of U and Pu concentrations in solutions indicate that bromide does not enhance the release of both actinides (Fig. 3). Within the observation interval of 212 days, U concentrations in solution were found to be ranging within the same levels, or show a certain decrease when bromide was added. Pu concentrations were found to be decreased at a factor of ≥ 10 in comparison to SNF corrosion experiments at $P(\text{H}_2) = 3.2$ bar in the absence of bromide.

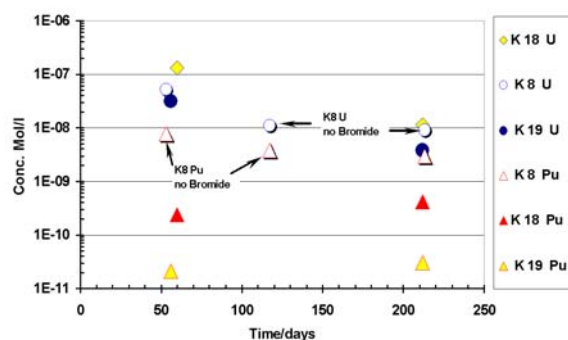


Fig. 3 Concentrations of U and Pu in SNF corrosion experiments under 3.2 bar H_2 overpressure in absence (K8) [16] and presence of 10^{-4} mol (kg H_2O) $^{-1}$ (K19) and 10^{-3} mol (kg H_2O) $^{-1}$ (K18) bromide [15].

In the second type of experiments (cf. 2), a steady state concentration of produced radiolysis gases was achieved after applying a γ -dose of > 1 MGy. In agreement with results of homogenous γ -radiolysis of $6 \text{ mol (kg H}_2\text{O)}^{-1}$ NaCl ($\text{UO}_2(\text{s})$ free experiments) [5,14] our results show that in presence of Br^- concentrations of the main radiolysis products, H_2 and O_2 , were significantly higher compared to the radiolytically hydrogen and oxygen yield in experiments without Br^- (Fig. 4). In the experiments with bromide, about the same production of radiolysis gases is observed independent of the initial H_2 concentration.

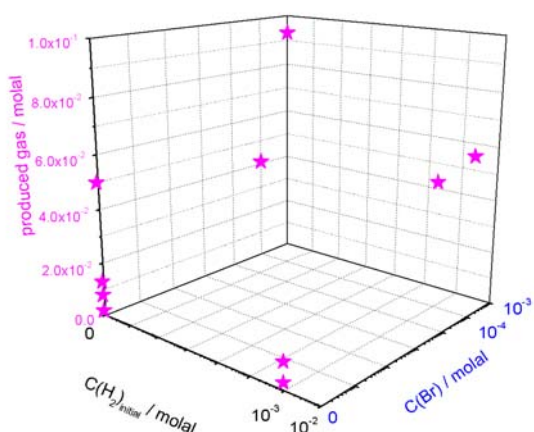


Fig. 4 Steady state concentrations of produced radiolysis gas as function of dissolved hydrogen and bromide [5,14].

A comparison of the radiolysis gas concentrations in the radiolysis experiments with $\text{UO}_2(\text{s})$ in NaCl brine and those in homogeneous ($\text{UO}_2(\text{s})$ free) NaCl brine at the same initial hydrogen and bromide concentrations shows that the presence of $\text{UO}_2(\text{s})$ does not affect the radiolysis yield.

In contrast to the observed increase of the radiolytic yield in the presence of bromide, no significant effect of bromide on uranium concentration, $[\text{U}]$, was observed. During the two experiments on γ -radiation induced $\text{UO}_2(\text{s})$ corrosion, $[\text{U}]$ in solution reached within error the same concentration level, i.e. $1 \cdot 10^{-6} \text{ mol (kg H}_2\text{O)}^{-1}$ and $4 \cdot 10^{-6} \text{ mol (kg H}_2\text{O)}^{-1}$, respectively (Fig. 5). Since U concentration was not monitored during irradiation, it is not evident if the final concentration of U represents a steady state concentration, where $d[\text{U}]/dt = 0$.

As shown in Fig. 5, uranium concentrations in the radiolysis experiments agree well with the solubility limits of the schoepite / $\text{UO}_3 \cdot 2\text{H}_2\text{O}(\text{cr})$ – Na-diuranate $\text{NaUO}_2\text{O}(\text{OH})(\text{cr})$ transition, measured in $5.6 \text{ mol (kg H}_2\text{O)}^{-1}$ NaCl solution

$(\text{kg H}_2\text{O)}^{-1}$ NaCl. U(IV) and U(VI) solubility

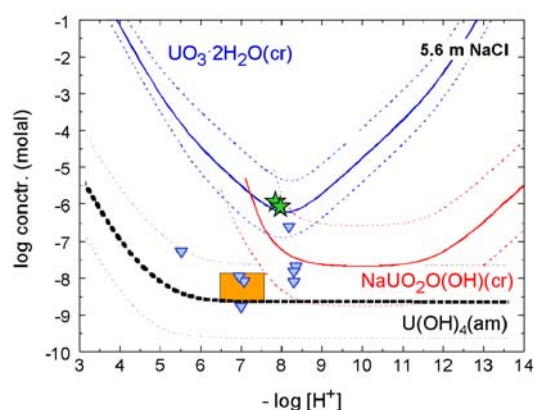


Fig. 5 Uranium concentrations in corrosion experiments under hydrogen overpressure compared to solubilities of $\text{U}(\text{OH})_4(\text{am})$, $\text{UO}_3 \cdot 2\text{H}_2\text{O}(\text{cr})$ & $\text{NaUO}_2\text{O}(\text{OH})(\text{cr})$ in 5.6 mol data taken from [19-21]: Experiments on SNF corrosion in the presence of bromide (concentration range denoted by rectangle) and experiments in absence of bromide (triangles, data taken from [3]). Experiments on γ -radiation induced $\text{UO}_2(\text{s})$ corrosion (stars).

[19-21]. These results are corroborated by results of SEM-EDS, EXAFS and XPS measurements, showing precipitates of secondary U(VI) phases on the pellets recovered from the experiments on γ -radiation induced $\text{UO}_2(\text{s})$ corrosion. The pellet recovered from the experiment without bromide is covered solely by a secondary phase having a (water free) composition close to $\text{Na}_2\text{U}_2\text{O}_7$ (Fig. 6). On the surface of the pellet from the experiment with bromide, a phase having a (water free) composition close to $\text{Na}_2\text{U}_2\text{O}_7$ and traces of a phase having a (water free) composition close to UO_3 is observed.

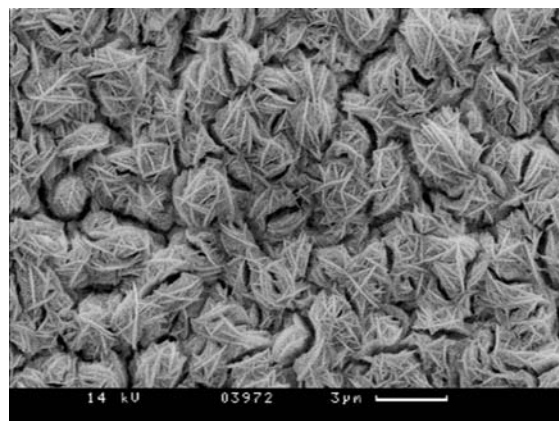


Fig. 6 SEM image of the pellet recovered from the experiment on γ -radiation induced $\text{UO}_2(\text{s})$ corrosion without bromide, showing U(VI) precipitate, having a composition close to $\text{NaUO}_2\text{O}(\text{OH})(\text{cr})$.

As in the experiments on γ -radiation induced $\text{UO}_2(\text{s})$ corrosion, measured concentrations of dissolved U in the SNF corrosion experiments are independent of the bromide in solution (Fig. 3). On the other hand, concentration of U released from spent nuclear fuel (within the observation interval of 212 days) are below concentrations in the γ -radiolysis experiments and below solubilities of the respective U(VI) phases (Fig. 5).

Discrepancies between the U release observed in the γ -radiolysis and the SNF corrosion experiments might be attributed (i) to catalyzing properties of the ϵ -phase in spent nuclear fuel, or (ii) to reduction of U(VI) species and precipitation of secondary U(IV) phases or (iii) to differences in the dose rate. Studies on corrosion of SIMFUEL and irradiated UO_2 fuel have shown that ϵ -phase exert a very significant effect on the corrosion behavior of the fuel. These metallic particles catalyze oxidation of hydrogen and reduction of oxidative radiolysis products, resulting in an inhibition of the $\text{UO}_2(\text{s})$ corrosion [22,23]. However, the enhanced release of redox insensitive radionuclides in the presence of bromide, i.e. Sr and Cs, indicates that the presence of bromide results in an alteration of the matrix. Since solution concentrations of redoxsensitive radionuclides were determined to be at the same level as in the absence of bromide (uranium) or below (plutonium) it is obvious that these radionuclides are involved in retention processes, as sorption or formation of secondary phases.

Conclusions

The results of the complementary experiments on SNF corrosion and γ -radiation induced $\text{UO}_2(\text{s})$ corrosion allow the conclusion that even trace concentrations of bromide reduces significantly the protective hydrogen effect with respect to release of certain radionuclides and yield of radiolysis products. Retention processes such as precipitation of secondary phases or sorption control the concentration of actinides in solution rather than radiation induced corrosion processes.

References

[1] K. Spahiu, L. Werme, and U.-B. Eklund, *Radiochim. Acta* 88, 507 (2000).
 [2] K. Spahiu, D. Cui, and M. Lundstöm, *Radiochim. Acta* 92, 625 (2004).
 [3] A. Loida, V. Metz, B. Kienzler, and H. Geckeis, *J. Nucl. Mat.* 346, 24 (2005).
 [4] K. Spahiu, P. Carbol, J. Cobos-Sabate, J. P. Glatz, C. Ronchi, V. V. Rondinella, D.

Wegen, T. Wiss, A. Loida, V. Metz, B. Kienzler, B. Grambow, J. Quinones, and A. Martinez-Esparza, *Svensk Kärnbränslehantering, SKB TR-05-09*, Stockholm, Sweden (2005).
 [5] M. Kelm and E. Bohnert, *J. Nucl. Mat.* 346, 1 (2005).
 [6] J. Bruno and R.C. Ewing (2006) Spent nuclear fuel. *Elements* 2, 343-349.
 [7] C. Wittwer, NTB 85-49 report, NAGRA, Wettingen, Switzerland (1986).
 [8] C. Ekberg, Uncertainties in actinide solubility calculations illustrated using the Th-OH-PO₄ system. Ph. D. thesis, Chalmers University, Göteborg, Sweden (1999).
 [9] F. J. Pearson, D. Arcos, A. Bath, J.-Y. Boisson, A. M. Fernandez, H.-E. Gäbler, E. Gaucher, E. Gautschi, L. Griffault, P. Hernan, and H. N. Waber, *Bundesamt für Wasser und Geologie, BWG*, Bern, Switzerland (2003).
 [10] A. G. Herrmann and L. E. v. Borstel, *N. Jahrb. Min. Monat.*, 1991, 263 (1991).
 [11] O. Braitsch, Entstehung und Stoffbestand der Salzlagerstätten, in W.V. Engelhardt and J. Zemann (eds.), *Mineralogie und Petrographie in Einzeldarstellungen*, vol. 3, Springer, Berlin, Germany (1962).
 [12] A. G. Herrmann and B. Knipping, *Fluide Komponenten als Teile des Stoffbestandes der Evaporite im Salzstock Gorleben*, Techn. Univ. Clausthal (1993).
 [13] A. Henglein, W. Schnabel, and J. Wendenburg, *Einführung in die Strahlenchemie*, Verlag Chemie, Weinheim, Germany (1969).
 [14] V. Metz, E. Bohnert, M. Kelm, D. Schild, J. Reinhardt, B. Kienzler, M. R. Buchmeiser, *Scientific Basis for Nuclear Waste Management XXX*, Materials Research Society (in press).
 [15] A. Loida, V. Metz, B. Kienzler, *Scientific Basis for Nuclear Waste Management XXX*, Materials Research Society (in press).
 [16] A. Loida, V. Metz, B. Kienzler, H. Geckeis, *J. Nucl. Mat.* 346, 24-31 (2005).
 [17] B. Grambow, A. Loida, P. Dressler, H. Geckeis, J. Gago, I. Casas, I., J. de Pablo, J. Gimenez, J., M.E. Torrero, *Wissenschaftliche Berichte FZKA 5702* (1996).
 [18] B. Grambow, L. Werme, R. Forsyth, J. Bruno, *Mater. Res. Soc. Proc* 176, 465-474 (1990).
 [19] T. Fanghänel and V. Neck, *Pure and Applied Chemistry* 74, 1895 (2002).
 [20] A. Altmaier, V. Neck, R. Müller, V. Metz, B. Kienzler, T. Fanghänel, 9th Intl. Conf. Chemistry Migration Actinides & Fission Products, p. 31, Gyeongju, Korea (2003).
 [21] V. Neck, M. Altmaier, R. Müller, M. Schlieker, and T. Fanghänel, 9th Intl. Conf. Chemistry Migration Actinides & Fission Products, p. 47, Gyeongju, Korea (2003).

- [22] D. W. Shoesmith, J. Nucl. Mat. 282, 1-31 (2000).
- [23] D. W. Shoesmith, Abstracts of the Int'l Spent Fuel Workshop, Uppsala, Sweden (2006).

5.2 Radionuclide retention in the Far Field

A. Bauer, N. Banik, M. Bouby, B. Fiehn H. Geckeis, A. Görtzen, W. Hauser, B. Kienzler, M. Klein, Chr. Marquardt, J. Römer, Th. Schäfer, H. Seher, D. Schild, Th. Rabung, P. Vejmelka

and partly S. Wold, M. Jonsson (KTH, Royal Institute of Technology, Stockholm, Sweden)

Introduction

Radionuclide migration in the far-field of a nuclear waste repository is controlled by advective and by diffusive processes. In aquifers or in fractured rocks, advectively controlled groundwater flow dominates causing radionuclide and colloid transport. In clay-rich host rocks, the low permeability of these geomatrices prevent groundwater flow by pressure gradients, in this case, radionuclide transport takes place by diffusion due to concentration /activity gradients.

Pu diffusion in the Opalinus Clay

The Opalinus Clay (OPA) is a potential host rock for a repository for spent fuel, vitrified high-level waste and long-lived intermediate-level waste in Switzerland. Owing to its small hydraulic conductivity (10^{-14} - 10^{-13} ms⁻¹), it is expected that transport of solutes will be dominated by diffusion. The diffusion is a very sensitive process in performance assessment (PA). The process is well understood for non-retarded solutes with simple chemistry, but little is known for retarded solutes. Therefore, the objective of this work is to understand the ²³⁸Pu diffusion in clay mineral-rich geological formations in order to provide support for improved representation of these processes in performance assessment and to enhance safety case credibility.

The objective of our work is to understand actinide diffusion in clay mineral-rich geological formations in order to provide support for improved representation of these processes in performance assessment and to enhance safety case credibility. The samples were collected in the Mont Terri underground laboratory where the OPA is situated -200 to -300 m below the surface. A sample cell - autoclave system (SCAS) was developed for carrying out actinide diffusion experiments in clay stones under their natural, confining pressure. The pressure applied in our experiments was 30 bar to simulate the in-situ confining pressure of the natural system.

Design of the experimental Set-up

To counteract the swelling of clay in contact with groundwater and to simulate the confining stress within the geological formation, a specifically adapted experimental set-up was developed. The heart of the diffusion cell is a

thin-walled stainless steel cell which holds the clay sample (Ø 20 mm, length 10 mm). All parts of the diffusion cell which are in contact with solution are coated with PEEK. The thickness of the wall of the stainless steel is 2/10 mm. After the positioning of the sample two PEEK distribution plates are placed on each side of the sample and the autoclave is sealed with screws. This cell is then placed in an autoclave. This autoclave has a volume of 300 ml and is filled with 250 ml of water. With help of a stainless steel pump we pressurized the autoclave with pressures between 0-100 bars. Due to the construction of the cell, the confining pressure acts isotropically onto the clay sample. The tubing for tracers and sampling are constructed in such a way that they are kept under ambient pressure and tracer injection and sampling can be performed in closed circulation loops.

The solutions are circularly pumped from 100 mL PE storage containers in split cycles with a 2-channel peristaltic pump (IPC, Ismatec, IDEX, USA). The Opalinus Clay samples were re-saturated by circulating these solutions in contact with the respective end of the sample for 5 weeks. This time was found to be sufficient to reach re-saturation [1]. Subsequently, the solutions were replaced by fresh ones and the solution in the large container was spiked with the desired tracer.

Sample preparation and characterisation

The Opalinus (OPA) clay stone sample used for our experiments was provided by NAGRA from the Mont Terri underground research laboratory (URL). The bore core (BEZ A24/3) with a diameter of 100 mm was sliced into 2-cm-thick pieces using a diamond saw (no lubricating fluid was used). Each slice was cut in two parts. A 20mm diameter core was drilled out of the inner part of each slice to avoid the use of artificially oxidized clay rock material. All samples were drilled perpendicular to the bedding plane.

The residue of the core was ground in a glove box and the mineralogy of the samples was determined using X-ray diffraction. Quantitative analysis was performed using the Rietveld method (TOPAS, Bruker AXS). The mineralogical composition is comparable to the one published in [2]. The porosity of the

sample was measured by mercury porosimetry and was found to be 10 %. The total organic matter (TOC) in the starting material was measured to be 0.5-1.3 wt % using a LECO-125 C/S analyser.

After completion of the diffusion experiments the clay stone cores were pushed out of the diffusion cell and embedded in epoxy-resin (Struers, Fellbach, Germany) to avoid drying out of the sample. These samples were cut perpendicular to the bedding (parallel to diffusion) in two pieces using a diamond saw in the glove box (no lubricating fluid was used) after the epoxy-resin had hardened. The intersection was cleaned with Tesafilm (Beiersdorf, Hamburg) to remove remaining sawdust.

One half of the sample was used for autoradiography. Therefore, the phosphor storage screen technology was used (Cyclone, Storage Phosphor System, Packard Instrument Company, USA). The measurement period was between 1 h and 7 days. Radiation is stored in reusable phosphor screens of BaFBrEu²⁺ crystals as defect energy. For reading out, the screens are scanned with a red laser and the emission of blue light stored in crystal defects is detected. The main advantages compared to film techniques are the higher sensitivity and the enhanced linear dynamic range. The lateral resolution is 600 dpi equal to about 40 µm. The α-activity of the ²³⁸Pu in the diffusion sample was determined against a 500 ppm NIST standard of natural ²³⁸U.

In the other half of the sample, the diffusive ²³⁸Pu profile in the rock was determined using the high-resolution abrasive peeling method [3]. Therefore, the sample was mounted on a sample holder and 46 grinding steps using a P220 abrasive paper and 32 grinding steps using a P80 abrasive paper were performed. The grinding paper was manufactured by Struers (Fellbach, Germany). The grinded samples were acidified (HNO₃, HF and HCl) and shaken for 24 hours.

Artificial Pore Water

The recipe for the artificial pore water used in the diffusion experiments is given in [5].

Activity measurements

The activity of the ²³⁸Pu in solution was measured by liquid scintillation counting (LSC). 100 µl of the sample was acidified with 20 µl of 65 % HNO₃. Then 20 µl was placed in a 20-ml polyethylene (PE) counting vial and 10-ml scintillation cocktail was added (Ultima Gold

XR, Canberra-Packard). The samples were vigorously shaken and placed in a liquid scintillation counter (Quantulus, WALLAC). The counting efficiency for each tracer was measured using artificial pore water with known amounts of activities. Background measurements were performed in a similar way using artificial pore water without radiotracers.

Sorption experiments

The ²³⁸Pu sorption pH edge was measured at 20°C in the OPA porewater. All experiments were performed in a glove box under Argon atmosphere. The pH was adjusted by adding analytical grade KOH or HNO₃. The experiments were performed in 10 ml Polypropylene Copolymer centrifuge vials (Oakridge) with a solid/solution ratio of 2 g/L. At the end of the experiment the solid was separated from solution by centrifugation.

Starting from pH ~4.8 the ²³⁸Pu concentration in solution is decreasing with increasing pH and reaches a sorption maximum at pH 7.2 (Fig. 1). Under alkaline conditions > 7 the ²³⁸Pu concentration in solution is increasing again. According to the results of the batch sorption data a strong ²³⁸Pu sorption under the experimental conditions of the diffusion experiments is expected.

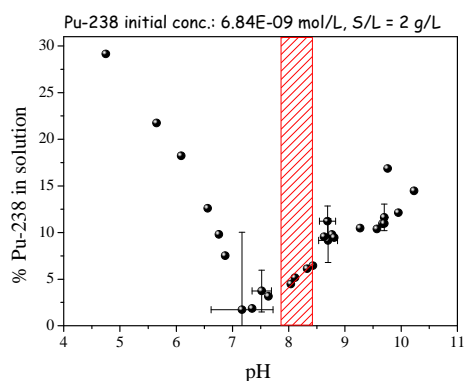


Fig. 1 Sorption experiments of ²³⁸Pu on Opalinus Clay. The filled pattern indicates the pH region of the diffusion experiments.

Results on the ²³⁸Pu diffusion in OPA

The diffusion experiments were performed at two different initial pH values. At pH 8.4 the initial ²³⁸Pu concentration was 5.63E-09 mol/L in SCAS 1. In SACS 2 the initial pH was 7.9 and the initial ²³⁸Pu concentration 5.38 E-09 mol/L. The pH of the OPA porewater remained unchanged throughout the experiment. The ²³⁸Pu concentrations dropped in SCAS 1 by one order of magnitude to reach a plateau value of ~1.93E-10 mol/L after 400 hours. In the SACS 2 experiments the decrease in the

^{238}Pu solution concentration appeared faster. After 724 hours the maximum decrease in ^{238}Pu concentration was observed, followed by a “steady state” concentration of $\sim 3\text{E-}10$ mol/L. The continuously in-line measured Eh value using an IONODE SI30 gel redox-electrode was found to be 440 mV for SCAS1 and 392 mV for SCAS 2. Although glove-box operations were performed as careful as possible two times an intrusion of oxygen (~ 8000 ppm for 12-24 hours) into the glove box was monitored

On the blank concentration side of the experiments the first α -activity was measured after 30 days experimental duration. A selective Pu extraction indicated that the detected α -activity was not due to through-diffusion of ^{238}Pu , but came from ^{228}Th released to the solution from the Opalinus clay sample.

At the end of the SACS 2 experiment the autoclave system and connected tubings were washed for two hours with 65 % HNO_3 to check sorption to the experimental set-up. This test showed that around 50-60 % of the initial ^{238}Pu concentration was sorbed on the container walls and tubings of the diffusion experiment.

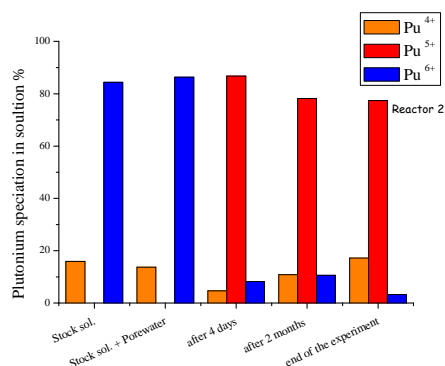


Fig. 2 ^{238}Pu speciation in the OPA porewater and in the solution of SACS 2 determined by BMBP-extraction. The ^{238}Pu concentration of the stock solution was $2\text{E-}07$ mol/L. In the OPA porewater the ^{238}Pu concentration was $4\text{E-}09$ mol/L and at the end of the experiment in Reactor 2 (after 93 days) $3.12\text{E-}010$ mol/L.

^{238}Pu Pu oxidation states in solution

The ^{238}Pu Pu oxidation states (Fig. 2) as a function of time in the Opalinus porewater were determined by BMBP-extraction [4]. Whereas in the stock solution 85 % Pu(VI) and 15 % Pu(IV) were observed the Pu oxidation state changed to predominantly Pu(V) (85%) after four days equilibration time in the OPA porewater. In the Opalinus porewater the pH was adjusted to pH 8.2. After two months the

^{238}Pu oxidation states changed to 10 % Pu(IV), 80 % of Pu(V) and 10 % of Pu(VI) in the OPA porewater. At the end of the experiment SACS 2 the Pu oxidation state in the solution was also determined. Like in the Opalinus porewater without contact to the Opalinus clay we found as the dominant oxidation state Pu(V) with 77 %, followed by Pu(IV) 17 % and 6% Pu(VI).

Autoradiography

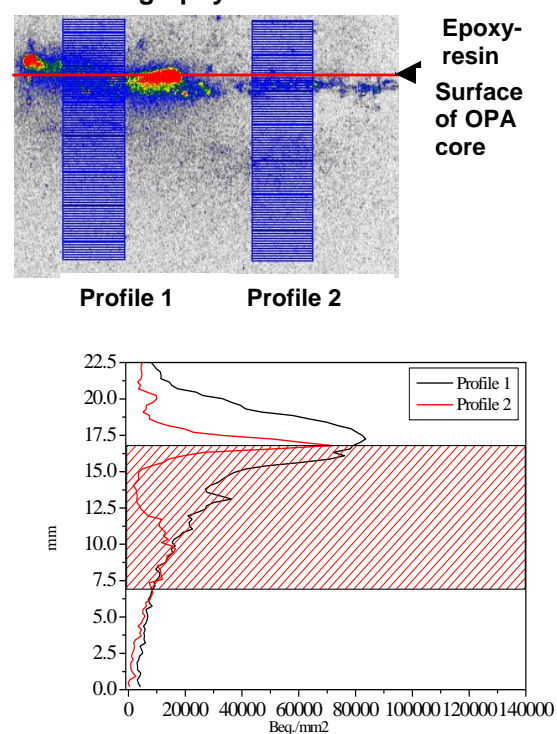


Fig. 3 Two different diffusion profiles measured with autoradiography. The filled pattern indicates the clay sample. The dotted line indicates the background radiation from the Opalinus clay. Each horizontal bar represents a data point in the diffusion profile. The different colors represent different concentrations. Red indicates the highest and the grey color the lowest concentration.

Traces of saw dust contaminated the embedding medium (epoxy-resin), therefore the interface between embedding medium and the clay sample was difficult to determine (Fig. 3). The figure also shows clearly that no preferential pathways for the migration of ^{238}Pu exist. It is evident that the ^{238}Pu diffusion within the Opalinus Clay is not homogenous. The ^{238}Pu is concentrated in Fig. 3 in two distinct areas (red spots) and on the left side of the picture. SEM-EDAX analysis showed no specific elemental concentration or any specific mineral phase in this area. The measured profiles are subsequently different for the two sides of the sample. Whereas profile 1 shows the diffusion of the ^{238}Pu of ~ 5 mm at the end

of the experiment (93 days) the diffusion in profile 2 is much more restricted (~ 1 mm). The background activity varied between 5000-10000 Bq/mm².

Conclusions

Trustworthy determination of the diffusion behavior of actinide ions in clay requires carefully designed experimental set-ups and development and application of a series of analytical techniques. Careful cross-checking is required in order to verify that the samples are not subject to undue disturbances, especially those resulting in preferential artificial transport pathways. Furthermore, delineation of natural activity inventory from the studied ions and identification of inventory lost in the equipment is a precondition for adequate interpretation of the experimental results. Trustworthy interpretation of transport experiments also requires batch sorption data and 3D distribution of along the diffusion samples. The present work shows that all these objectives have been demonstrated for an in-house built diffusion experiment system and development and application of the required associated analytical techniques. For this purpose Pu transport in an Opalinus clay core was studied. This initial demonstration and experimental development experiment shows that (i) about 40 % of Pu is sorbed on components of the experimental set-up, (ii) there is considerable impact of the samples natural alpha-emitting inventory, (iii) the mobile Pu inventory is dominated by Pu(V), and there is no preferential transport pathway for Pu in the clay sample.

These ongoing investigations will provide the necessary basis for credible description of sorbing radionuclide mobility in clay for the nuclear waste disposal safety case.

Colloid stability and radionuclide-colloid-rock interaction under Äspö groundwater conditions

Those studies aim at the investigation of radionuclide behaviour in a colloid-groundwater-fracture infill mineral system. Background of the experiments is the scenario of a potential release of clay colloids from the bentonite barrier in a repository and their subsequent transport with the groundwater flow in a water conducting fracture. Those colloids may sorb radionuclides and thus can act as carriers for the colloid-mediated radionuclide migration.

Experiments

The stability of clay colloids prepared from MX 80 bentonite (platelet like particles; 30-180 nm in diameter) in solutions of varying ionic strength and pH and in a groundwater sampled at the Äspö Hard Rock Laboratory (HRL) site (TRUE-1 site, Feature A, KXTT4; composition see Table 1) has been studied within the reported period. The impact of MX80 bentonite colloids, fracture filling material (FFM; taken from the Äspö HRL; composition see [6]; a size fraction of 2 to 8 mm was taken and conditioned prior to use with anaerobic ÄGW) and fulvic acid on the speciation of various radionuclides including the actinides was observed in Äspö groundwater (ÄGW) over a period of 3 months.

Table 1 Physico-chemical parameters of ÄGW

pH	7.5 ± 0.1	
E _{h(SHE)}	~ 62.2 mV	
		Particulates+ colloids *
[Mg ²⁺]	70.9 mg.L ⁻¹	no
[Ca ²⁺]	1.06 g.L ⁻¹	no
[Fe ^{2+,3+}]	760 µg.L ⁻¹	~ 34 %
[Sr ²⁺]	15.9 mg.L ⁻¹	no
[Cs ⁺]	3.8 µg.L ⁻¹	no
[La ³⁺]	0.2 µg.L ⁻¹	~ 85 %
[U]	0.28 µg.L ⁻¹	no
[Al ³⁺]	37.7 µg.L ⁻¹	~100 %
[Na ⁺]	1.2 g.L ⁻¹	n.d.
[Cl ⁻]	3.9 g.L ⁻¹	n.d.
[SO ₄ ²⁻]	270 mg.L ⁻¹	n.d.

*Calculated from supernatant analysis after ultracentrifugation, 2h at ~ 500 000 g;
n.d.: not determined

Colloid stability measurements

The colloid stability ratios (W) were calculated from the coagulation rates of the bentonite MX80 colloids measured as a function of the ionic strength and pH by Photon Correlation Spectroscopy (PCS). The initial mean colloid size was at 220 ± 30 nm. Size evolution is then recorded after the simultaneous addition of concentrated electrolyte aliquots (NaCl 2 M or CaCl₂ 2 M) and NaOH or HCl to reach the desired final ionic strength (from 0.001 M up to 1 M) and a pH varying in the range 4-10. Additional Laser-Induced Breakdown Detection (LIBD) measurements of suspensions after coagulation and sedimentation were performed after more than 6 months.

Batch sorption experiments

Sorption of radionuclides to colloids and FFM has been studied in four batch type experiments.

- Set 1: Äspö groundwater (TRUE-1 site, Feature A, KXTT4) has been spiked with radionuclides: Sr90($2.2 \cdot 10^{-9}$ M), Cs137($2.3 \cdot 10^{-9}$ M), Am241($1.10 \cdot 10^{-10}$ M), Np237($1.06 \cdot 10^{-8}$ M), U233($2.3 \cdot 10^{-8}$ M) and Pu244($1.07 \cdot 10^{-9}$ M). These concentrations have been chosen to remain below the solubility limits of the elements at the final pH of 7.5 ± 0.2 especially for Am(III) and Pu(IV) as given in [6].

- Set 2: This solution is prepared as in Set 1, but MX80 bentonite colloids (2.4 mg.L^{-1}) have been added.

- Set 3: Pre-conditioned FFM has been weighed and contacted with fresh ÄGW (solid-liquid ratio 1:4 g.mL^{-1}). Radionuclides are added at concentrations as in Set 1.

- Set 4: For this set of experiments a FFM suspension as prepared for Set 3 experiments has been spiked with MX80 bentonite colloids (2.4 mg.L^{-1}) and fulvic acid (10 mg.L^{-1}) prior to radionuclide addition.

All solutions were then left and the evolution of the radionuclide and bentonite colloid concentrations have been followed for over 4 months by direct analysis of the supernatant and sample aliquots after ultracentrifugation (2 h at $\sim 500\,000$ g). Sr90, Cs137, Am241 concentrations were measured by LSC, while Al (bentonite colloid), Np237, U233 and Pu244 concentrations were determined by ICP-MS.

Results and discussion

Characterisation of Äspö groundwater (ÄGW)

The ÄGW shows a high salinity with an ionic strength around 0.2 M dominated by CaCl_2 . LIBD analysis reveals the presence of colloidal species in the natural groundwater as indicated by a BDP = 0.8. ICP-MS analysis shows that colloids contain $\sim 34\%$ Fe, $\sim 100\%$ Al and $\sim 85\%$ lanthanides while naturally present Cs, Sr and U do not reveal colloidal behaviour. Colloid concentrations decrease rapidly and are the consequence of oxygen intrusion during or after the sample transfer resulting in Fe(III)OOH precipitates. This shows clearly the necessity of controlling the experimental conditions when planning in-situ radionuclide migration experiments at Äspö HRL. The Fe concentration (most likely Fe(II)) drops to $\sim 2 \cdot 10^{-6}$ M and remains constant.

Contact with FFM does not cause a major concentration change of the groundwater main components (Ca, Mg, Na, pH) indicating an overall equilibrium state of the solid/liquid system. However, the clear increase of Al and

Fe concentrations, which can be removed by centrifugation demonstrates the existence of particulate and colloidal matter in the FFM, which can be mobilized after agitation of the sample. Cs concentration is clearly reduced by a factor of ~ 3 by sorption to the solid. The release of uranium from the rock agrees with recent observations [7] showing a mobilization of natural uranium. This has been explained by the presence of oxidized uranium in the solid due to air contact of the sample during sampling and storage.

MX80 bentonite colloid stability

Colloid stability ratios (W) were calculated from the coagulation rates of the bentonite MX80 colloids. The results are presented in Fig. 4 and indicate clearly that at the high ionic strength of the Äspö groundwater (IS ~ 0.2 M), the stability ratio equals to 1 in all systems, which means that the colloids are instable. Additional LIBD measurements of dispersion supernatants after sedimentation of agglomerates were performed over 5 months. LIBD breakdown probability drops to a value measured for ultrapure water demonstrating the colloid agglomeration/sedimentation being complete in experiments with ionic strengths > 0.01 M.

Various Äspö groundwaters contain significant DOC concentrations. Fulvic acid dominates the organic component of organic matter in deep granite groundwater and was already isolated from various Äspö groundwaters [8]. A well characterised fulvic acid from the Gorleben site (GoHy-573) was taken to simulate the influence of natural organic matter on colloid and radionuclide behaviour in ÄGW. Organic matter originating from the site was not available. The influence of fulvic acid (7.7 and 77 mg.L^{-1}) on colloid agglomeration was found

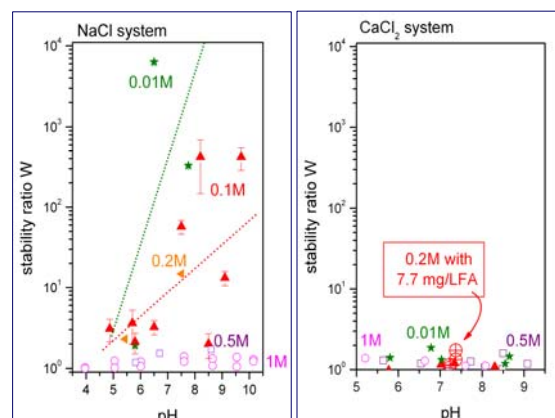


Fig. 4 Stability ratio of the MX80-bentonite colloids as a function of pH and ionic strength induced by addition of NaCl or CaCl_2 and in presence of organic matter.

negligible. The presence of fulvic acid only decreases the sedimentation kinetics depending on the organic matter: inorganic colloid ratio.

Radionuclide behaviour in Äspö groundwater in presence of bentonite colloids, fracture filling material and fulvic acid.

The sorption behaviour of the radionuclides onto FFM in presence of bentonite colloids is illustrated in Figs. 5a, 5b, 5c. The upper part of each figure shows the radionuclide portion remaining in solution while the lower part represents the colloidal fraction.

The following conclusions can be drawn from the results.

- MX80-bentonite colloids: in agreement with the results of the colloid stability study, the MX80 bentonite colloids are unstable under these conditions and sediment after 2 days. These conclusions are drawn from the analysis of the Al concentration evolution in the supernatant, which are not explicitly plotted here. The concentration of Al as a main constituent of bentonite is taken as an indicator for the clay colloids.
- Cs(I) and Sr(II) do neither significantly interact with bentonite and groundwater colloids nor with fulvic acid. Cs is found to sorb partly to FFM.
- U(VI): U233 does not show any significant colloidal behavior in presence or absence of MX80 bentonite colloids. In contact with fracture filling material the natural U238 concentration increases (from 0.3 µg.L⁻¹ up to 6 µg.L⁻¹ after 3 weeks) as mentioned before.
- Am(III): Am241 forms colloids when spiked to

the ÄGW. These colloids, consisting most likely of Fe(III)oxyhydroxide phases formed due to oxygen contact during sampling and storage from the barrel even though performed under Ar atmosphere, sorb trace metal ions such as Am(III). They are instable and disappear from solution after 2 months. In presence of MX80-bentonite colloids, Am is associated with the instable MX80-bentonite colloids and disappears even faster from solution. Colloidal Am is removed from solution after 2 months. In contact with fracture filling material Am sorbs strongly within 3 weeks. In presence of fulvic acid, a part of Am seems to be stabilized, at least for 3 weeks due to complexation by fulvic acid. The influence of fulvic acid on the sorption of Am will be observed further.

- Pu(IV): Pu-244 forms as well colloids when spiked to the ÄGW in presence and absence of bentonite colloids similar to the behaviour of Am. As found for Am no more Pu is found in solution after 2 months. Pu is also removed from solution in presence of FFM and, like Am, is kept partly in solution by complexation with fulvic acid (~ 25 %).
- Np(V): Np-237 spiked to the ÄGW disappears almost completely from solution after 3 months. This is explained by a slow reduction of Np(V) under given redox conditions (Eh ~ 60 mV). Np(IV) phases may either sorb to container walls or coagulating and sedimenting Fe(III)OOH colloids. In presence of MX80-bentonite colloids, the Np is removed even faster. This indicates a possible Np(IV) sorption to sedimenting MX80-bentonite colloid agglomerates. Sorption to FFM and an influence of fulvic acid yet cannot be observed.

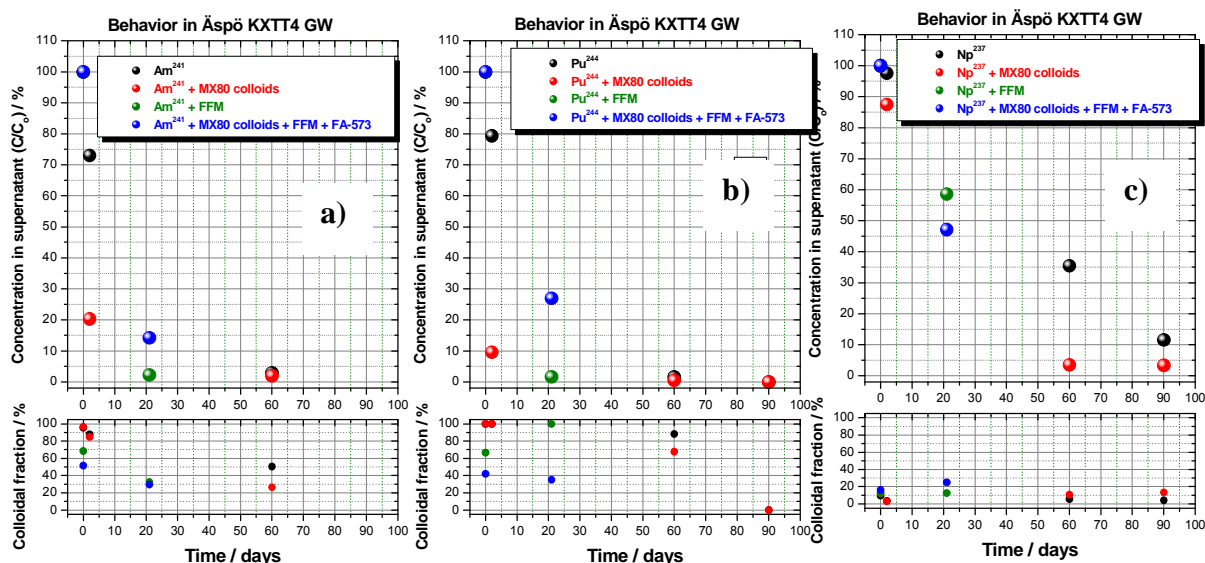


Fig. 5 Behavior of a) Am241, b) Pu244 and c) Np237 in ÄGW in presence of added MX80-bentonite colloids, fracture filling material (FFM) (1g : 4 mL water) and fulvic acid

Conclusions-Outlook

The colloid composition in Äspö groundwater is very sensitive to contact with even trace oxygen content of the atmosphere and pressure changes. This has to be considered for planned in-situ experiments.

Bentonite colloids (as those supposed resulting from the bentonite barrier erosion) are shown to be instable in this medium, coagulate and sediment. Under given conditions, we have to conclude that colloids eroding from bentonite rather retain radionuclides such as actinides and do not act as mobilizing carriers.

The presence of organic matter does not enhance bentonite colloids stability in ÄGW but acts as a complexing agent keeping tri- and tetravalent actinides partly in solution. The impact of fulvic acid on radionuclide sorption will be investigated further.

Future experiments will focus on radionuclide and colloid migration experiments using a bore core from Äspö. Geochemical calculations will be performed in order to specify prevailing radionuclide speciation under given experimental conditions and to confirm to a certain extent the conclusions. Considering the presently discussed scenario of low mineralized glacier melt water intrusion towards the bentonite barrier, one has to discuss as well an extension of the experiments to study the influence of low mineralized groundwater on colloid mobilisation.

Acknowledgement

This work was financed by SKB (Swedish waste management organisation, Stockholm, Sweden)

References

- [1] Van Loon, L. R., Soler, J. M., and Bradbury, M. H., 2003. Diffusion of HTO, Cl-36(-) and I-125(-) in Opalinus Clay samples from Mont Terri - Effect of confining pressure. *J. Contam. Hydrol.* 61, 73-83.
- [2] NAGRA, 2002. Projekt Opalinuston; Synthese der geowissenschaftlichen Untersuchungsergebnisse, Wettingen.
- [3] Van Loon, L. R. and Eikenberg, J., 2005. A High Resolution Abrasive Method for Determining Diffusion Profiles of Sorbing Radionuclides in Dense Argillaceous Rocks. *Applied Radiation and Isotopes* , , 11-21.
- [4] Nitsche, H., Roberts, K., Xi, R., Prussin, T., Becraft, K., Mahamid, I. A., Silber, H. B., Carpenter, S. A., and Gatti, R. C., 1994. Long Term Plutonium Solubility and Speciation Studies in a Synthetic Brine. *Radiochim. Acta* 66.
- [5] Pearson, F. J., 1998. Opalinus Clay experimental water: A1 Type, Version 980318. In: TM-44-98-07, P. I. r. (Ed.). Paul Scherrer Institut, Villigen PSI, Switzerl
- [6] Vejmelka, P.; Fanghänel, Th.; Kienzler, B.; Korthaus, E.; Römer, J.; Schüssler, W.; Artinger, R.; Wissenschaftliche Berichte, FZKA 6488, Forschungszentrum Karlsruhe, 2000
- [7] Kienzler, B.; Vejmelka, P.; Römer, J.; Schild, D.; Jansson, M.; MIGRATION'05 Conference, Sep. 18-23, 2005, Avignon, France
- [8] Buckau, G.; Molf, M; Technical report TR-05-20 from SKB, "The colloids investigations conducted at the Äspö Hard Rock Laboratory during 2000-2004", 2005, p.77-85

5.3 Influence of natural organics

G. Buckau, F. Claret*, C.M. Marquardt, P. Michel, M. Plaschke, J. Rothe, T. Schäfer

* CEA Saclay, CEA/DEN/DANS/DPC/SECR/LSRM, Gif sur Yvette, France

Introduction

Natural organic matter (NOM) can occur in a wide variety of structures starting with low molecular weight compounds (LMWC) as e.g. found in the porewater of claystone formations (Opalinus clay), humic substances (HS) and finally the immobile most mature organics called kerogen. The focus of the research at INE in the last decade was clearly lead on the characterization, radionuclide interaction and mobility of HS (humic and fulvic acids). Humic and fulvic acids (HA and FA) are a class of organic compounds with a large number of similarities, for example in the comparably long residence time/chemical stability. The elemental composition varies around $\text{CHO}_{0.5}$, the total proton exchange capacity around 5-8 meq/g (mainly from carboxylic and phenolic groups) and the number-weighted average mass is around 450 to 500. Furthermore, HS have an inventory of redox sensitive functional groups and the redox state will reflect their physico-chemical environment or can be seen as a "memorized" chemical environment of their formation. These redox sensitive functional groups are very important for reactions with redox sensitive actinide ions.

A new focus within recent years is the characterization of mineral associated organic matter. The fractionation of HA/FA via mineral adsorption might be an approach to explain the observed discrepancies between laboratory data and the predictive modeling of ternary systems (mineral-organics-RN) using linear additive models. Combination of spectroscopic methods in collaboration with CEA is a very promising approach (see below). The studies on isolation, characterization and reactivity of kerogen found in natural host-rock formations (Callovo-Oxfordian, Opalinus Clay, Toarcien) was continued. It could be shown that natural organic matter/humic substances on natural mineral surfaces are generally strongly bound, partly by covalently bonds, and show a low inventory of oxygen containing carboxylic groups. These low functionalized organics can block mineral surface functional groups and might lead to a different radionuclide sorption behavior than predicted by the "bottom-up" approach using pure mineral systems.

There are still many open questions for adequate description of the overall influence of NOM on the geochemical behavior of actinide ions and their mobility in deep groundwater

systems. Three of these topics are discussed in more detail below, namely basic description of radionuclide complexation, influence on the redox state of actinide ions and the characteristic properties of mineral bound natural organic matter.

Basic description of complexation with radionuclides

The INE has developed an approach for systematic description of metal ion humate complexation. The description combines the binding capacity, i.e. the amount of complex formed by humic acid under specific physico-chemical conditions with recent findings on the mass distribution of humic acid as well as the number of proton exchanging functional groups per average molecule. The approach shows that strongly complexing metal ions form one complex per humic acid molecule, followed by association of complexes to form larger clusters, finally resulting in the well known flocculation. The protonation induced flocculation also form part of this process description. The approach is very promising because it brings together recently acquired knowledge, especially reflecting dramatic changes relatively to the previous grave overestimation of the humic acid molecular mass distribution. It also opens the possibility to describe competition by parallel complexation processes resulting in mixed clusters/flocculates.

One particularity is that the approach does not make use of the frequently assumed polyelectrolyte/double layer properties that can hardly be defended based on the recent development with respect to the much smaller molecules than previously thought.

There are, nevertheless, still open questions. The original approach was based on studying strongly complexing metal ions, namely Am(III) and U(VI). It is also shown to be applicable to the strong ternary U(OH)- and Cm(OH)_x-HA complexation. One open question refers to the complexation accessibility of metal ions forming weaker complexes. In Fig. 1 the complexation capacities of Np(V) is shown as a function of pH, in relation to the Binding Capacities of the strongly complexing Am(III) and U(VI) ions (Np(V) data from [1,2]). The binding capacities of Np(V) humate complexation, with a complexation constant of 3.7, is about half of those found for the stronger complexing Am(III) and U(VI). This interpretation is that the lower

complexation accessibility is associated with the lower complexation strength. It shows that the simple monomolecular interaction approach is applicable also to other metal ions than the strongly complexing ones used in the original development. For further development of the approach, however, more data from the complexation of different ions with same humic acid under comparable experimental conditions would be required.

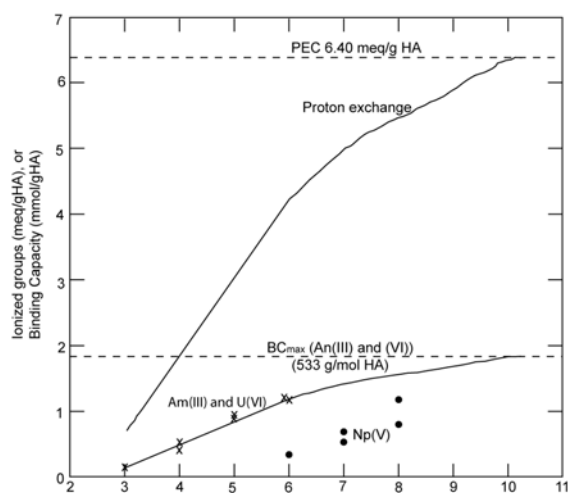


Fig. 1 Binding capacities of Np(V) shown together with those of the strongly complexing Am(III) and U(VI) and the proton exchange behaviour of Gohy-573 humic acid in 0.1 M NaClO₄.

Understanding humic acid / Zr(IV) interaction – a spectromicroscopy approach

Depending on the geochemical milieu, polyvalent actinide cations form oxo/hydroxide colloids following hydrolysis and oligomerization. The chemical properties and colloid stability of these inorganic particles may be altered by surface reactions with humic acid (HA). As part of the assessment of HA impact on actinide transport phenomena, it is crucial to characterize both the nature of HA/actinide ion complexes and HA hetero-aggregates with actinide oxo/hydroxide colloids. In the present study, Zr(IV) acts as a chemical homologue for Pu(IV).

We apply Scanning Transmission X-ray Microscopy (STXM) to study the interaction between HA and tetravalent Zr or its hydrolysis products. Polyacrylic acid (PAA) is chosen as an appropriate model compound to clarify the role of carboxyl groups in the HA / metal ion interaction. In our previous studies striking similarities are found in spectral trends of the C 1s-NEXAFS (Near Edge X-ray Absorption Fine Structure) signatures before and following complexation of trivalent metal ions by HA and PAA [3].

Aqueous suspensions of purified commercial HA (Aldrich) and PAA are contacted with solutions of Zr(IV) at different pH. Addition of metal cations to saturate HA and PAA loading capacities ($[Zr(IV)] = 1.1E-3$ mol/L) or acidification of HA suspensions to pH 1 induces the polymers to precipitate from solution. Resulting aggregate flocs are of ideal dimension to be probed by soft x-ray microscopy at the carbon K-edge. STXM investigations are performed at beamline X-1A at the NSLS in Brookhaven, New York [4] with a spatial resolution of about 100 nm. Zr(IV)-HA and -PAA aggregates are investigated sandwiched between two silicon nitride membranes in fully hydrated state. Stacks of images from selected sample regions are recorded as a function of incident photon energy E . C 1s-NEXAFS spectra are extracted from vertical projections onto aligned image stacks. Details on wet cell sample preparation and stack data analysis can be found in Refs. [5] and [6], respectively.

Results

The C 1s-NEXAFS of Zr(IV)-PAA strongly depends on the solution pH (Fig. 2). At pH 5, we observe the spectrum of uncomplexed PAA, with a NEXAFS comparable to the Na-form [1]. At pH 4.3, the decrease of the carboxyl peak and the appearance of a shoulder adjacent to the carboxyl peak (arrow) points to complex formation, as recently observed for Eu(III) and other polyvalent metal cations [5]. This shoulder becomes more pronounced at pH 3. We offer the following interpretation: at pH 5, Zr(IV) hydrolysis and oxo/hydroxide formation is dominant [6]. PAA is merely coating and co-precipitating with these inorganic particles; no specific metal organic interaction is discernible from the C 1s-NEXAFS. This interpretation is corroborated by Zr K-EXAFS measurements, giving evidence

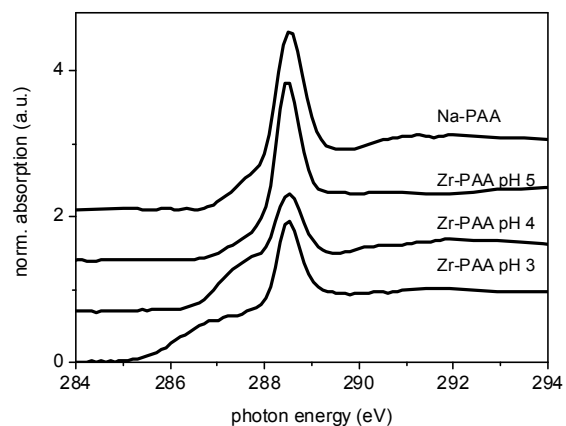


Fig. 2 Normalized C 1s-NEXAFS for Na-PAA and Zr(IV)-PAA at different pH.

for Zr(IV) colloid formation under these conditions. Decreasing the pH leads to an increased fraction of ionic Zr(IV) which can be complexed by PAA carboxyl groups. This reaction becomes more favorable at pH 3, indicated by the stronger complexation effect in the C 1s-NEXAFS.

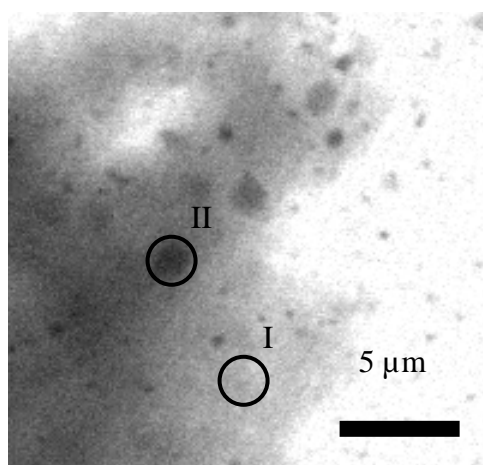


Fig. 3 Specific carbon absorption by STXM of Zr(IV)-HA at pH 4, recorded at 288.5 eV (corresponding to the carboxyl resonance). Circles indicate regions used to extract NEXAFS data in Fig. 4.

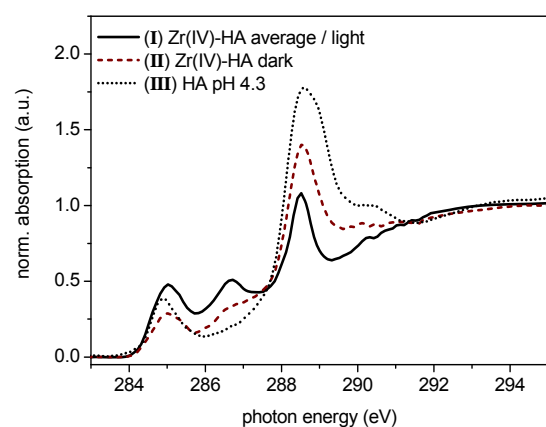


Fig. 4 Normalized C 1s-NEXAFS recorded for HA at pH 4.3 and Zr(IV)-HA fractions after metal cation induced aggregation and segregation.

We previously observed that HA aggregation induced by addition of polyvalent metal cations at slightly acid pH (~5.0) is always accompanied by segregation into zones with different optical densities [7]. Both dense or 'dark' and less dense or 'light' zones possess characteristic C 1s-NEXAFS signatures. Similar segregation into different HA fractions induced by Zr(IV) addition is observed in the STXM image in Fig. 3, where confined dark patches embedded into a lighter matrix of carbonaceous material are visible. The

corresponding C 1s-NEXAFS signatures are compared in Fig. 4. The aromatic peak at ~285 eV and the dominant carboxyl peak at ~288.5 eV are evident. The spectrum of the light zones (I) shows a distinct peak at ~286.7 eV, generally attributed to phenolic carbon. The spectrum of the dark zones (II) exhibits a somewhat weaker aromatic peak and a shoulder leading to the more pronounced carboxyl resonance. Spectrum III, taken from [3], was extracted from a HA precipitate observed at pH 4.3 without addition of metal cations. HA aggregates at pH 1 without added Zr(IV) exhibit a spectrum similar to signature I (not shown). Averaging the spectroscopic signal over entire aggregates at pH 4 with added Zr(IV) also yields spectrum I. We conclude that signature II obviously characterizes a minority fraction. The shoulder in II resembles the complexation feature observed for Zr(IV)-PAA at pH 3-4. II also resembles the signature of HA at pH 4.3 (III), indicating lack of strong complexation.

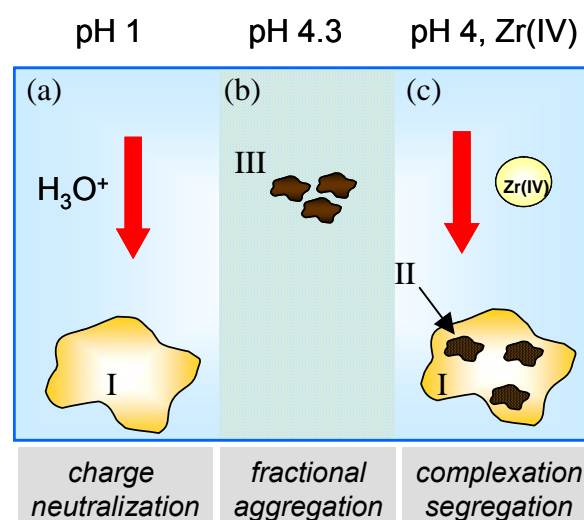


Fig. 5 Mechanistic model describing HA precipitation vs. fractionation under various pH conditions and following metal cation complexation. Signatures I-III corresponding to spectra in Fig. 4.

Based on these observations, we suggest a simple mechanistic model of HA behavior and Zr(IV) / HA interaction as illustrated in Fig. 5. At low pH (a), saturation of HA functional groups by protons leads to HA precipitation via charge neutralization and subsequent agglomeration. The C 1s-NEXAFS (similar to signature I) is characteristic for the HA majority fraction rich in aromatic and phenolic subunits. This fraction is dissolved at pH 4.3 (b), leaving behind a less soluble minority fraction exhibiting signature III. Saturating the HA loading capacity at pH 4 by adding Zr(IV)

cations (c) leads to complexation and segregation. The dark zones (signature II) can be attributed to the pH 4.3 minority fraction rich in carboxyl groups. It has a stronger affinity for metal cations, as already observed for Eu(III)-HA [8]. The corresponding C 1s-NEXAFS (signature II) exhibits a significant shoulder associated with a strong complexation reaction similar to that observed in Zr(IV)-PAA. The light zones represent the majority fraction aggregating due to charge neutralization as observed for pH 1 without Zr(IV) (signature I).

Interaction of humic substances and hydroquinones with redox sensitive Actinide ions

The reduction sequence of Pu starting with Pu(VI) in presence of hydroquinone (HQ) and fulvic acid (FA) as reducing compounds at various pH values between pH 1 and 7 was investigated in detail. The Pu species were monitored by UV-Vis spectroscopy and liquid-liquid extraction. The experiments showed that Pu(V) and (VI) are not stable in aqueous solutions containing hydroquinone or fulvic acid (FA) at pH 1 to 7. With 200 mg/L FA the reduction of Pu(VI) to Pu(V) is fast and complete after 30 minutes at pH 3. Compared to the reduction reaction at similar concentration of HQ, the FA reduction is slower. Pu(V) in same solutions is converted to Pu(IV), the most stable oxidation state in aqueous solutions containing FA at pH 3 - 7 (relevant for natural aquifers). Reduction of Pu(IV) to Pu(III) was found only at pH values < 5 for HQ and < 3 for FA. The reactions were also monitored by Eh measurements.

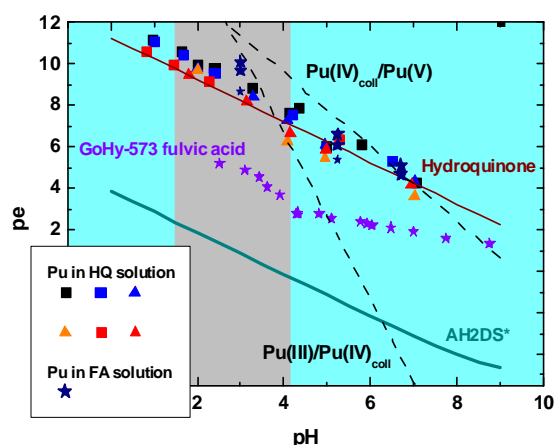


Fig. 6 Eh measurements of hydroquinone (HQ) and fulvic acid (FA) solutions. The HQ and FA concentrations exceeded the total Pu concentration. Lines (solid, dashed) show thermodynamic calculations and the grey area symbolises the Pu(III)/Pu(IV) transition zone obtained from the experiment. (* AH2DS is 9,10-anthraquinone-2,6-disulfonate)

The present studies show that a correlation between Eh values and thermodynamic calculations might be a capable tool for modeling redox reactions between Pu ions and hydroquinone or hydroquinone-like compounds like FA (see Fig. 6). It cannot be excluded that Pu(III) is more stable in solutions containing organic compounds with lower redox potential than the GoHy-573-FA batch used in the present studies.

Further studies focused on the chemical (sulfur K-edge XANES) and stable isotope analyses ($\delta^{18}\text{O}$ and $\delta^{34}\text{S}$) on fulvic acids (FAs) associated sulfur to determine on one hand the S cycling in a well known aquifer system (Franconian Alb, Southern Germany) and elucidate the influence of the FA formation environment on redox sensitive functional groups [6].

Characterization of mineral bond natural organic matter

Sorption to mineral surfaces and complexation by Natural Organic Matter (NOM) are two important processes influencing the cycling of potentially toxic trace metals in the environment. Both, the sorption of metal cations onto pure oxides/clay minerals and the binding of trace metals to NOM (e.g. humic and fulvic acids) have been extensively studied. However, the specific interactions between metal cations and mineral surface absorbed NOM are still matters of debate. Indeed, the use of additive models, i.e. linear combination of binary systems metal/surface, NOM/surface, and metal/NOM, to describe the ternary system showed significant deviations. One tentative explanation of this discrepancy can be the chemical and physical fractionation of NOM during the interaction with mineral surfaces. In collaboration with CEA we studied the fractionation of Suwannee River Fulvic Acid (SRFA) and the Gorleben Humic Acid (GoHyHA) at the mineral surface of $\alpha\text{-Al}_2\text{O}_3$ using spectroscopic techniques (UV/VIS, C(1s)-NEXAFS). For SRFA, a clear fractionation consisting of enrichment in aromatic functional groups on the alumina surface has been detected by both UV/VIS and NEXAFS spectroscopy, whereas for GoHyHA fractionation understanding is still pending.

Understanding and modelling confinement properties over the long term of a deep geological repository for nuclear waste is the heart of performance assessments. In this context, specific experimental works have been addressed on the impact of thermal or chemical perturbations on either the clay minerals or organic matter. Argillites are a

complex system formed of multiple minerals (i.e. various clays minerals, calcite, quartz, pyrite) and organic phases. Process understanding regarding the clay mineral-organic matter interactions can be gained by observing at submicron-scale the transformations occurring during pyrolysis of simplified systems in which the nature of the mineral phase as well as the type of organic matter is well defined. Confined pyrolysis ($T=200^{\circ}\text{C}$ - 365°C , $P_{\text{tot}}=300$ bars, $t_{\text{reac}}=72$ hours) experiments in argon filled gold cells were performed with mixtures of Volclay bentonite containing mainly smectite phase and isolated kerogen from the Toarcian shale (Paris Basin) and water [7]. Microscopic observations and spectroscopic measurements have been conducted by using Electron Energy-Loss Spectroscopy coupled to Transmission Electron Microscopy (TEM-EELS) and Scanning Transmission X-Ray Microscope (STXM) in order to (1) observe at submicron-scale the nature of kerogen-type organic matter and the potential interactions with bentonite and (2) compare the information provided by both spectroscopic methods.

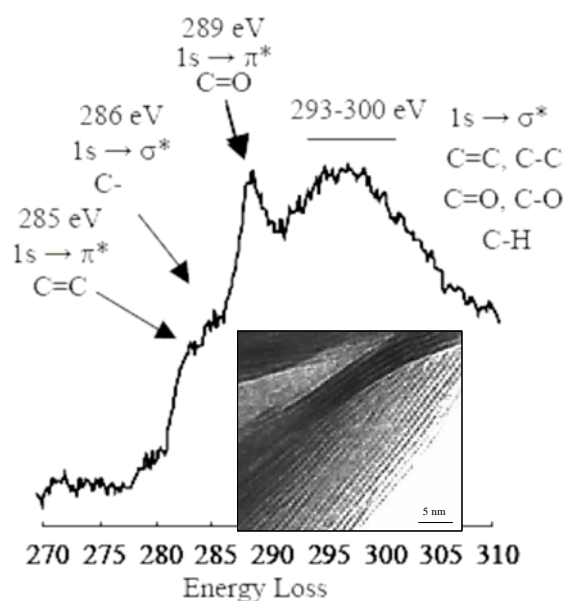


Fig. 7 EELS spectra of bentonite associated kerogen after pyrolysis at 350°C and organic matter phase observed on the surface of smectite particle and TEM image showing cloudy organic structures observed on the clay outer surface.

Measurements on pyrolysis products clearly show the presence of organic carbon predominantly as isolated particle of organic matter. EELS spectra of such particles are similar to those obtained on the isolated kerogen (amorphous organic material) before pyrolysis. Moreover, organic carbon was also found on smectite surfaces (Fig. 7). EELS spectra of such cloudy organic matter

structures revealed well discriminated C K-edge bands, in particular (1) a band around 288/289 eV assigned to the $1s \rightarrow \pi^*$ transition of the C=O bond of carboxylic groups and (2) a shoulder at 286/287 eV corresponding to either the $1s \rightarrow \sigma^*$ transition of the C-H bonds or the $1s \rightarrow \pi^*$ transition of the C=O bond of phenol type groups. The smectite could be identified by additional measurements at the calcium $L_{2,3}$ -edge around 350 eV.

Scanning Transmission X-Ray Microscopy (STXM) investigations confirmed TEM-EELS measurements. C K-edge spectra showed again distinctive different spectra for clay-associated organic matter and particulate organic matter found (Fig. 8).

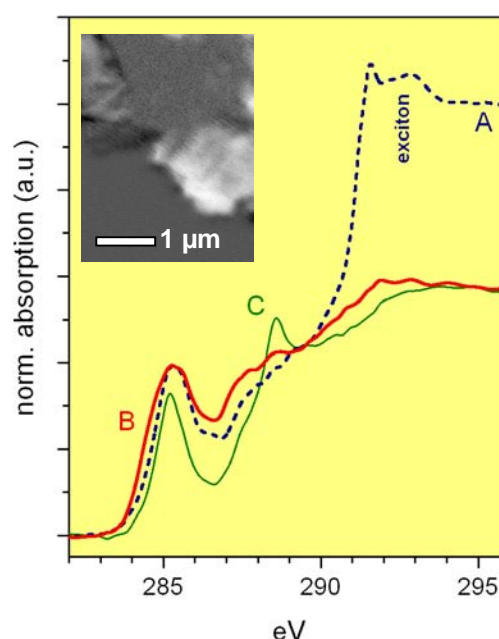


Fig. 8 C 1s-NEXAFS of (A) Toarcien kerogen before pyrolysis reaction at 365°C , (B) isolated particles of kerogen-type organic matter not associated with smectite and (C) Volclay smectite associated kerogen showing the enhanced absorption band at 288.6 eV assigned to the $1s \rightarrow \pi^*$ transition of carboxyl-type groups. The inserted STXM ratio image shows in light grey colors the distribution of organics as patchy structures on the clay surface.

In summary, the investigations show a clear consistency of the data obtained by both TEM-EELS and STXM on the carbon K-edge. Furthermore, the spectromicroscopic observations demonstrate that thermal stress simulated by confined pyrolysis induces changes on clay associated kerogen-type organic matter, whereas pure particulate organic matter seems to be structurally similar in experiment with or without clay. The initial

swelling properties of the clay are conserved and not affected by the occurrence of clay associated organic matter as cloudy/patchy structures. This implies that the association is restricted to the external surface. Further studies are underway to elucidate the involved organic matter association/reaction processes.

References

- [1] J.I. Kim and T. Sekine, *Radiochim. Acta*, 55, 187-192 (1991).
- [2] Marquardt, C. and Kim, J.I., *Radiochimica Acta*, 80(3): 129-137 (1998).
- [3] M. Plaschke, J. Rothe, M.A. Denecke and Th. Fanghänel, *J. Electron Spectrosc. Relat. Phenom.* 135, 53 (2004).
- [4] C. Jacobsen, S. Williams, E. Anderson, M. T. Browne, C. J. Buckley, D. Kern, J. Kirz, M. Rivers and X. Zhang, *Opt. Commun.* 86, 351 (1991).
- [5] Neuhausler, U., Jacobsen, C., Schulze, D., Stott, D. and Abend, S., *Journal of Synchrotron Radiation*, 7: 110-112 (2000).
- [6] Einsiedl, F., Schäfer, T. and Northrup, P., *Chemical Geology*, 238: 268-276 (2007).
- [7] Michel, P. *Etude expérimentale des interactions organo-minérales de roches argilo-carbonatées*. Ph.D. Thesis, University Louis Pasteur, Strasbourg (2006).

5.4 TRANSAL: Development of a Code for Coupled Transport and Reaction Modelling

E. Korthaus, E. Bozau, B. Kienzler

Introduction

In a deep geological repository, contact of groundwater to the wastes cannot be excluded. In this case, groundwater acts as corroding media for the technical, geo-technical barriers and the waste forms but also as transport media to and from the wastes. Both, advective and diffusive transport processes may occur depending on the hydro-geological and geochemical characteristics of the host rocks and the design of the disposal. Groundwater constituents will be consumed by the corrosion / dissolution processes, simultaneously, dissolved species increase concentrations directly at the surfaces of the corroding solids. Consequently, transport processes will re-distribute the groundwater constituents to and dissolved components from the corroding waste form surfaces. Various reactions will take place, including dissolution of solid radionuclide phases, formation of complexes of the radionuclides and other components of the waste form with constituents of the groundwater and precipitation which will lead to new thermodynamically stable phases. Even if the long-term behaviour of a quasi closed disposal system can be described by thermodynamic equilibrium models, interpretation of kinetically controlled reactions, as observed in many laboratory experiments, requires consideration of coupled transport and reaction processes. This method allows to predict if observed rates are controlled by reaction kinetics or by transport phenomena.

Considerable progress has been made in the field of reactive transport modelling during the last decade. Specific approaches have been developed [1] e.g. for cement systems. Commercial codes are also available. In use at INE is the code "The Geochemist's Workbench" [2], a set of interactive software tools for solving problems in aqueous geochemistry, including those encountered in geology and nuclear waste disposal. However, commercial codes do not account for specific questions to be modelled for German disposal systems. For this reason the TRANSAL code was developed and applied to various systems.

In TRANSAL, a series of features applicable to specific problems are implemented which are characterized below.

Modelling of one-dimensional advective flow driven by convergence

Modelling of advective flow in a saturated porous system under the assumption of one-dimensional Darcy flow is described by eq. 1.

$$v_D = \frac{k}{\mu} \frac{\partial p}{\partial x} \quad (\text{eq. 1})$$

with the permeability k and viscosity μ of the fluid. v_D is the Darcy velocity which is correlated to the average flow velocity v ($v_D = v \cdot \Phi$, Φ : porosity). v_D is also related to the flux Q according to $v_D = Q/A$ (A : cross sectional area). Additionally, the continuity equation (eq. 2) must be met

$$\frac{\partial \Phi}{\partial t} + \frac{\partial v_D}{\partial x} = S \quad (\text{eq. 2})$$

S: source or sink.

Especially for compacted crushed rock salt, a relation between porosity and permeability is given by Müller-Lyda [3] eq.3.

$$k = c \cdot \Phi^n \quad (\text{eq. 3})$$

Advection is driven by pressure difference between the boundaries and/or by geomechanical convergence of the flow system causing a reduction of the pore volume. Furthermore, changes in the pore volume may occur as consequence of dissolution or precipitation of solid materials in the flow path. These processes are treated in TRANSAL. Specific material models are implemented for various dependencies:

- convergence rate depending on compressibility of the porous material (rock salt) and fluid pressure.
- compressibility of the porous material (rock salt) under dry and wet conditions and variable temperature.

Advectively and diffusively controlled transport of dissolved substances

The transport of dissolved material by advection and/or diffusion is described by eq.4.

$$\frac{\partial(\Phi \cdot c)}{\partial t} - \frac{\partial}{\partial x} \left(\Phi \cdot D \cdot \frac{\partial c}{\partial x} + v_D \cdot c \right) = Q + R \quad (\text{eq. 4})$$

c: concentration, D: diffusion constant, Q: external source, R: reactive source for each component.

In the case of a variable cross sectional area A, the term porosity Φ is replaced by the product $\Phi \cdot A$.

The reactive source R of each species depends on the concentrations of several other species involved in the reaction and additionally on space and time. Therefore, eq. 4 represents a system of coupled differential equations, one for each species involved. The R values have to be calculated stepwise iteratively. The same procedure is applied for the porosity and for v_D where changes are the result of convergence and/or dissolution and precipitation processes.

For solving the problem, initial and boundary conditions are required: These include the initial concentrations of all involved components, as well as initial porosity and flow rate. Boundary conditions reflect either constant boundary concentrations or zero fluxes at the model boundaries.

A specific problem is connected with application of dispersion in advective transport. In this case, diffusion constants are replaced by effective dispersion coefficients depending on permeability, tortuosity, diffusion constant and the flow rate. According to Bear [4], the numerical values are derived for a large range of Peclet numbers Pe (eq. 5).

$$Pe = \frac{d_{\text{grain}} \cdot v_D}{(\Phi \cdot D)} \quad (\text{eq. 5})$$

d_{grain} : average grain diameter.

In principle, TRANSAL is able to deal with different diffusion/dispersion constants for each species. For charged species, however, charge-neutrality will not be maintained. This effect has also to be considered, if surface complexation is modelled where counter ions show different mobility than the sorbed species.

Thermodynamic equilibrium

Local (spatial and temporal) equilibrium between dissolved and solid (immobile) phases are calculated by mass balance and mass action equations. For a given inventory of n basic components a non-linear equation system has to be solved.

$$B_j + \sum_{i=1}^{n_c} v_{i,j} \cdot c_i + \sum_{k=1}^{n_s} v_{k,j} \cdot P_k = B_{\text{tot},j} \quad (\text{eq. 6})$$

$$(\gamma_i \cdot c_i)^{-1} \cdot \prod_{j=1}^{n_b} (\gamma_j \cdot B_j)^{v_{i,j}} = K_i \quad (\text{eq. 7})$$

$$\prod_{j=1}^{n_b} (\gamma_j \cdot B_j)^{v_{k,j}} = K_k \quad (\text{eq. 8})$$

B_j : concentrations of n_b basis components
 c_i : concentrations of n_c aquatic complexes
 P_k : concentrations of n_s solid/gaseous phases
 B_j^{tot} : total conc. of basic component
 $v_{i,j}$: stoichiometric coefficients
 K_i : complexation constant of complex i
 K_k : solubility product of solid/gas k

The non-linearity comprises additionally the activity coefficients γ_j , as these coefficients depend on the ionic strength non-linearly. All concentrations in each increment are varying as function of the transport processes and sources.

For treating concentrated salt solutions, the activity coefficients γ_j are calculated by means of the Pitzer formalism [5].

In TRANSAL parts of the THCC code [6] are used to solve the speciation/reaction problems.

Reaction kinetics

Many cases are observed where the adjustment of the thermodynamic equilibrium is delayed or hindered compared to the rate of changes caused by transport processes. In TRANSAL, rate laws are implemented for complexation in solution and for dissolution and precipitation reactions. Numerical treatment of aquatic complex kinetics in TRANSAL is performed by applying space and time depending factors to the equilibrium constants which are suitably adapted during the iteration process.

Sorption modelling

In TRANSAL, sorption, surface complexation and surface precipitation can be modelled by thermodynamic equilibrium calculations analogue to the aquatic species and solids. However, calculation of electrical surface potentials is needed. This is performed according to the constant capacity model. Sorption equilibrium for a species is given by eq. 9.

$$(c_i)^{-1} \prod_{j=1}^{n_b} (B_j)^{v_{i,j}} = K_i \cdot e^{-\frac{zF\Psi}{kT}} \quad (\text{eq. 9})$$

for the surface potential Ψ

$$\Psi = \frac{F}{s \cdot a \cdot C} \cdot \sum (z_j \cdot c_j) \quad (\text{eq. 10})$$

s: specific surface, a: conc. of sorbed species, z: (transferred) charge, C: specific capacity, F:

Faraday constant, k : Boltzmann constant, T : temperature.

The term $\Sigma(z_j \cdot c_j)$ takes into account all charged surface complexes. In the list of basic species, one represents the concentration of sorption sites. The complexation constant K_i is used as intrinsic constant. Multiplication with the exponential term results in the apparent complexation constant K_i^{app} . TRANSAL treats surface complexes as immobile species. The counter ions are part of the mobile aqueous system. Deviations from electro-neutrality are expected to be small even for higher concentrated solutions.

Sorption modelling using different sorption sites or applying other sorption modes are not yet implemented in TRANSAL.

Modelling of general metal corrosion

In contrast to the conditions of non-conductive solids, the surface potential of metallic surfaces is not controlled by sorbed species. The potential is adjusted according the condition of a balance between anodic and cathodic electrode currents. For iron (steel) the following currents are considered in TRANSAL:

- anodic reaction of Fe dissolution
- cathodic current density of H_2 formation by H^+ reduction
- cathodic current density of H_2 formation by water decomposition and reduction
- cathodic current density of O_2 reduction

The current densities are related to the species flux densities by eq.11.

$$i = j_s \cdot n \cdot F \quad (\text{eq. 11})$$

n : number of electrons, These reactions are implemented by application of sources and sinks of involved species in TRANSAL.

Applications

Various applications were computed with TRANSAL. However, only few measurements are available for testing modelling results against experimental findings. One of the first test cases considered the flow of salt brines along a temperature gradient in a rock salt high-level waste repository.

Experimental verification

For modelling of corrosion processes of metallic disposal canisters in close contact with backfill materials, TRANSAL was applied, first results are presented elsewhere [7]. The corrosion phenomena are considered by electrochemical corrosion rates and electrical

potentials. Validation of the code was performed by modelling counter diffusion experiments where Fe^{2+} and OH^- are diffusing in a porous medium [8]. Narrow precipitation zones of $Fe(OH)_2$ or "green rust" and magnetite were predicted and observed in experiments over periods of almost 1 year.

The code was applied to modelling different corrosion experiments in salt brines at temperatures up to $150^\circ C$. Results of these calculations showed only in the initial phase (< 1 year) variations in the solution compositions close to the metal surface. During this relatively short period, protective layers can be formed influencing the long-term corrosion rates. This also provides information for conditioning the near-field in a repository to increase life-time of canisters.

Radionuclide retention by a corroded canister

In many PA studies, canisters are considered in a rather simplified approach: As long as a canister is intact, release of radionuclides is zero, after a certain time after disposal, retention by a canister is neglected, completely. This approach is in contradiction to observations of radionuclide retention onto iron oxides/hydroxides. The source term for radionuclides depends on the geochemical boundary conditions. Based on results of various investigations a geochemical modelling approach by means of TRANSAL is adapted to provide for radionuclide concentrations including speciation inside and outside of a corroded steel iron canister. This work is part of the integrated EU Project PAMINA. The approach will be valid for different types of host rocks and groundwater compositions. The approach will take into account interactions between groundwater and waste/canister materials, dissolution, precipitation and sorption processes. Calculations are performed by coupled reactive codes for specific concentrations of sorption/redox sites and mobilized U(VI).

First calculations were performed for transport of the radionuclides and their retention by a corroded canister in a one-dimensional geometry having a total length of ~ 10 m. The region was divided into 3 material zones. The inner zone (10 cm) consists of spent nuclear fuel which slowly dissolves by radiolytic oxidation. The adjacent zone (10 cm) is treated as corroded canister material (Fe_3O_4 , having an estimated concentration of sorption sites of $10^{-5} \text{ mol (kg H}_2\text{O)}^{-1}$). This zone is followed by the geo-matrix (10 m). The whole region is divided in 4 + 4 + 12 increments. Diffusion is

assumed as the only relevant transport mechanism. The flux at the model boundaries is set to zero. It is assumed that the zone of spent fuel has a porosity of 5 %. The other model zones provide a porosity of 10 %. All zones and species have the same diffusion properties. A constant UO_2 release from the spent fuel in zone 1 ($10^{-10} \text{ mol (kg H}_2\text{O)}^{-1} \text{ s}^{-1}$) is used in the model. In the first calculations only thermodynamic equilibrium reactions are considered. For the complexation reactions 13 species, for sorption 6 species ($\equiv\text{S-OH}$, $\equiv\text{S-OH}_2^+$, $\equiv\text{S-O}^-$, $\equiv\text{S-OFe}^+$, $\equiv\text{S-OFeOH}$, $\equiv\text{S-OUO}_2\text{OH}$) are taken into account and precipitation/dissolution of 8 solids is modelled. Uranium reduction is involved by implementing the redox couples $\text{U}_{\text{IV}}/\text{U}_{\text{VI}}$ and $\text{Fe}_{\text{II}}/\text{Fe}_{\text{III}}$. The pore water used in the calculation is anoxic and its main components are Na^+ , Cl^- , and Fe^{2+} . The initial pH is 9.6 in contact with the corroded Fe. Calculations are performed over a period of 50000 years.

After about 10000 years the calculated concentrations of U_{IV} and U_{VI} species of the pore water in the geo-matrix are nearly constant (Fig. 1). Due to the model boundary conditions the precipitation of schoepite only occurs in the zone of the spent fuel. This process continues to the end of the period under investigation. Mass balance studies and application of realistic sorption site density are not yet completed.

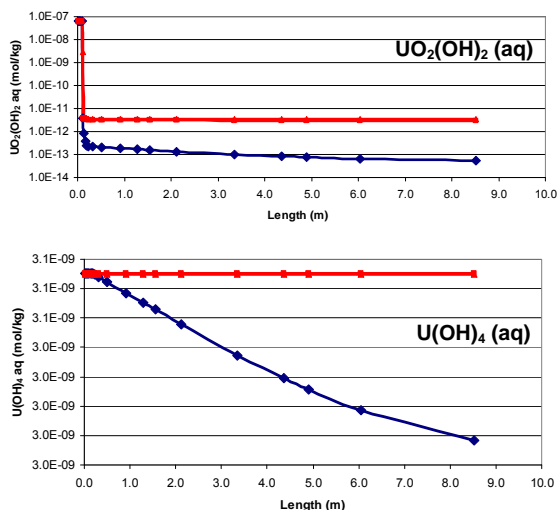


Fig. 1 Modelled concentrations of the aqueous species $\text{UO}_2(\text{OH})_2$ and $\text{U}(\text{OH})_4$ after 3000 (blue line) and 10000 (red line) years

Redox phenomena

For performance assessments, modelling of redox phenomena has not been developed to a level comparable to geochemical modelling

or transport modelling. The reason is that the redox potentials are not necessarily controlled by thermodynamics but to a large extent by kinetics. In general, different redox couples are simultaneously present in the groundwaters such as $\text{Fe}(\text{II})/\text{Fe}(\text{III})$, $\text{H}_2(\text{g})/\text{H}^+$, and $\text{O}_2(\text{g})/\text{H}_2\text{O}$, sulphate/sulphide, methane/carbonate. Most of these couples are kinetically hindered and are not in a thermodynamic equilibrium state. Reactions may be strongly retarded or inhibited. Complexity increases significantly, if redox sensitive surfaces are in contact with the groundwater. In these cases, the surface areas, coatings of the surfaces, etc. are assumed to dominate the effective redox system. In geochemical modelling codes, the redox state is usually calculated by the $\text{H}_2(\text{g})$ and $\text{O}_2(\text{g})$ partial pressures, which means by kinetically hindered redox couples.

TRANSAL provides with specific utilities for kinetically controlled processes is used to model these phenomena.

Summary

TRANSAL was developed to treat a series of specific problems in geochemically, and transport/kinetically controlled processes in context with high-level waste disposal. TRANSAL is coded in Fortran and runs under UNIX and LINUX. Computation time depends on the actual problem: Model calculations shown in Fig. 1 - migration of $\text{U}(\text{VI})$ through a corroded canister under consideration of reductive sorption and precipitation - requires about 2 weeks for a 50000 years period on a LINUX cluster.

References

- [1] Schmidt-Döhl, F., *Ein Modell zur Berechnung von Kombinierten chemischen Reaktions- und Transportprozessen und seine Anwendung auf die Korrosion mineralischer Baustoffe*. IBMB (Institut für Baustoffe, Massivbau und Brandschutz der TU Braunschweig) 1996. **125**.
- [2] Bethke, C.M., *"The Geochemist's Workbench" Rel. 6.0*. 2006, Rockware, Inc.: Golden, USA.
- [3] Müller-Lyda, I., H. BIRTHLER, and E. FEIN. *A permeability-porosity relation for crushed rock salt derived from laboratory data for application within probabilistic long-term safety assessment*. in *DisTec'98*. 1998. Hamburg: Kontec.
- [4] Bear, J., *Dynamics of Fluids in Porous Media*. Environmental Science Series, ed. A.K. Biswas. 1972, New York: American Elsevier Publishing Company, INC.

[5] Pitzer, K.S., *Activity coefficients in electrolyte solutions*. 2. ed. 1991, Boca Raton: CRC Press.

[6] Carnahan, C.L. *Simulation of Uranium Transport with Variable Temperature and Oxidation Potential: The Computer Program THCC*. 1987. Mat. Res. Soc. Symp. Proc. 84.

[7] Korthaus, E. *Code development for modelling of coupled effects at corrosion of carbon steel containers under repository conditions*. in *TRePro 2002 - modelling of coupled transport reaction processes*. 2002.

Forschungszentrum Karlsruhe 20th and 21st of March 2002: Forschungszentrum Karlsruhe.

[8] Seher, H., *Gegendiffusionsexperimente zur Bildung sekundärer Eisen(II)-Phasen aus wässrigen Lösungen in einer chemisch inerten porösen Polyethylenmatrix: Experimentelle Validierung geochemischer Modellrechnungen*, in *Lehrstuhl für angewandte Geologie*. 2005, Universität Karlsruhe.

6. Development of speciation methods: Speciation of actinides at trace concentrations

The application of sensitive speciation techniques is crucial for the elucidation of radionuclide reactions on a molecular level. INE made a lot of efforts in the past and will continue this strategy in the future to further develop advanced tools for the characterization of radionuclide species. Activities at INE's dedicated actinide beamline are summarized. Experiments on corundum surface characterization by sum frequency vibrational spectroscopy have been continued and for the first time, spectroscopic findings have been correlated with theoretical quantum chemical calculations. Polymerization and colloid formation belongs to the predominant reactions of tetravalent elements in solution. Those reactions have now been followed successfully by electrospray mass spectrometry and EXAFS for Zr. Further studies will now focus on the tetravalent actinides. Various examples are given in the last section for the implementation of theoretical quantum chemical calculations in order to interpret or complement experimental spectroscopic findings.

6.1 The INE-Beamline for Actinide Research at ANKA

Melissa A. Denecke, Boris Brendebach, Kathy Dardenne, Jörg Rothe

Introduction

The INE-Beamline at the FZK synchrotron source ANKA completed its first full year of operation in 2006. Official operation commenced on Oct. 1st, 2005. A major activity of INE-Beamline personnel was dedicated to perform in-house research and support for external users. In addition, a number of upgrades were installed and tested in 2006. The beamline also serves as a learning center and in 2006 it hosted students for training in practical laboratory work and two international workshops. The following report summarizes these activities, concentrating on 2006 highlights. In addition, an outlook of improvements and upgrades planned for the near future is given at the conclusion.

In-house research

The INE-Beamline is designed to ensure variability, in order to optimize the diverse actinide speciation applications associated with safe disposal of high level nuclear waste. The in-house research investigations performed in 2006 involve a broad range of themes including, for example, colloid formation and stability [1], actinide oxide/hydroxide solubility [2], characterization of actinide oxides as nano-sized particles and as thin films down to monolayers [3], identification of corrosion products on UO₂ fuel pellets, studies of actinide incorporation into secondary phases [4], characterization of partitioning ligand-actinide complexes [5], and combined XAFS and XRD investigations (cf., next section) [6]. The results of many of these investigations can be found elsewhere in this report. The following two examples are selected highlights of these activities.

Discovery of ternary Ca-M(IV)-OH complexes:

New aqueous ternary Ca-M(IV)-OH complexes have been characterized using EXAFS [2]. Ca₃[Zr(OH)₆]⁴⁺ is comprised of a distorted [Zr(OH)₆]²⁻ octahedron surrounded by three edge bound Ca²⁺ ions. The Ca₄[Th(OH)₈]⁴⁺ coordination structure is derived from the fluorite-type structure in solid actinide dioxides MO₂(cr), with four Ca²⁺ ions distributed over the edges of the central [Th(OH)₈]⁴⁻ cubic polyhedron. Formation of these ternary Ca_n[M(OH)_m]^{4+2n-m} complexes leads to unexpectedly high Zr(IV) and Th(IV) hydrous oxide solubilities in alkaline CaCl₂ solutions. Stabilization of anionic M(IV) hydroxide complexes via ion pair formation observed in these hitherto unknown species may be a general phenomenon with significant impact on the solubility and aqueous speciation of actinide ions that deserves further investigation.

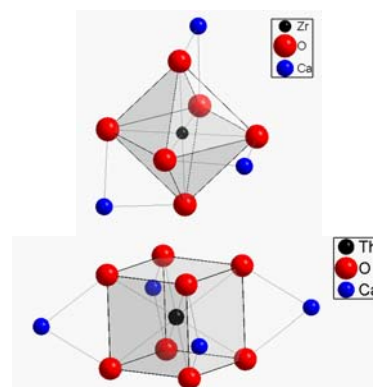


Fig. 1 Idealized coordination structures for aqueous Ca₃[Zr(OH)₆]⁴⁺ (top) and Ca₄[Th(OH)₈]⁴⁺ (bottom) complexes. Hydrogen atoms omitted for clarity.

Combined quantum chemical and EXAFS study of the coordination structure of metal-PAA complexes:

Results from scanning transmission X-ray microscopy (STXM) and C 1s-NEXAFS studies of metal ion complexation with a simple model polymer for humic acids, polyacrylic acid (PAA), indicate a stronger uranyl cation-ligand molecule interaction than the metal cation-ligand interaction in Eu(III)-PAA.

U and Eu L3-edge EXAFS analysis combined with density functional theory (DFT) level energy minimization calculations using the TURBOMOLE package reveal this to be associated with differences in primary metal cation-PAA interaction [7]. Eu(III) is coordinated by four water molecules and four carboxylate groups in a monodentate fashion in the aqueous Eu(III)-PAA complex. There are three bidentate coordinated carboxylate groups in the equatorial plane of the dioxo cation in the UO_2^{2+} -PAA complex, resulting in a molecular structure similar to that in crystalline $\text{UO}_2(\text{C}_2\text{H}_3\text{O}_2)_3$. This investigation is an example of INE's present efforts to combine experimental with theoretical, quantum chemical methodology.

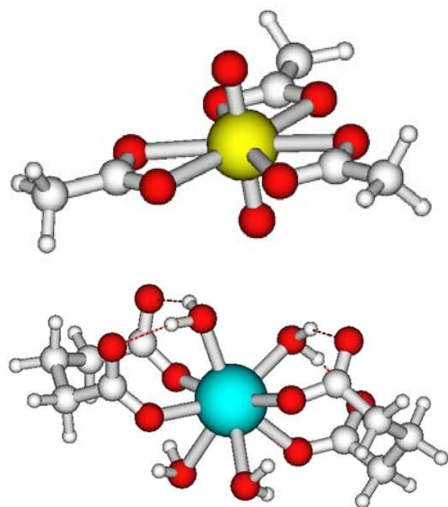


Fig. 2 UO_2^{2+} -PAA and Eu(III)-PAA molecular structure from *ab initio* energy minimization calculations and EXAFS analysis.

External users

A total of thirteen external groups came to use INE-Beamline in 2006. Their investigations and results led to eleven contributions to the ANKA Annual Report 2006. External users of the INE-Beamline obtain access essentially via three routes: as an approved ACTINET project, through the ANKA proposal system, or via cooperation with INE. The INE-Beamline and

INE active laboratories are one of the pooled facilities of the EU European Network of Excellence for Actinide Science (ACTINET) and eight groups with team members from six different countries (Germany, England, Sweden, France, Hungary, and Russia) performed experiments at the beamline via this avenue in 2006. A portion of annual beamtime at the INE-Beamline (30%) is available through the standard ANKA facility proposal procedure (for detailed information see [8]). A number of external users obtaining access through the ANKA proposal system were students and young researchers from near lying universities and from institutions on the FZK campus. A measure of the INE-Beamline's success is a doubling of requested beamtime for INE-Beamline proposals for the first cycle of 2007, compared to the last ANKA proposal period. Access to the INE-Beamline is also possible through cooperation with INE. The strongest such cooperation is between INE and the Universität Bonn, Physikalisches Institut (PI-Uni Bonn). As in the past, cooperation in 2006 was not limited to use of the INE-Beamline by students from PI-Uni Bonn, but also continued efforts in instrumentation development and beamline improvement.

Some of the external user investigations performed in 2006 represent advances and/or are highlights at the beamline. For example, a group from the French CNRS – Laboratoire de Chimie Métallurgique des Terres Rares and CEA Valduc performed experiments at the Pd

Cooperation at the INE-Beamline

External groups involved in experiments at the INE-Beamline in 2006:

- Universität Bonn, Physikalisches Institut
- Universität Mainz, Kernchemie
- TU München, Radiochemie
- Institute for Transuranium Elements
- FZK-INT
- FZK-ISS
- Kungliga Tekniska Högskolan (KTH), Stockholm (ACTINET)
- Lomonosov Moscow State University (ACTINET)
- Institute de Recherches Subatomiques, Strasbourg (ACTINET)
- CNRS – Lab. de Chimie Métallurgique des Terres RaresSubatech, Nantes (ACTINET)
- University of Manchester (ACTINET)
- CEA Grenoble (ACTINET)

K-edge (24.35 keV) on tritium containing Pd^0 , PdT_x , to study structural defects from ^3He formed upon tritium decay. Because of the tritium in the samples, these investigations are not possible elsewhere in Europe. In addition, this experiment was performed at energies above the absorption edge of the beamline optics mirror coating (Rh K = 23.22 keV), showing that the INE-Beamline can deliver sufficient photon flux at these higher energies.

Upgrades and improvements

Numerous beamline improvements were made and upgrades installed in 2006. These include a Quick-XAFS mode of operation, commissioning of a CCD camera for beam spot characterization, optimization of instrumentation for low energy studies down to the P K-edge (2.1 keV), development and testing of a position sensitive XRD detector for combined XAFS/XRD investigations, and acquisition and initial tests of a hexapod positioner for planned micro-focus capabilities. Specific information of selected improvements/upgrades follows.

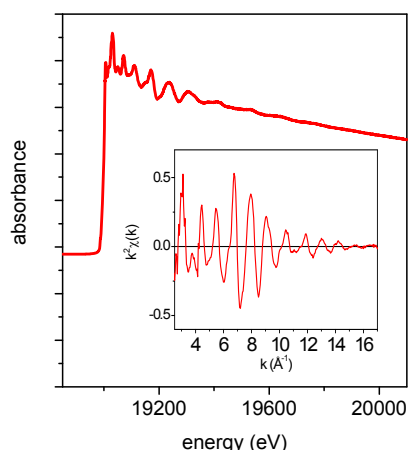


Fig. 3 First Quick-XAFS of a Nb foil at the INE-Beamline. Measuring time=60s.

A special data acquisition mode allowing investigations of dynamic processes, Quick-XAFS, was installed and successfully tested this year at the INE-Beamline. Initial tests showed remarkably good measurement statistics out to a k -value of 17\AA^{-1} for a Nb^0 foil recorded in 60 s.

A CCD camera (SESO, Aix-en-Provence) is now installed at the INE-Beamline to be used for beam characterization. It allows optimization of optic component geometry and subsequent measurement of beam spot dimensions. The measured beam spot at 12 keV is $500\mu\text{m}$ in diameter (1σ -width), with an approximate Gaussian profile in both the horizontal and vertical dimensions. Using the

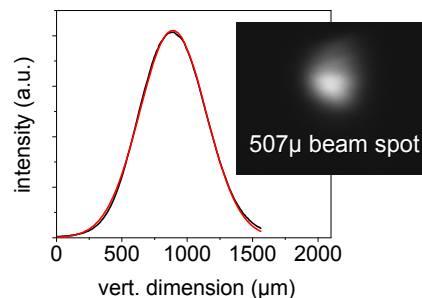


Fig. 4 Beam spot CCD image (right); measured vertical profile (--) and Gaussian fit (--).

CCD camera signal, beamline components were re-adjusted to minimize beam spatial drift at the sample position over a broad energy range. Typically there is less than $50\mu\text{m}$ vertical beam drift and about $200\mu\text{m}$ horizontal drift over a typical EXAFS spectral range. The optimized beam, focused by the toroid mirror, will enable getting as much possible flux into a micro-focusing optic aperture for planned micro-focus capabilities of the beamline.

INE has designed and constructed an inexpensive position sensitive XRD setup for performing combined XAFS/XRD investigations using flexible image plates made of radiation sensitive, europium-doped barium fluoride films with a high dynamic range. The image plates are mounted on a curved holder with a 8 mm exposure slit and can be automatically shifted across the slit, thereby allowing around 10-12 exposures onto one film plate. The films are read out using a scanner with a laser beam and can be re-used after exposure to day UV-light. First test measurements of Y_2O_3 , with quartz added as internal calibrant for the 2θ -axis, at the Y K-edge and using 0.727\AA XRD photon wavelength gave good results.

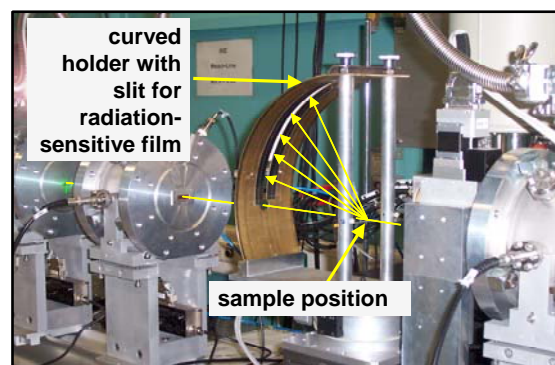


Fig. 5 Self-built combined XAFS/XRD setup. Incoming, transmitted and diffracted beam paths indicated as thin lines.

The INE-Beamline as learning center

Beamline staff members taught and experiments were performed at the INE-Beamline during recurring courses in 2006: FTU's Radioisotopenkurs/Radiochemisches Praktikum and the graduate course for mineralogists held by the Deutsche Mineralogische Gesellschaft. In 2006 two doctoral candidates and one "Diplom" student finished their theses, which included work performed at the INE-Beamline [9, 4]. In addition to recurring educational activities, a three day ACTINET sponsored workshop "ACTINET Workshop on Actinide Speciation using XAFS" was held at the beamline in March 2006. This workshop provided individualized training in planning and conducting actinide XAFS speciation experiments, as well as in evaluating and interpreting the data, for students and young researchers in small groups. In September 2006 INE hosted the "4th Workshop on Speciation, Techniques, and Facilities for Radioactive Materials at Synchrotron Light Sources, Actinide-XAS-2006". The Actinide-XAS series addresses the specialized field of the application of synchrotron techniques for investigating radioactive materials and is a forum for scientific discussion, thereby strengthening existing and establishing new transnational cooperative scientific networks. Nearly 70 participants from seven European countries, Japan, and the USA presented more than 30 talks and over 30 posters in six topical



Fig. 6 Participants of the Actinide-XAS-2006.

sessions comprising the workshop, covering a wide spectrum of research fields including fundamental aspects of the chemistry and physics of the actinide elements, as well as applied studies of radioactive materials. The workshop proceedings are being published by the Nuclear Energy Agency (NEA) and are now in print.

Outlook for 2007

Instrumentation development and upgrades planned at the INE-Beamline for 2007 are related to lowering the attainable energy,

implementing a microfocus option at the beamline, and designing new sample holders for special requirements. The Be window separating the ANKA storage ring and first mirror vacuum from the rest of the beamline will be replaced by a thinner 50 μm thick Be window. The Be window thickness and its inherent absorption is the determinant factor for the lower energy limit. An InSb monochromator crystal pair will be acquired and tested to reach energies down to the Si K-edge (1.8 keV). A number of improvements will be made in order to implement a microfocus option. One is an upgrade of the beamline detector electronics from analogue to digital. Storing complete fluorescence radiation in digitized form will enable construction of elemental distribution maps through multi-line peak fitting of digital data collected using a focused beam in a scanning mode. It also offers other advantages such as increased sensitivity and a method for dealing with overlapping fluorescence lines. A number of different μ -focusing optics (polycapillary, monicapillary, compound refractive lenses) will be tested in 2007. First tests will involve using new one dimensional focusing planar CRLs, fabricated at the FZK-Institute for Microstructure Technology (IMT), as a virtual slit in surface sensitive grazing incidence measurements. At least two new sample environments will be tested in 2007. First a cryostat capable of cooling down to liquid nitrogen temperatures will be fitted with a special sample containment for radioactive materials. The cryostat / sample containment system will be tested on a previously investigated crystalline solid solution. The second sample environment to be developed is an upgrade of an already existing inert gas purged holder for air sensitive samples. This system worked successfully for transporting U(III) solution samples to the beamline and their subsequent investigation over at least five hours [5]. The new system will be easier to load and mount onto the positioning instrumentation at the beamline.

Acknowledgements

Cooperation with FZK-ISS, especially the computing group headed by W. Mexner for development of the Quick-XAFS mode, is acknowledged with gratitude. Part of the INE-Beamline development is a contractual cooperation between FZK-INE and the Physikalisches Institut, Universität Bonn.

References

- [1] C. Walther, J. Rothe, M. Fuss, S. Büchner, S. Koltsov, T. Bergmann, *Anal. Bioanal. Chem.* 2007 (in print).
- [2] B. Brendebach, M. Altmaier, J. Rothe, V. Neck, M.A. Denecke, *Inorg. Chem.* (submitted).
- [3] In cooperation with ITU and Lomonosov Moscow State University, Radiochemistry.
- [4] F. Heberling, Diplom thesis, "*Structural Incorporation of Neptunium(V) into Calcite*", Institut für Geographie und Geoökologie der Universität Karlsruhe(TH), 2006.
- [5] M.A. Denecke, F. Burdet, M. Weigl, M. Mazzanti, *Compte Rendu Chimie Académie des Sciences Special Issue "Nuclear Energy and Radiochemistry"* (invited contribution, accepted).
- [6] B. Brendebach, K. Dardenne, M.A. Denecke, J. Rothe, (accepted American Institute of Physics publication).
- [7] J. Rothe, M. Plaschke, B. Schimmelpfennig, M.A. Denecke, Proceedings to the 4th Workshop on Speciation, Techniques, and Facilities for Radioactive Materials at Synchrotron Light Sources, Karlsruhe, Germany, 18.-20. Sep. 2006.
- [8] <http://ankaweb.fzk.de/>
- [9] Doctoral theses by Hye-Ryun Cho "*Chemistry of tetravalent plutonium and zirconium: hydrolysis, solubility, colloid formation and redox reactions*" and M. Marques-Fernandez "*Spektroskopische Untersuchungen (TRLFS und XAFS) zur Wechselwirkung von dreiwertigen Lanthaniden und Actiniden mit der Mineralphase Calcit*", both completed for the Naturwissenschaftlich-Mathematische Gesamtfakultät der Ruprecht-Karls-Universität Heidelberg, 2006.

6.2 Speciation of the Functional Groups at Mineral/Water Interfaces Probed by Vibrational Sum Frequency Spectroscopy and Quantum Chemistry

M. Flörsheimer, R. Polly, K. Kruse, A. Abdelmonem, B. Schimmelpfennig, R. Klenze

Introduction

The adsorption of radioisotopes at mineral surfaces of the aquifer is an important process which leads to the retention of the contaminants. That means that their transport by the ground water is either suppressed or considerably slowed down. For the reliable long-term modelling of the elements' migration, the adsorption/desorption properties and the reactivity of the mineral surfaces must be understood at the molecular level.

The interaction of a mineral with an electrolyte is controlled by the surface functional species. We use sapphire ($\alpha\text{-Al}_2\text{O}_3$) as a model mineral which is related to natural clay minerals and analogous iron phases. At the surfaces, there are aluminol groups. At a sapphire (001) surface, for example, a single type of a doubly coordinated OH species (see middle formula in Fig. 1) is expected to occur [1]. The most basic

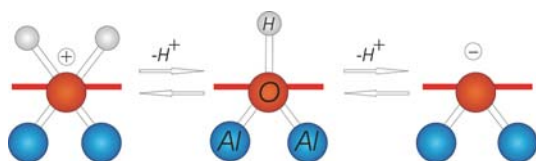


Fig. 1 Scheme of sapphire/water interface, protonation and deprotonation of aluminol species

and most important reaction of the surface functional species is their protonation and deprotonation which occurs upon the change of the pH of the water. As a result, the surface properties change dramatically, for example the interaction capability with actinide and lanthanide ions. In our combined experimental and theoretical study we observe a surprising diversity of species and unexpected processes at the interface leading to a picture of the interface at the molecular level which is much more detailed as compared to the simple model assumed in Fig. 1.

Vibrational Sum Frequency Spectroscopy

In the sum frequency (SF) experiment (scheme see inset of Fig. 2a), a crystallographically well-defined cut of a single crystalline mineral is in contact with the electrolyte. The interface is illuminated with intense light from two lasers. Due to the high intensities, photons from the

two beams can couple to the sample at the same time in order to generate photons at the sum of the individual frequencies. This SF signal [2] can always be generated at a surface or an interface due to the polar order of its electric dipoles. In the bulk of centrosymmetric media such as water or sapphire, however, SF generation is symmetry forbidden. As a result, we obtain SF light selectively from the mineral/water interface and from the polar water film adjacent to the mineral surface. Additionally one of the lasers is tunable over a large region of the infrared (IR) spectrum. Due

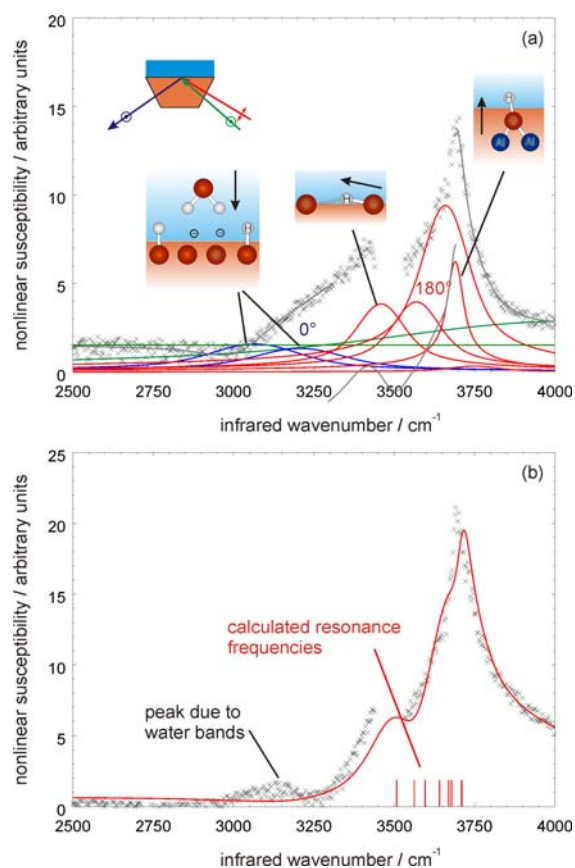


Fig. 2 (a) Sum frequency spectrum of sapphire (001) surface under water at pH 12 together with scheme of experiment, result of deconvolution and with interpretation. (b) Comparison of measured data (pH 6) with spectrum calculated from independent results of quantum chemical theory. The excellent agreement proves that our molecular picture is adequate. The arrows in (a) indicate the dipoles of the OH species.

to the interaction of the IR light with the sample the SF spectrum provides information on the vibrational resonances of the surface species.

Fig. 2a gives the OH stretch region of the SF spectrum obtained from a sapphire (001)/electrolyte interface at pH 12 (ionic strength $I = 50$ mM, NaCl). The black crosses are the measured data points. Fig. 2a shows also a fit to the data, the deconvolution of the spectrum and a few molecular models as interpretation.

In the nonlinear optical experiment, we consider the field of the generated SF light as the signal. The deconvolution of the spectrum leads to the magnitudes of the contributing bands (red and blue lines in Fig. 2a) and to their phases indicated in Fig. 2a for the resonance maxima. This phase information, which cannot be obtained in the corresponding linear optical experiment, provides information on the absolute orientation of the molecular dipoles which are responsible for the generation of the signal.

The two blue bands in Fig. 2a are due to the polar water film near the mineral surface which is well known from various aquatic interfaces [2]. At high pH, our spectrum shows that the water dipoles point into the direction of the mineral surface (phase 0°). This is consistent with the negative surface charge which we expect at high pH.

Additionally we observe a surprisingly large number of additional bands (red curves in Fig. 2a) which are due to different aluminol species. From the spectral position of the four species with resonance maxima between 3460 and 3690 cm^{-1} , we conclude that their OH groups are doubly coordinated. We have also measured their surface concentrations as a function of the electrolyte's pH as well as the axial orientation of their OH bonds (quantitative comparison of spectra obtained with different polarizer orientations). The result is:

- The tilt angles of the OH bonds with respect to the surface normal increase with decreasing wavenumber (two species shown in Fig. 2a)
- The concentrations of the species with larger tilt angles (three species with resonances between 3460 and 3660 cm^{-1}) increase considerably with decreasing pH.

It can be expected that the difference in the tilt angles leads to different properties of the aluminol species. With increasing tilt angle, the oxygen atom, which is a hydrogen bond acceptor, becomes better exposed to neighboring molecules such as water.

We have also studied the absolute polar orientation of the water molecules adjacent to the mineral surface as a function of the pH. From the simple model of surface charging given in Fig. 1, we expect flipping of the dipoles upon passing the point of zero charge. Actually, however, we observe repeated flipping. At medium pH, the net water dipole points into the water phase. Between pH 1.3 and 4, the net dipole orientation, however, is the same as in Fig 2a (high pH). This phenomenon cannot be explained with electrostatic interactions. It must be due to hydrogen bonding which dominates the mineral/water interaction within a large pH range. Two populations of hydrogen bonded water molecules are expected which differ in their orientation:

- At low pH (high concentrations of aluminol species with large tilt angle), we expect an increased concentration of water molecules with their hydrogens attached to the oxygens of aluminol species leading to a net dipole moment of this population which points to the mineral surface. This expectation is in agreement with the measured phase of the SF signal.

- At medium pH (larger concentrations of aluminol species with small tilt angle), we expect the dominance of a water population whose oxygens interact as hydrogen bond acceptors with the surface species so that the arising net water dipole moment points into the water phase in agreement with the measured phase of the water signal.

The interpretation of the SF data leads to a detailed, consistent model. For a verification, we need, however, the results of an independent method.

Quantum Chemical Calculations

For the task of supporting and confirming the experimental results we complemented the experimental study of the functional groups at the mineral/water interface with a quantum chemical investigation of the problem. This allows a better insight into and a better understanding of the problem. Experimentally the sum frequency spectrum and a correlation between the tilt angles and the vibrational frequencies are observed.

The quantities of interest to understand/simulate the observed spectrum are the harmonic vibrational frequencies, the tilting angles and the dipole moments of the OH groups. These can be readily obtained by means of ab initio or DFT calculations. Details

on the calculations and structural results are presented in section 6.4 of this report.

Applying these methods we determined the structures of several small Al/O clusters (Al_4O_6 , Al_8O_{12} , $\text{Al}_7\text{O}_{12}\text{H}_3$) with MP2, CCSD(T) and DFT. The frequencies were obtained by means of MP2 and DFT. This assessment of the quality of the DFT results showed that this method is well suited to describe the quantities of interest in this study.

As a model for the calculation we used a $\text{Al}_{20}\text{O}_{38}\text{H}_{12}$ cluster. This model represents the sapphire (001) surface around the point of zero charge. All the OH species in the model are doubly coordinated. The calculation shows that they differ in their OH tilt angle. With increasing tilt angle of the species their OH resonance frequency decreases as observed experimentally. Using the theoretical angles and resonance frequencies we calculated also the expected SF spectrum (red line in Fig. 2b) For a comparison we select the experimental spectrum taken at pH 6 (point of zero charge).

The excellent agreement of the measured and the simulated spectrum shows that the chosen model is a realistic representation of the surface. Most recently we have also included water molecules into the calculations and observed the two populations of hydrogen bonded molecules as proposed above.

Therefore these calculations represent a completely independent theoretical proof of the experimental findings. All experimentally observed features can be theoretically reproduced and confirmed.

Conclusion and Outlook

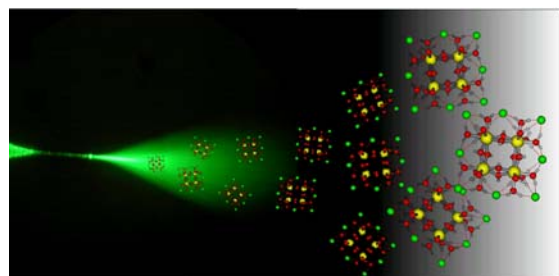
Applying two independent methods we obtained a detailed, consistent model on the speciation of the functional groups of a mineral surface and on the interaction of the functional species with the adjacent water molecules. In the next steps we include actinide ions as well as organic molecules

References

- [1] V. Barrón, J. Torrent, J. Colloid Interface Sci, 177, 407 (1996)
- [2] Y. R. Shen, Surface Properties Probed by Second-harmonic and Sum Frequency Generation, Nature, 337, 519-525 (2004).
- [3] G. L. Richmond, Molecular Bonding and Interactions at Aqueous Surfaces as Probed by Vibrational Sum Frequency Spectroscopy, Chem. Rev. 102, 2693-2724 (2002).

6.3 Direct observation of polynuclear Zr(IV) hydroxide complexes in solution by nano-electrospray MS and EXAFS

S. Büchner, M. Fuß, J. Rothe, C. Walther



Introduction

Zr(IV) is well known for forming polynuclear hydroxide species in solutions of millimolar concentration [1]. In particular the tetramer, $Zr_4(OH)_8^{8+}$, is a dominating species even at rather high acidity. Knowledge of the species distribution as function of pH and Zr(IV) concentration is a prerequisite for the correct interpretation of solubility data and the evaluation of measurements on the solubility of Zr(IV) amorphous hydroxide. A previous study by LIBD and EXAFS suffered from exactly this lack of information [2]. Nano-electrospray time-of-flight mass-spectrometry [3, 4] (ESI TOF) was used in the present work for measuring the species distribution of $Zr_x(OH)_y^{4x-y}$ (short: (x,y)) complexes in acidic solution.

Sample preparation and experimental methods

Samples ($1\text{mM} < [Zr(IV)] < 10\text{mM}$, $0.3 < \text{pH}_C < 3$) were prepared by dissolving $ZrOCl_2 \cdot xH_2O$ in hydrochloric acid of required pH_C . $1\mu\text{l}$ aliquots were filled into nanospray capillaries and measured by ESI TOF. In order to minimize the invasiveness of the electrospray process the source was operated at very mild declustering conditions, *i.e.* during the transfer into the vacuum the Zr(IV) complexes were not completely stripped but retained a shell of ca. 20 solvent molecules. (For further experimental details see [5]). The time-of-flight mass-spectrum, more precisely the mass-to-charge ratio of the ionized species of the sample at $[Zr]=2.5\text{mM}$, $\text{pH}_C 0.2$ is shown in Fig.1 (top) in a logarithmic representation. Three major species are distinguished: the hydrolyzed monomers (1,y), the tetramers (4,9) and the pentamers (5,11). The charge of the complexes is partly compensated by chlorine ions (see Fig.2). Due to the varying number of water molecules, the peaks group into clusters (Fig1, middle). Further magnification (bottom) reveals a substructure (black: measured data) due to the natural isotope distributions of Zr and Cl, which agrees well

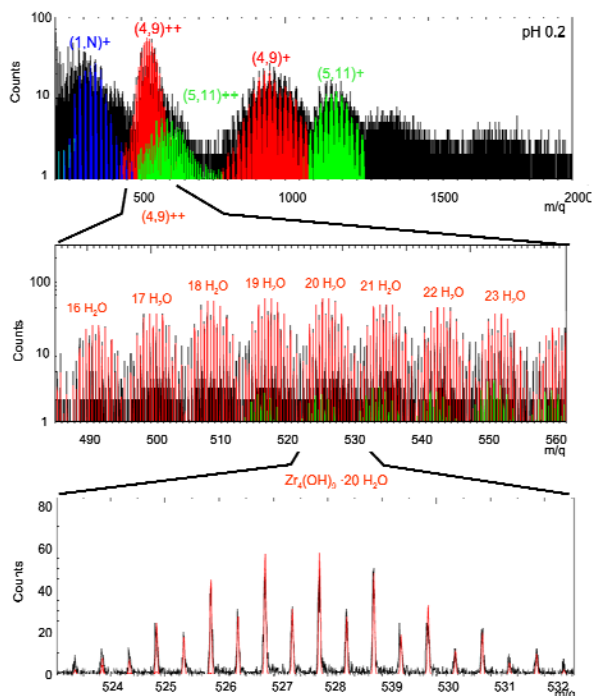


Fig. 1 Mass spectra of a solution with $[Zr]=2.5\text{mM}$, $\text{pH}_C 0.2$. **Top** Monomers (blue) tetramers (red) and pentamers (green) are identified **Middle**: A magnification reveals that the cluster of doubly charged tetramers is in turn composed of peak clusters representing different numbers of water molecules in the solvation shell. **Bottom**: The isotope distribution (Cl and Zr isotopes) of each group is shown by further magnification. The measured spectrum (black) agrees excellently with the theoretical distribution (red).

with the theoretical distribution (red). By use of a homebuilt C++ routine the isotope distribution is evaluated for the complete mass spectrum (up to 5000 peaks) and the detected complexes $[Zr_x(OH)_y^{4x-y} mCl^+ nH_2O]^{q+}$ are identified unambiguously.

Due to the high mass resolution of the spectrometer [6] (up to $m/\Delta m \sim 26.000$) even isobaric interferences are suppressed, which is illustrated in Fig.2 (magnification of the mass spectrum of Fig.1 around $m/q = 341$). The isobars $[^{90}\text{Zr}^{4+} {}^{35}\text{Cl}_2 {}^{37}\text{Cl} 8\text{H}_2\text{O}]^+$ (or $[^{92}\text{Zr}^{4+} {}^{35}\text{Cl}_3 8\text{H}_2\text{O}]^+$, respectively) (blue) and $[^{90}\text{Zr}(\text{OH})^{3+} {}^{35}\text{Cl} {}^{37}\text{Cl} 9\text{H}_2\text{O}]^+$ (or $[^{92}\text{Zr}(\text{OH})^{3+} {}^{35}\text{Cl}_2 9\text{H}_2\text{O}]^+$, respectively) (green) are well resolved, which allows the identification of the number of hydroxide ligands of the complex within its solvent shell. The peak at $m/q \sim 341.3$ is due to

organic contamination and is discriminated against the peaks of the Zr(IV) complexes.

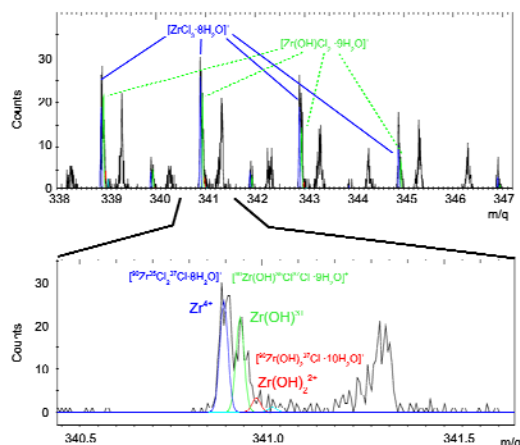


Fig. 2 Section of the mass spectrum of Fig. 1 **Top:** Isotopic distributions of the complexes $[\text{ZrCl}_3 \cdot 8\text{H}_2\text{O}]^+$ and $[\text{Zr}(\text{OH})\text{Cl}_2 \cdot 9\text{H}_2\text{O}]^+$ due to the natural isotopic abundances of Zr and Cl. **Bottom:** The isobars $[\text{Zr}^{4+} \cdot \text{Cl}_2 \cdot \text{Cl} \cdot 8\text{H}_2\text{O}]^+$ (or $[\text{Zr}^{4+} \cdot \text{Cl}_3 \cdot 8\text{H}_2\text{O}]^+$, respectively) (blue) and $[\text{Zr}(\text{OH})]^{3+} \cdot \text{Cl} \cdot 9\text{H}_2\text{O}]^+$ (green) are well resolved as are the peaks slightly above each mass unit (e.g. at $m/q \sim 341.3$) which originate from organic contaminations and are clearly discriminated from the Zr species.

ESI and EXAFS Results

With increasing pH the fractions of Zr(IV) monomeric species decrease and larger complexes form, which contain an increasing number of Zr(IV) ions (Fig.3). Pentamers and larger complexes form at the expense of tetramers resulting in a complex mixture of many solution species. No dimers or trimers are observed. Surprisingly, at $\text{pH}_C > 1.7$ the number of species decreases and the octamer accounts for more than 70% of the detected ions. To exclude artefacts caused by the possibly invasive electrospray process, six samples at $[\text{Zr}(\text{IV})]=10\text{mM}$ and pH_C 0.1-1.8 were measured by EXAFS (Fig.4). The data of

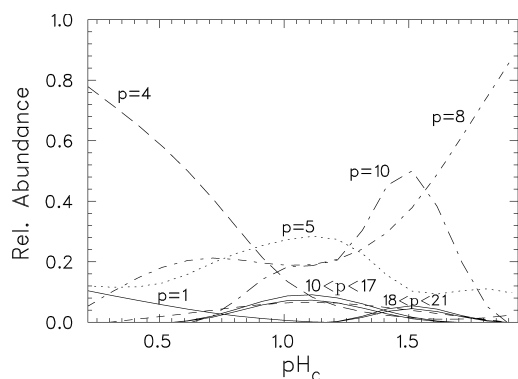


Fig. 3 Species distribution according to ESI TOF (relative number of detected ions) ($[\text{Zr}]=10\text{mM}$)

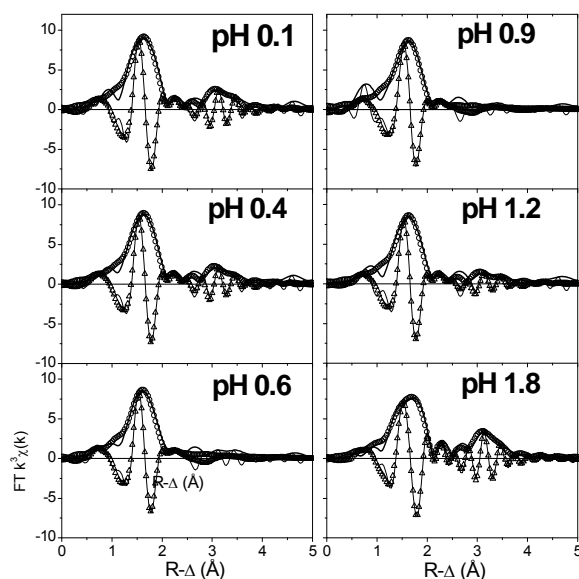


Fig. 4 Zr K-EXAFS R-space fit results for samples ($[\text{Zr}]=10\text{mM}$), FT magnitude of EXAFS data (thick solid line), and corresponding fit (open circles) are shown, as well as FT real part of data (thin line) and corresponding fit (open triangles).

the samples at pH_C 0.1 and pH_C 0.4 show a FT peak centered at $\sim 1.7 \text{ \AA}$ ($R-\Delta$), i.e. $R \sim 2.2 \text{ \AA}$ radial distance) corresponding to Zr-O backscattering and a less pronounced and broadened peak centered at $\sim 3.1 \text{ \AA}$ ($R-\Delta$), i.e. $R \sim 3.6 \text{ \AA}$ radial distance) due to Zr-Zr backscattering. The EXAFS data are a strong evidence for the presence of tetramers (c.f. discussion on tetrameric Zr-Zr and Zr-O distances in [2]) and in good agreement with the 80% relative abundance of the tetramer found by ESI TOF at high acidity (Fig.3).

At $\text{pH}_C > 0.5$ ESI-TOF detects increasing amounts of pentamers. Accordingly, in the EXAFS spectra the Zr-Zr scattering peak eventually vanishes (samples pH_C 0.6-1.2). Based on the EXAFS data alone, one might erroneously conclude from the absence of a Zr backscattering signal that mononuclear Zr-hydroxide complexes ($\text{Zr}(\text{OH})_y^{4-y}$) were present. However, the vanishing Zr-Zr peak is caused by the presence of many different Zr-Zr distances and this interpretation is strengthened by the results from the sample at pH_C 1.8: At this pH the number of different species is strongly reduced and according to the ESI-TOF results (Fig.3) the octamer accounts for more than 80% of the Zr solution species. In good agreement the EXAFS data show a distinct Zr-Zr backscattering signal and yield a Zr-Zr distance of $3.66(3)\text{\AA}$ with a mean coordination number close to two ($1.5(4)$).

ESI TOF allows us to identify, as a function of pH_C , not only the size (polymerization x), but also the number of hydroxide groups (y) and via $q=4x-y$ the charge of each polymer. Often several hydroxide complexes with the same degree of polymerization (x) but different number of hydroxide groups y are present simultaneously. In this case a number-weighted mean charge is calculated. A pronounced decrease of the charge $4x-y$ and hence an increase in the number of hydroxide groups y is observed, which is fitted empirically by a linear dependence (Fig.5). It is worth noting, that for pentamers as well as octamers at all measured concentrations the mean charge approaches ~ 2 under conditions (H^+ and Zr concentrations) close to the solubility of $Zr(OH)_4(am)$. This is in agreement with the slope analysis of previous work [2].

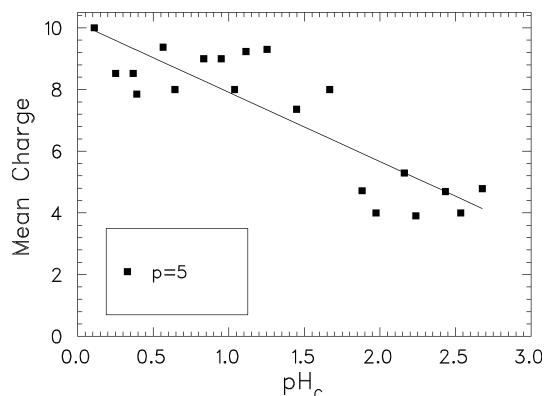


Fig. 5 The mean charge of the pentamers decreases almost linearly as a function of pH_C ($[Zr]=1.5mM$)

Speciation model

This finding that the hydrolysis of polynuclear Zr-species is a continuous process which leads to charge compensation by sequential substitution of water molecules by hydroxide ligands requires an extended speciation model. In a first approximation 9 different polynuclear complexes and the monomers $Zr(OH)_y^{4-y}$ ($y=0-4$) were considered. Formation constants for the hydrolysis complexes of the monomers were taken from literature [1], the respective values for the larger polymers were fitted to the data. SIT coefficients for all complexes were estimated according to the models proposed in [1] and [2]. With these assumptions the measured data (symbols see caption) are well reproduced for all measured concentrations ($[Zr(IV)]=1.5mM -10mM$). By using a lower number of species, the data of $[Zr]=1.5mM$ could not be satisfactorily described, due to the strong variation in charge of the pentamers and octamers between pH_C 0 – 3.

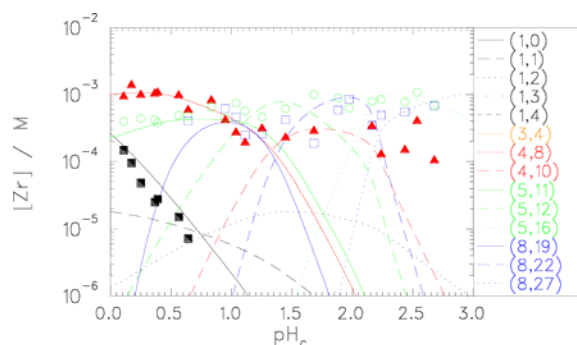


Fig. 6 Species distribution at $[Zr(IV)]=1.5mM$ in units of molar Zr concentration within each size class for the ESI-TOF data (monomers (black squares), tetramers (red triangles) pentamers (green circles) and octamers (blue open squares)). Lines: speciation model. (x,y) denotes the complex $Zr_x(OH)_y^{4x-y}$. For details on the speciation model see text.

Summary

The present results on the hydrolysis of Zr(IV) are consistent with observations reported in the literature, however, they provide additional information which is not available by other experimental methods. For Zr concentrations in the millimolar concentration range mononuclear species are shown to be minor species at $pH_C > 0.1$. The expected stability range of the tetramer $Zr_4(OH)_8^{8+}$ is confirmed and the observed formation of octamers is in agreement with literature data based on X-ray scattering [7]. In addition, it is shown that the degree of polymerization gradually increases if the conditions (Zr and H^+ concentration) approach the solubility limit of $Zr(OH)_4(am)$. The polymerization process culminates in the formation of colloids and finally precipitation. Simultaneously, the number of OH^- ligands per Zr(IV) ion increases with increasing pH (charge compensation). The charge of the polynuclear species which are found to be dominant under conditions close to the Zr and H^+ concentrations in solutions saturated with $Zr(OH)_4(am)$ agrees with the slope analysis from solubility measurements. The simple models proposed for instance in the NEA-TDB review [1] are adequate as a tool to model solubility data but they do not reflect the complexity of the Zr(IV) hydrolysis process which continuously produces a considerable number of polymers as function of pH and total Zr concentration. On the other hand, it is not yet possible to construct an accurate set of thermodynamic constants for all the species detected by nano-electrospray mass-spectrometry because of the exceeding number of unconstrained model parameters.

References

- [1] P.L. Brown, E. Curti, B. Grambow, C. Ekberg, F.J. Mompean, J. Perrone, M. Illemassene, Chemical Thermodynamics of Zirconium. CHEMICAL THERMODYNAMICS, ed. D.B. OECD Nuclear Energy Agency. Vol. 8. 2005, Amsterdam: ELSEVIER.
- [2] H.R. Cho, C. Walther, J. Rothe, V. Neck, M.A. Denecke, K. Dardenne, T. Fanghänel, Anal. Bioanal. Chem., 383 (2005) 28-40.
- [3] R.B. Cole, Electrospray Ionization Mass Spectrometry. 1997, New York: John Wiley and Sons.
- [4] M. Wilm, M. Mann, Anal. Chem., 68 (1996) 1-8.
- [5] C. Walther, J. Rothe, M. Fuss, S. Büchner, S. Koltsov, T. Bergmann, Anal. Bioanal. Chem., in print (2007).
- [6] T. Bergmann, T.P. Martin, H. Schaber, Rev. Sci. Instr., 61 (1990) 2592-2600.
- [7] A. Singhal, L.M. Toth, J.S. Lin, K. Affholter, J. Am. Chem. Soc., 118 (1996) 11529-11534.

6.4 Computational Chemistry

Bernd Schimmelpfennig, Michael Patzschke* and Robert Polly
* since Aug. 2006 at Helsinki University/Finland

Introduction

Computational Chemistry is a powerful tool to describe atoms, molecules and solids on the basis of the fundamental equations of quantum mechanics at the sub-atomic level. In contrast to approximate schemes describing the interaction between atoms or building blocks by force constants, we pursue the computationally more demanding approach to describe the interaction between nuclei and electrons explicitly by means of density functional theory (DFT) or ab initio methods, such as Møller Plesset perturbation theory of second order (MP2), coupled cluster theory (CCSD(T)) or multireference ab initio methods (CASSCF, CASPT2, MRCI). The main task of the computational chemistry group is to support experiment with additional reliable information about the systems under experimental investigation. A wide range of properties is tackled with quantum chemical methods such as structural parameters including coordination numbers, vibrational frequencies, thermodynamic data, electronic excitations from core or valence shells as well as an analysis of the bonding between f-elements and ligands.

Solvent effects

The majority of experimental investigations at our institute are carried out in aqueous solution and an reliable understanding and modelling of solvent-solute interactions is therefore a key prerequisite for an accurate description of complexes in solution. Polarizable continuum models have been considered as a useful tool to treat the interaction with solvent molecules beyond the first coordination shell, but our studies of actinide ions in water have indicated that the reliability of energetic differences between differently coordinated metal ions is strongly hampered by the range of results which can be obtained with different schemes of such models. We found for Cm(III) in water an effect of the solvent model in the same order as the investigated difference in ΔH . A comparable effect of the applied continuum model was later found for the water exchange at uranyl(VI) by V. Vallet(Lille/France).

Two approaches are currently pursued to overcome these uncertainties:

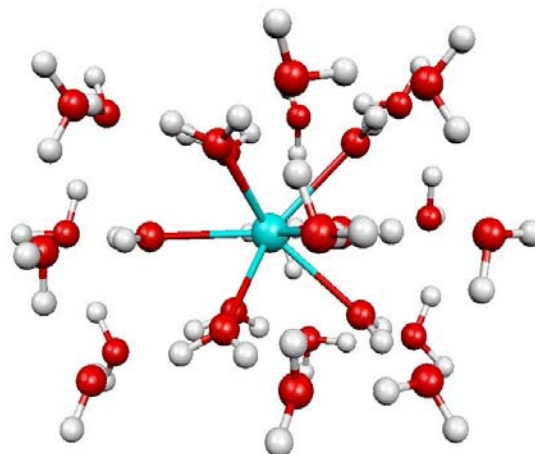


Fig. 1 Nine-coordinated Cm(III) with an explicit second shell of 18 water molecules.

- Explicit inclusion of the second coordination shell and confirmation of the structures using molecular dynamics.
- A combination of a quantum mechanical description of the solute with molecular mechanics for the solvent in cooperation with V. Vallet and F. Real (ACTINET post-doc) in Lille (France) within an ACTINET project.

Zr(IV) clusters

C. Walther and co-workers investigate clusters with several Zr(IV) centers bridged by either O or OH (see section 6.3 of this report). Whereas the tetramer system is clearly understood as a ring system (see Fig.2) the structure and rela-

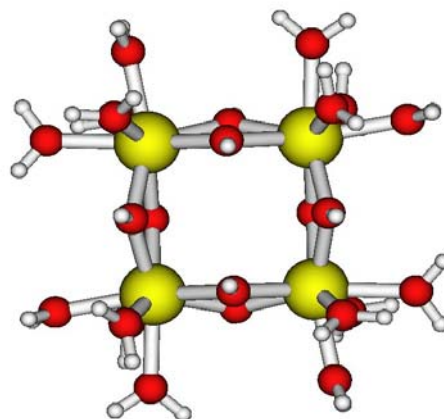


Fig. 2 A possible structure of the Zr(IV)(OH)₂ tetramer with quadratic anti-prismatic coordination of Zr.

tive stability of larger clusters is still under investigation. Thanks to the limited number of coordinated water molecules in the outer spheres, a gas-phase model with explicit water molecules is can be presumed to describe the clusters accurately. This project is continued.

Speciation of the Functional Groups at Mineral/Water Interfaces

The adsorption of radioisotopes at mineral surfaces of the aquifer is an important process which leads to the retention of the contaminants. This theoretical work is aimed to support surface sensitive vibrational sum frequency spectroscopy (SF) experiments probing the corundum (Al_2O_3)/Water surface (see section 6.2 of this report). The experimental results provide information about the vibrational frequencies of the surface as well as the tilt angles of the OH groups with respect to the surface. Our quantum chemical calculations allow an independent access to these experimental observables, confirming and supporting the experimental results.

Experimental evidence shows that the corundum surface in contact with water is oxygen terminated. For the theoretical investigation of this problem we use several Al/O/H clusters representing the corundum surface in contact with water.

We started this investigation with a determination of the structures of several small Al/O/H clusters (Al_4O_6 , Al_8O_{12} , $\text{Al}_7\text{O}_{12}\text{H}_3$) with (RI-) MP2 and CCSD(T) as well as (RI-) DFT methods. CCSD(T) is very accurate, but com

putationally very demanding and can only be applied to the smallest cluster. Due to the reduced computational demands MP2 can be applied to larger clusters, too, to determine the structure. Both, the highly accurate CCSD(T) calculations and the less accurate (RI-) MP2 method serve to calibrate the (RI-) DFT method, which is the only method which can be applied to the larger systems ($\text{Al}_{20}\text{O}_{38}\text{H}_{12}$ (+ n H_2O) or $\text{Al}_{31}\text{O}_{60}\text{H}_{21}$ (+ n H_2O)). The results of this study shows that the structural information of (RI-) DFT is very reliable and very close to the CCSD(T) or MP2 results for this class of systems.

Vibrational frequencies can only be obtained by means of (RI-) MP2 or (RI-) DFT. The agreement of both methods is excellent for the smaller clusters. Hence the (RI-) DFT methods for larger systems can be regarded as reliable. The vibrational frequencies of the OH groups on the surface, together with the tilt angles and the occupation numbers can be used to simulate the experimental sum frequency spectra at the mineral/water interface (see Fig. 2b in section 6.2). The agreement of the theoretical and the experimental spectra is outstanding. Therefore the theoretical results strongly support the experimental results and leads to an improved understanding of the physics on the corundum/water interface.

Extraction chemistry

The separation of Ln(III) and An(III) ions from acidic solutions is a long-term project with strong interaction between theory and experiment. A deeper analysis of donation / back-donation effects was expected to give a deeper insight into the differences between actinide and lanthanide complexes. Complementing our previous work investigating the difference density between Gd(III) and Cm(III) complexes. The tool of Natural Population Analysis (NPA) became available in the TURBOMOLE software package and was applied to Gd(III) and Cm(II) 1:3 complexes with BTP and Terpyridine ligands. The M(III) Terpyridine complexes are currently investigated experimentally (see section 7.1 of this report), and there are strong indications for a 1:3 complex not to be formed. Still, this complex serves as a hypothetical system which should have a close similarity to the BTP complex. In order to check the dependency on the quantum chemical approach applied, we also compared different DFT functionals and Unrestricted Hartree-Fock (UHF). In general, our study found no differences in M(III)-N binding distances between the Gd(III) and Cm(III) complexes, although the results depended strongly on the method employed,

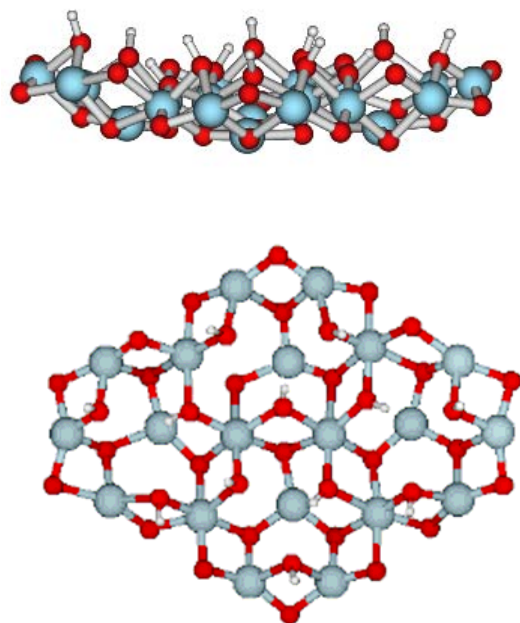


Fig. 3 $\text{Al}_{20}\text{O}_{38}\text{H}_{12}$ cluster used to represent the corundum surface in contact with water in this study.

except for the occupation of the 6s orbital of Gd, which differ by approx. 0.4 electrons depending on the method. No donation to the corresponding 7s orbital of Cm could be found by the analysis. Donation to the d-shell is found to be in the order of 0.1-0.2 electrons whereas no donation is found to / from the p and f shells. The standard explanation of different bonding behaviour by a stronger covalence in the Cm(III) complexes can not be confirmed by this study and a deeper analysis is in progress to understand this surprising behaviour.

Conclusions

Computational chemistry is a powerful tool for looking deep inside molecular systems and to get an understanding of the mechanisms involved in reactions and the bonding situation. The main obstacles to computations on actinide compounds are an adequate description of the complicated coupling in the partially occupied f-shell and for the systems investigated of solvent effects in aqueous solution. The quantum chemistry group is involved in international cooperations to overcome these challenges.

7. Separation of long-lived minor actinides

7.1 Separation of Minor Actinides

A. Geist, M.A. Denecke, P.J. Panak, F. Burdet, M. Weigl, B. Schimmelpfennig, U. Müllich, K. Gompper

Introduction

The separation of plutonium and the minor actinides (neptunium, Np; americium, Am; curium, Cm) from spent nuclear fuels and their subsequent transmutation by nuclear fission in advanced reactors could significantly reduce the radiotoxicity of the highly active waste to be stored in a final repository [1]. This is the so-called *Partitioning & Transmutation* strategy [2]. We study aspects of two separations processes based on liquid-liquid extraction, in the frame of the EC Integrated Project, EURO-PART [3], and a joint FZK-INE/CEA-Grenoble ACTINET project [4]:

1. The DIAMEX process, which is the co-extraction of Am, Cm, and the lanthanides from the PUREX raffinate solution.
2. The SANEX process, involving separation of Am and Cm from the chemically similar lanthanides, from the DIAMEX product solution.

Whereas the DIAMEX process can be considered mature, the SANEX process is still under development, owing primarily to the fact that SANEX extracting agents developed so far all have their shortcomings.

The separation chemistry involved in the SANEX process is not understood from a fundamental point of view: Why do nitrogen (N)-donor extractants preferentially extract trivalent Am and Cm over the lanthanides, in spite of their chemical similarity? We look into this using EXAFS (extended X-ray absorption fine structure), TRLFS (time-resolved laser fluorescence spectroscopy), and quantum chemistry.

Besides, we studied the mass transfer kinetics of Am(III) extraction into an alkylated 2,6-ditriazinylpyridine (BTP). Furthermore, DIAMEX and SANEX process development studies were carried out in EUROPART.

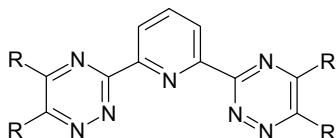


Fig. 1 Alkylated 2,6-ditriazinylpyridine (BTP)

n-Pr-BTP EXAFS Studies

In continuation of previous EXAFS studies [5, 6, 7] on Am(III), Cm(III), and Eu(III) complexed with *n*-Pr-BTP (Fig.1, R = *n*-C₃H₇) we also

prepared the respective U(III), Gd(III), and Lu(III) complexes in organic solution [8] and measured them at the INE-Beamline [9]. The considerable challenge of preparing, transporting, and measuring U(III) solution samples was mastered.

The EXAFS were fit with a four-shell model (the four shells comprising of N, N/C, N/C and C atoms; see Fig.2, R = *n*-C₃H₇). As previous results confirmed the 1:3 complex stoichiometry [5], the coordination numbers were fixed to 9/18/18/9. Table 1 compiles the major results from the four-shell fits (coordination numbers *N* and M(III)–N bond lengths *R*; σ^2 , ΔE_0 , and *r*-factor are found in [5, 8]).

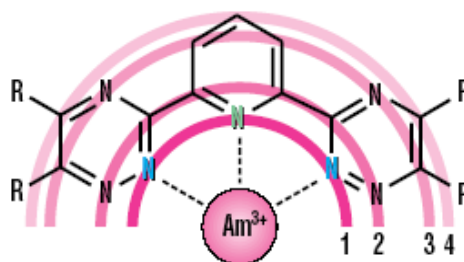


Fig. 2 Visualisation of the four shells in the M(III)-BTP complexes; only one ligand shown.

At a first glance, the M(III)–N bond lengths from the first shell, with the exception of M = Lu, are identical within the error of EXAFS analysis (0.02 Å). However, the differences between the first shell M(III)–N bond lengths and tabulated M³⁺ radii are more meaningful. These are 1.56 Å for U(III), 1.61±0.01 Å for Am(III), Cm(III), Eu(III), and Gd(III), and 1.67 Å for Lu(III).

The result for the [U(BTP)₃]³⁺ solution structure confirms solid state results [10]. The 0.05 Å shorter distance for U(III) compared to the lighter lanthanides could indicate stronger covalency for U(III). However, in the case of Am(III) and Cm(III) no significant difference to Eu(III) and Gd(III) complexes is found. This indicates that BTP's good selectivity for the former over the latter is not due to structural or bonding properties. The longer distance for the much smaller Lu(III) may be attributed to steric effects.

Table 1 Coordination numbers N (held constant at the given value) and bond lengths R determined from four-shell fits to the L3 EXAFS of the M(III)-BTP complexes studied.

Sample	Shell	N	R [Å]
U(III)-BTP [8]	1	9	2.57(2)
	2	18	3.44(2)
	3	18	4.85(8)
	4	9	5.34(9)
Am(III)-BTP [6,7]	1	9	2.562(5)
	2	18	3.423(7)
	3	18	4.77(6)
	4	9	5.25(7)
Cm(III)-BTP [5]	1	9	2.568(7)
	2	18	3.431(9)
	3	18	4.81(3)
	4	9	5.30(4)
Eu(III)-BTP [5]	1	9	2.559(8)
	2	18	3.42(1)
	3	18	4.82(2)
	4	9	5.30(3)
Gd(III)-BTP [8]	1	9	2.554(5)
	2	18	3.41(3)
	3	18	4.80(3)
	4	9	5.29(4)
Lu(III)-BTP [8]	1	9	2.52(1)
	2	18	3.35(2)
	3	18	4.77(3)
	4	9	5.26(3)

TPZA EXAFS Studies

Tris[(2-pyrazinyl)methyl]amine (TPZA, Fig. 3) extracts An(III) preferentially over Ln(III) [11]. Crystal structures [12] of M(III)-TPZA complexes ($M = U, La$) show that the metal ion is coordinated to four N (from TPZA), one O (from THF) and three anions (here, I⁻). U(III)-N bond lengths are distinctly shorter, suggesting more covalence in the U(III)-N bonds than in the La(III)-N bonds.

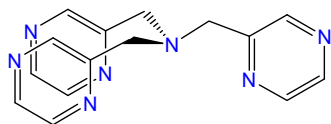


Fig. 3 TPZA.

We prepared solid and liquid $U_3(TPZA)(THF)$ and $SmI_3(TPZA)(THF)$ samples, and studied them at the INE-Beamline [8]. L3 EXAFS were fit with a two-shell model, the first shell consisting of N (from TPZA) and O (from THF), and the second shell consisting of I. Then, a three-shell fit was made, with fixed coordination numbers, and 1st shell = O, 2nd shell = N, 3rd shell = I. Coordination numbers and bond lengths are compiled in Table 2.

To conclude, coordination numbers from the two-shell fits are in good agreement with the crystal structures (i.e., 5 O/N and 3 I); two- and three-shell fits agree with one another; bond distances in the solid and liquid samples agree well (with the exception of Sm(III)-I). Comparing the U(III) and Sm(III) solution complexes, similar bond lengths are observed; however it must be considered that the U(III) cation radius is approx. 0.05 Å larger than that for Sm(III). This is in agreement with similar findings for the U(III)-BTP complex (see above).

Table 2 Coordination numbers N ($f =$ held constant at the given value) and bond lengths R determined from fits to the L3 EXAFS of the M(III)-TPZA complexes studied.

Sample	Shell	N	R [Å]
U(III)-TPZA (solid)	N/O	6(1)	2.61(3)
	I	3.0(8)	3.14(1)
U(III)-TPZA (liquid)	O	1(f)	2.42(7)
	N	4(f)	2.64(2)
	I	3(f)	3.12(2)
Sm(III)-TPZA (solid)	N/O	5(1)	2.56(2)
	I	2.7(9)	3.06(1)
Sm(III)-TPZA (solid)	O	1(f)	2.45(6)
	N	4(f)	2.61(2)
	I	3(f)	3.06(1)
Sm(III)-TPZA (liquid)	O	1(f)	2.43(3)
	N	4(f)	2.63(1)
	I	3(f)	3.12(1)

n-Pr-BTP TRLFS Studies

It was previously demonstrated in a TRLFS study titrating solutions of Cm(III) or Eu(III) in kerosene/1-octanol with *n*-Pr-BTP ($R = n-C_3H_7$) that the extractable $[M(BTP)_3]^{3+}$ complexes form at widely different $[M(III)]/[BTP]$ ratios [5], in agreement with BTP's selectivity for An(III) over Ln(III).

Meanwhile, the 1:1, 1:2, and 1:3 complexes could be identified for Cm(III). For Eu(III), only two species were detected. One is the 1:3 complex, the other one was identified as the 1:1 complex by slope analysis and lifetime measurement [8]. The 1:2 Eu(III) complex could not be detected. With these findings and peak deconvolution, the speciation for Cm(III)/*n*-Pr-BTP and Eu(III)/ *n*-Pr-BTP was identified, as shown in Figs. 4 and 5.

Whereas the $[Eu(BTP)_3]^{3+}$ complex forms quantitatively only for $[BTP]/[Eu(III)] > 300$, $[BTP]/[Cm(III)] > 5$ suffices to exclusively form $[Cm(BTP)_3]^{3+}$, despite the 100 times lower me-

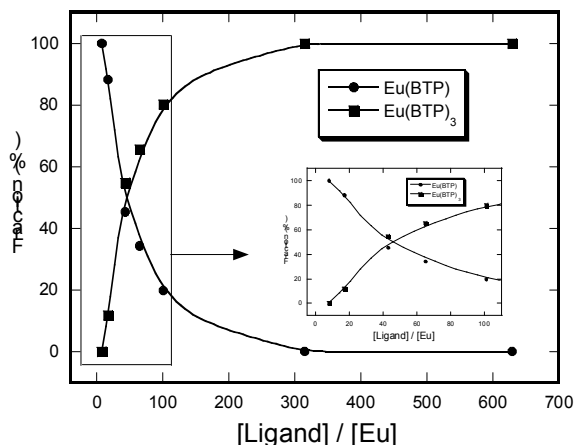


Fig. 4 Eu(III)/*n*-Pr-BTP speciation in kerosene/1-octanol. [Eu(III)] = 10^{-5} M.

tal ion (and accordingly BTP) concentrations used in the Cm(III) experiment. These results are currently under quantitative evaluation, in order to estimate K_1 , K_2 , and K_3 for the stepwise addition of BTP ligands to Eu(III) or Cm(III) in organic solution.

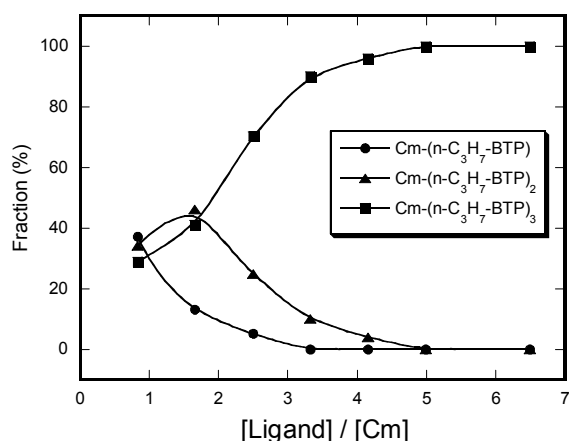


Fig. 5 Cm(III)/*n*-Pr-BTP speciation in kerosene/1-octanol. [Cm(III)] = 10^{-7} M.

n-Pr-BTP Mass Transfer Kinetics

n-Pr-BTP (Fig. 1, $R = n\text{-C}_3\text{H}_7$) extracts trivalent actinides from nitric acid with high separation factors over the lanthanides. The kinetics of Am(III) extraction and back extraction of this extraction system was studied in a constant-interface stirred cell [13].

Am(III) extraction rate was found independent of stirring speed. Thus the rate of mass transfer is limited by a slow chemical complex formation reaction ("chemical regime"), allowing for a full kinetic investigation.

Am(III) extraction rate was found to increase linearly with the concentration of *n*-Pr-BTP. Nitrate concentration had virtually no influence on Am(III) extraction rate. However, nitric acid concentration had a strong influence on the rate of Am(III) extraction, see Fig. 6: due to an

increasing co-extraction of nitric acid, the concentration of free BTP decreases, which in turn reduces the rate of extraction.

Interesting with respect to process optimisation is the following: Decreasing the feed nitric acid concentration from 1 M to 0.5 M results in better process performance as the increase in extraction rate by a factor of two (cf. Fig. 6) overcompensates the small decrease in distribution ratio.

By investigating the influence of the interfacial area on Am(III) extraction rate, the interface was identified as the site of the chemical reaction. Am(III) back extraction rate increased linearly with stirring speed, indicating that back extraction is limited by diffusion.

From these findings, kinetic equations were derived and implemented into a simple model based on measured equilibrium data for the co-extraction of Am(III) and nitric acid. Extraction and back extraction rates could thus be calculated with good agreement to experiments (see e.g., the line in Fig. 6).

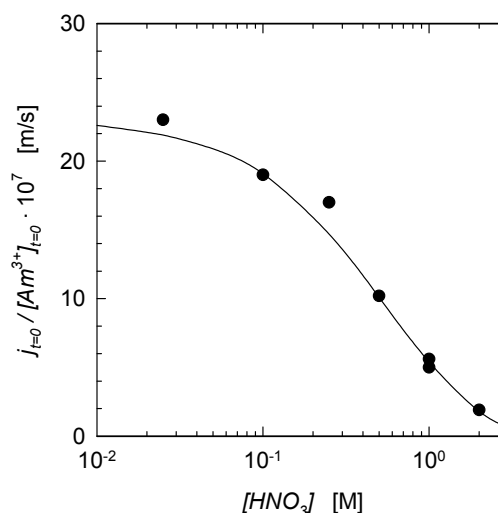


Fig. 6 Dependency of normalised initial Am(III) extraction rate on aqueous nitric acid concentration. $n = 300/\text{min}$, $[\text{NH}_4\text{NO}_3] = 2$ M, $[\text{BTP}] = 0.04$ M. Symbols, experiments. Line, calculated.

SANEX Process Development

6,6'-bis(5,5,8,8-tetramethyl-5,6,7,8-tetrahydrobenzo[1,2,4]triazin-3-yl)-[2,2']bipyridine (Fig. 7, CyMe₄-BTBP), first synthesised at Reading University (UK), was selected as reference extractant for An(III)/Ln(III) separations (SANEX) process development in EUROPART [3].

Much of the assessment of its extraction performance has already been performed at FZK-INE [14]. As it is planned to run a spiked CyMe₄-BTBP SANEX test at FZJ-ISR and a

hot one at ITU, additional experiments needed for flow sheet development were made.

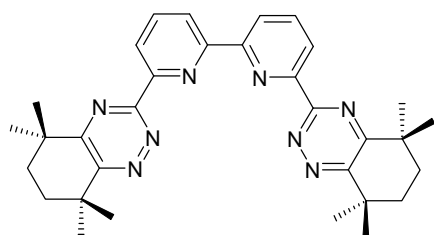


Fig. 7 CyMe₄-BTBP.

DIAMEX Process Development

A final spiked DIAMEX (i.e., co-extraction of An(III) and Ln(III) from PUREX raffinate solution) process test was performed in our HFM micro-plant [15]. Raffinate decontamination factors were > 30000 (americium) and > 900 (curium). Back extraction efficiency was > 99.8%. With a small modification to the flow sheet, the problem of low mass balances encountered in previous tests could be resolved; Am(III) and Cm(III) mass balances of 100% and 99% were achieved [16]. This flow sheet will be used for the hot DIAMEX test to be performed in the second HFM micro-plant at ITU.

Conclusions

The research on minor actinide separation covers aspects from fundamental studies contributing to understanding the selectivity of N-donor extracting agents for trivalent actinides to process development.

For the first time, complexes formed between N-donor ligands (BTP and TPZA) and U(III) were prepared and investigated by EXAFS in solution. This study confirmed what we previously assumed based on solid state structures: results from using U(III) as a surrogate for studying the behaviour of N-donor extractants towards Am(III) and Cm(III) are of limited significance.

Using TRLFS, the speciation in the Cm(III)/*n*-Pr-BTP and Eu(III)/*n*-Pr-BTP systems was identified based on peak deconvolution, lifetime measurement, and slope analysis.

Besides these basic studies on the extracting and complexing properties of N-donor extractants, we performed work on the optimisation of solvent systems to be used in future SANEX tests, and on flow sheet optimisation for a hot DIAMEX test to be carried out at ITU in a HFM micro-plant developed and built at FZK-INE. These tasks are part of our commitment to the integrated project EUROPART.

Financial support from the Commission of the European Community is acknowledged (contract FI6W-CT-2003-508854 EUROPART and ACTINET project JP 03-11).

References

- [1] J. Magill, V. Berthou, D. Haas, J. Galy, R. Schenkel, H.-W. Wiese, G. Heusener, J. Thommasi, G. Youinou, Nucl. Energy 2003, 42 (5), 263-277.
- [2] Actinide and fission product partitioning and transmutation; status and assessment report. OECD-NEA (1999).
- [3] EUROpean research programme for the PARTitioning of minor actinides from high active wastes issuing the reprocessing of spent nuclear fuels (contract no. FI6W-CT-2003-508854).
- [4] JP 03-11, Performance and coordination structure of N-donor extracting agents for partitioning of trivalent actinides from lanthanides.
- [5] M.A. Denecke, A. Rossberg, P.J. Panak, M. Weigl, B. Schimmelpfennig, A. Geist, Inorg. Chem. 2005, 44 (23), 8418-8425.
- [6] M.A. Denecke, A. Geist, M. Weigl, P.J. Panak, B. Schimmelpfennig, ANKA Annual Report 2005, S. 86-87, Forschungszentrum Karlsruhe GmbH.
- [7] A. Geist, M.A. Denecke, P.J. Panak, M. Weigl, B. Schimmelpfennig, K. Gompper, Nachrichten – Forschungszentrum Karlsruhe 2005, 37 (4), 191-196.
- [8] M.A. Denecke P.J. Panak, F. Burdet, M. Weigl, A. Geist, R. Klenze, M. Mazzanti, K. Gompper, C. R. Chim. (2007), doi: 10.1016/j.crci.2006.12.010 (in press).
- [9] M.A. Denecke, J. Rothe, K. Dardenne, T. Fanghänel, H. Blank, H. Modrow, J. Hormes, Physika Scripta 2005, T115, 1001–1003.
- [10] P.B. Iveson, C. Rivière, D. Guillaneux, M. Nierlich, P. Thuéry, M. Ephritikhine, C. Madic, Chem. Commun. 2001, 1512-1513.
- [11] L. Karmazin, M. Mazzanti, C. Gateau, C. Hill, J. Pécaut, Chem. Commun. 2002, 2892-2893.
- [12] M. Mazzanti, R. Wietzke, J.-M. Latour, J. Pécaut, P. Maldivi, M. Remy, Inorg. Chem. 2002, 41, 2389-2399.
- [13] M. Weigl, A. Geist, U. Müllich, K. Gompper, Solvent Extr. Ion Exch. 2006, 24 (6), 845-860.
- [14] A. Geist, C. Hill, G. Modolo, M.R.S. Foreman, M. Weigl, K. Gompper, M.J. Hudson, C. Madic, Solvent Extr. Ion Exch. 2006, 24 (4), 463-483.
- [15] A. Geist, M. Weigl, K. Gompper, Proc. Internat. Solvent Extraction Conf. (ISEC 2005), Beijing, China, Sep. 19-23, 2005, 659-664.
- [16] A. Geist, K. Gompper, (submitted)

8. Vitrification of High-level radioactive liquid waste

8.1 Commissioning of Process Systems of VEK

W. Grünwald, J. Knobloch, W. Metzger, W. Tobie, G. Roth, K.H. Weiß, H. Braun, S. Weisenburger

Introduction

The HLLW vitrification plant VEK (Verglasungseinrichtung Karlsruhe) is currently in the state of final commissioning and preparation for a 2.5 months cold test operation with processing of 15 m³ of simulated HLLW to 27 glass canisters each with 400 kg of glass. INE experts are responsible for commissioning of the major processing systems of VEK. The focus of this work covered the HLLW receipt system, the feeding systems for HLLW and glass frit, the glass melter and the melter offgas line. In the following a portion of the entire commissioning work done in 2006 by the INE-staff is outlined and focused on melter.

Commissioning of VEK melter

The commissioning work for the VEK melter included melter start-up and test of the melter's key subcomponents including the glass pouring system. From these activities the melter start-up heating and the tests of the glass pouring system are described below in more detail.

a. Melter start-up heating

The melter start-up heating procedure until Joule-heating of the glass pool has been performed from May 23 to June 20, 2006. At first the five external SiC-heating elements

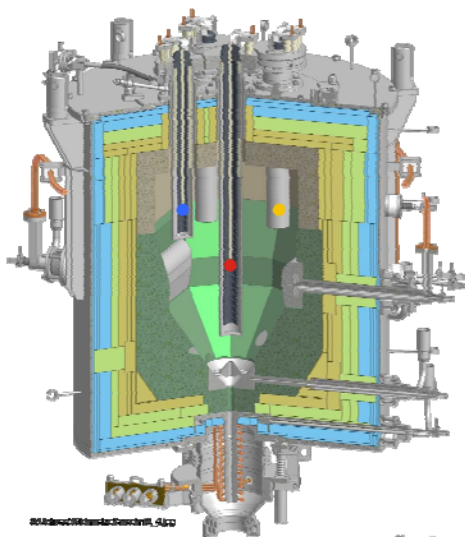


Fig. 1 Heating up of the internal VEK-melter structure by 5 SiC heating elements inside melter plenum. Coloured points correspond to the position of the temperature monitoring points plotted in Fig. 2.

encased in INCONEL 690 tubes were inserted into the empty melter (see Fig. 1) and connected to the electric power supply system.

b. Commissioning of the glass pouring system

Safe operation of the glass pouring system requires the accurate knowledge of several key parameters including the longitudinal temperature profile of the glass pouring pipe and the maximum applicable induction power by the MF-Generator. A new method has been applied to get such detailed information of the pouring system, i.e. among other tools the use of a thermovision system which allows in situ visual viewing of the temperature profile of the pouring pipe.

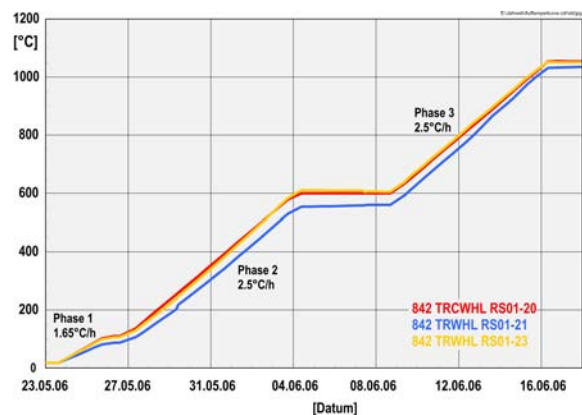


Fig. 2 Heat-up of melter vs. time during the tempering phase of the VEK-melter to 1050°C starting May 23, 2006 until June 16, 2006.

The measurements of induction power vs. the resulting temperature profile of the pouring pipe were first carried out on a dummy of the pouring pipe made of INCONEL 690. Afterwards the actual pouring pipe of the melter was heated up and measured. Fig. 3 shows the dummy and the defined temperature monitoring points M1-M8 on this pipe. Fig. 4 gives the position of the thermovision camera during the temperature measurements of the glass pouring pipe. By this system the temperature profile of the pouring pipe could be qualitatively recognized based on the colour. By a hand pyrometer typical temperature profiles could quantitatively be measured. The data are given in Fig. 5. It shows the temperatures of the defined

monitoring points in dependence on the applied MF-induction power.



Fig. 3 Temperature monitoring points M1 to M8 along a dummy of the glass pouring pipe for measurements by the thermovision camera. The tests have shown that the MF-power for the VEK-melter must be limited to 25 kW at the MF-Generator in order to not exceed a pouring pipe temperature of 1150°C.

c. First glass pouring operation of VEK melter

At Dec. 14, 2006 the first glass pouring test has been carried out after the glass pool had been heated up since Dec. 13 to approximately 1100°C and demineralized water had been fed into the melter at a rate of about 15 l/h to keep

the melter plenum (and thus the melter roof) below 500-800°C. At the time point the glass started to flow and at the end of pouring the following parameters had been monitored:

MF-power	Begin	15	kW	Max	21	kW
Glass pool	Begin	1085	°C	End	1085	°C
Bottom electrode	Begin	745	°C	End	896	°C
Pouring pipe flange	Begin	471	°C	End	654	°C



Fig. 4 Thermovision camera in the hot cell V3 viewing into melter cell V2

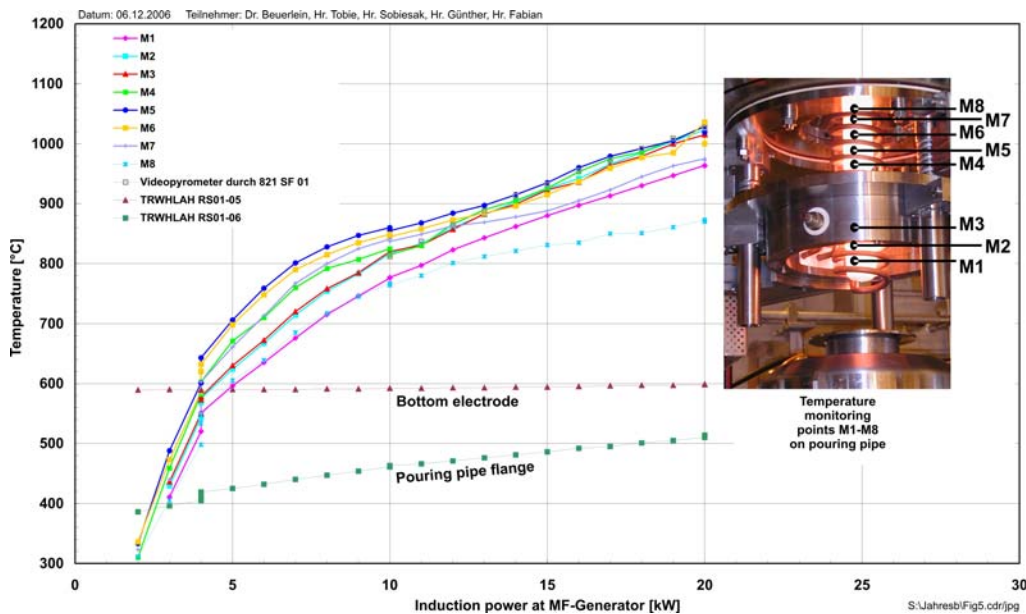


Fig. 5: Measurement results of temperature at various points at the pouring pipe dependent on applied induction power at MF-Generator. An induction power of 20 kW led to the highest pouring pipe temperature at monitoring point M6. Temperature data measured by hand pyrometer Impac IGA 8 plus. $\epsilon = 0.96$

8.2 Application of vitrification technology

Introduction and problem

A future application of FZK's vitrification technology is foreseen within the envisaged China-Project. A contract for design and delivery of the core technology for a vitrification plant to be built in China's Sichuan Province has been presigned between CNEIC (China Nuclear Engineering Industry Corporation) and a German consortium. A preliminary HLLW reference composition for this plant shows an oxide residue of 97.35 g/l (see table 1) and a content of 4.15 g/l sulphur in terms of SO₃ (1.66 g/l sulphur). The generally low solubility of sulphur in borosilicate glass can result in sulphur becoming the waste loading limiting constituent. On the other hand a waste oxide loading of the glass of at least 16 wt% is required for this project in order to limit the amount of glass to be produced and comply with the limited space capacity of the interim storage facility at the site the glass will be interim stored for 50 years. This means that the glass must have sufficient capacity to incorporate at least 0.664 wt% of sulphur in terms of SO₃ (corresponding to 0.80 wt% in terms of SO₄). It was the objective of lab-scale work to develop a glass frit composition by which the resulting waste glass has an incorporation capacity for sulphur of < 0.75 wt% in terms of SO₃ (< 0.9 wt% in terms of SO₄) without generation of a separated yellow phase (Na₂SO₄) from the bulk of the glass. The lab-scale results achieved so far are promising and are described below.

The guideline for a glass formulation with enhanced sulphur incorporation capacity under oxidizing conditions in the glass pool included (1) increase of basic oxides in the glass matrix like CaO and MgO in order to introduce more O²⁻ ions into the glass melt which shifts the thermodynamic equilibrium of the reaction $SO_4^{2-} \rightleftharpoons SO_2 + 1/2 O_2 + O^{2-}$ to the sulfate site (2) introducing barium oxide because barium is known to stabilize sulphur in the glass network (3) introduce small amounts of antimon pentoxide Sb₂O₅ which releases O₂ at operation temperatures between 1000-1150°C for microscale mixing of the glass melt below the cold cap, and (4) moderate temporary mechanical stirring of the melt to avoid oversaturation of glass melt areas near the processing zone (cold cap), because the diffusion (of temporarily unavoidable formation) of sulfate from the cold cap into the glass melt is relatively slow.

Table 1 Preliminary chemical reference composition of the high level waste (in terms of oxide residue)

HLLW		
	Oxide residue	
	g/l	wt%
SrO	0.226	0.232
Y ₂ O ₃	0.097	0.100
MoO ₃	1.181	1.213
MnO ₂	0.081	0.083
BaO	0.128	0.131
UO ₂	12.355	12.693
TiO ₂	0.910	0.935
Cr ₂ O ₃	1.810	1.859
Fe ₂ O ₃	19.700	20.238
NiO	3.600	3.698
Na ₂ O	42.650	43.815
Al ₂ O ₃	8.820	9.061
K ₂ O	0.573	0.589
SO ₃	4.040	4.150
P ₂ O ₅	0.434	0.446
Cs ₂ O	0.730	0.750
Total	97.35	100.00

Table 2 Candidate waste glass compositions designated CIAE-1 and CIAE-5

Oxide	Former waste glass composition		Optimized waste glass composition	
	waste wt%	CIAE-1 glass ¹⁾ wt%	waste wt%	CIAE-5 glass ¹⁾ wt%
SrO	0,232	0,037	0,232	0,037
Y ₂ O ₃	0,100	0,016	0,100	0,016
MoO ₃	1,213	0,194	1,213	0,194
MnO ₂	0,083	0,013	0,083	0,013
BaO	0,131	0,021	0,131	0,021
La ₂ O ₃ ²⁾	12,693	2,031	12,693	2,031
TiO ₂	0,935	0,150	0,935	0,150
Cr ₂ O ₃	1,859	0,298	1,859	0,298
Fe ₂ O ₃	20,238	3,238	20,238	3,238
NiO	3,698	0,592	3,698	0,592
Na ₂ O	43,815	7,011	43,815	7,011
Al ₂ O ₃	9,061	1,450	9,061	1,450
K ₂ O	0,589	0,094	0,589	0,094
SO ₃	4,150	0,664	4,150	0,664
P ₂ O ₅	0,446	0,071	0,446	0,071
Cs ₂ O	0,750	0,120	0,750	0,120
	100,00	16,00	100,00	16,00
Glass matrix				
SiO ₂	59,80	50,23	57,20	48,05
B ₂ O ₃	22,00	18,48	14,60	12,26
Na ₂ O	5,00	4,20	7,00	5,88
Li ₂ O	2,30	1,93	2,60	2,18
Al ₂ O ₃	3,50	2,94	4,40	3,70
CaO	5,40	4,54	8,00	6,72
TiO ₂	1,00	0,84	1,00	0,84
MgO	1,00	0,84	5,20	4,37
	100,00	84,00	100,00	84,00
Total		100,00		100,00

¹⁾ 16 wt.% waste oxide loading

²⁾ UO₂ replaced by La₂O₃ for glass development

S:\Jahresbi\Tabelle 3.xls

Experimental

a. Glass samples

Two candidate glass matrix compositions have been investigated as given in Tab. 2, designated CIAE-1 and CIAE-5. The latter

contains more basic oxides like CaO and MgO compared to CIAE-1. Glass samples were manufactured at INE glass lab by first melting the glass matrix separately from the waste constituents. The oxides of SiO₂, B₂O₃, MgO, TiO₂ and compounds of Na₂CO₃, Li₂CO₃, Al(OH)₃ and CaCO₃ were mixed in the appropriate ratio as fine powders, sieved through 280 μm mesh, melted for 20 min at 1300°C in a lab furnace, cooled and grinded, remelted for 2h at 1300°C and finally grinded to powder.

The simulated waste (composition see Tab. 1) was made from oxides except in the cases of Sr, Cs, Na, Al and S, for which Sr(NO₃)₂, Cs₂CO₃, Na₂CO₃, Al(OH)₃, and Na₂SO₄ were used. The mix of waste were sieved through 280 μm sieve and then mixed with the glass matrix powder prepared as described above. Melting was done for 2h at 1050 and 1100°C, respectively. The resulting glass sample mass was about 40 g. During melting of the glass the melt was mechanically stirred every 10 min for 10 sec. However, parallel samples had been molten without agitation as to show the stirring effect.

b. Glass investigation methods

Glass samples were investigated for their sulphur content by ion chromatography. The redox state of S in the glass was investigated by X-ray absorption spectroscopy (XAS) using the XAS-beamline of ANKA, Angströmquelle Karlsruhe. The X-ray absorption near edge fine structure (XANES) and the extended X-ray absorption fine structure (EXAFS) were used to clarify the coordination of the sulphur atoms by their number and type of neighbours. By Transmission Electron Microscopy (TEM) glass surface investigations were performed. The work related to TEM included investigation of inclusions in the glass and their chemical composition.

Results

a. Formal oxidation state of sulphur in the glass and coordination

Fig. 1 shows typical X-ray absorption near edge fine structure spectra. They were obtained from two CIAE-5 glass samples manufactured at 1050°C. Measurements of pure sodium sulfate and calcium sulfate served as references.

The diagram indicates that the X-ray near edge fine structure peaks of the two references and of the two glass samples lie on the same energy position in the absorption spectra.

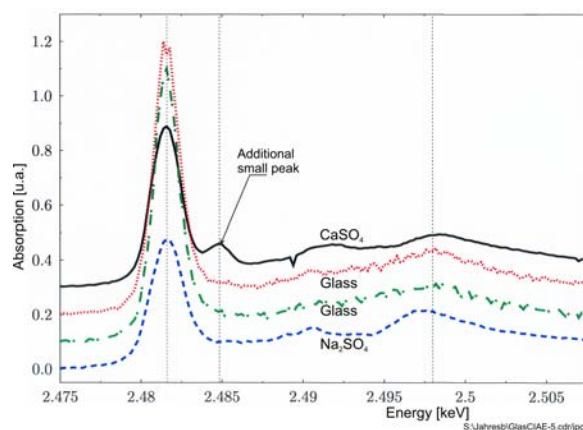


Fig. 1 X-ray absorption near edge fine structure (XANES) spectra of CIAE-5 glass samples and comparison with spectra of pure sodium sulfate Na₂SO₄ and pure calcium sulfate CaSO₄. Glass samples manufactured at 1050°C containing 1.59 wt% SO₄ in the raw glass batch material. One of two parallel samples agitated every 10 min for 10 s.

A small peak of the CaSO₄ at energy position 2.485 keV is neither visible in the spectra of Na₂SO₄ nor in the glasses. From this measurements it is thus most likely that the sulphur in the glass is present as sulfate, i.e. in the formal oxidation state S⁶⁺ and that the charge compensating cation of the sulfate in our glass is Na⁺. Coordination by cations of calcium Ca²⁺ appears unlikely although the glass contains Ca in significant amounts. The findings are supported by literature data obtained by Raman spectroscopic measurements on sulphur containing borosilicate glass samples [1].

b. Measured incorporation capacity of candidate waste glass compositions

Fig. 2 shows a typical result of the measurements of sulfate concentration in the glass by ion chromatography. The measured value of SO₄ is plotted vs. the target values according to the glass batch compositions of the glass. Ideally the measured values should be on the red line (i.e. no loss of sulphur during melting of glass batch material, no sulfate phase separation from bulk of the glass). Data are given for CIAE-5 glass samples (composition see tab. 2, increased amounts of basic oxides CaO, MgO). Sample manufacturing temperature has been 1050°C and 1100°C, respectively. Filled symbols in Fig. 3 refer to samples not mechanically agitated during melting. Open symbols refer to samples agitated during melting every 10 min for approximately 10 s.

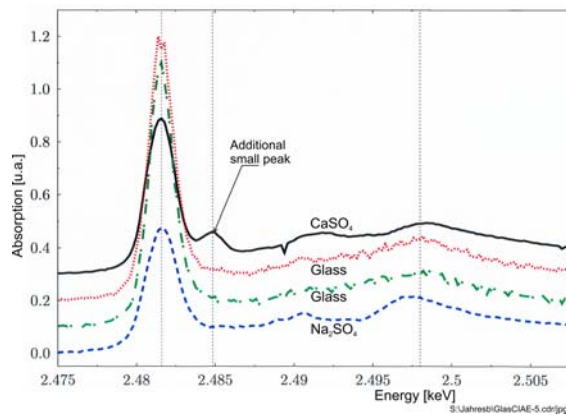


Fig. 2 Measured sulphate concentration in CIAE-5 glass product vs. target values according to glass batch composition. Data given for lab samples without agitation (filled symbols) and with agitation (every 10 min for 10 s). Data for 1050°C and 1100°C.

The data show that non-agitated samples did not incorporate more than about 0.75-0.80 wt% SO_4 , although the sample batches contained up to 3 wt% of SO_4 . In contrast, the agitated samples incorporated more sulphate as can be seen from Fig. 2.

TEM investigation showed only minor inclusions of Na_2SO_4 crystals in the glass. If the basic oxides CaO and MgO are taken out from the glass frit and mixed directly with the waste constituents before batch melting the sulfate incorporation of the glass for unstirred samples increased as can be seen from Fig. 3. But no increase can be seen for the samples which were temporarily stirred.

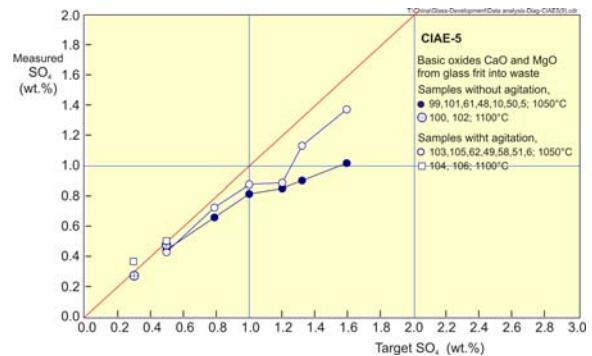


Fig. 3 Measured sulphate concentration in CIAE-5 glass product vs. target values. Data given for lab samples without agitation (filled symbols) and with agitation (every 10 min for 10 s). Data for 1050°C and 1100°C. Basic oxides CaO and MgO from glass frit mixed to the waste.

Outlook

The experiments will be continued. Preliminary experiments with Sb_2O_5 for supporting microscale mixing of the glass are very promising as well as preliminary experimental results with increased BaO in the glass. The goal to achieve a glass matrix the resulting glass of which can incorporate at least 0.9 wt% of sulfate without yellow phase separation seems to be realistic. As a technical support mild bubbling of the glass pool on three positions in the upper part of the glass tank will be envisaged.

- [1] David A. McKeown et al, "Raman studies of sulphur in borosilicate waste glass », J. of Non-Crystalline Solids 288 (2001) 191-198

9. List of Publications

Papers in Peer Reviewed Journals

ALONSO, U.; MISSANA, T.; GARCÍA-GUTIÉRREZ, M.; TURRERO, M.J.; GECKEIS, H.; SCHÄFER, T.; MÖRI, A.; PATELLI, A.; RIGATO, V.
Uncertainties in the assessment for the role of colloids generated in a high level waste repository for radionuclide migration.

Iberian Journal of Geology 32 (2006), 79-94

ALTMAYER, M.; NECK, V.; DENECKE, M.A.; YIN, R.; FANGHÄNEL, T.
Solubility of $\text{ThO}_2 \cdot x\text{H}_2\text{O}(\text{am})$ and the formation of ternary Th(IV) hydroxide-carbonate complexes in NaHCO_3 - Na_2CO_3 solutions containing 0 - 4 M NaCl.

Radiochim. Acta 94 (2006), 495-500

BAUER, A.; LANSON, B.; FERRAGE, E.; EMMERICH, K.; TAUBALD, H.; SCHILD, D. VELDE, B.
The fate of smectite in KOH solutions.

American Mineralogist 91 (2006) 1313-22

BECKER, U.; RISTHAUS, P.; BRANDT, F.; BOSBACH, D.
Thermodynamic properties and crystal growth behavior of the hashemite (BaSO_4 - BaCrO_4) solid solution.

Chemical Geology 225 (2006) 244-55

BLACK, L.; GARBEV, K.; BEUCHLE, G.; STEMMERMANN, P.; SCHILD, D.
X-ray photoelectron spectroscopic investigation of nanocrystalline calcium silicate hydrates synthesised by reactive milling.

Cement and Concrete Res 36 (2006) 1023-31

BOLEA, E.; GORRIZ, M.P.; BOUBY, M.; LABORDA, F.; CASTILLO, J.R.; GECKEIS, H.
Multielement characterization of metal-humic substances complexation by size exclusion chromatography, asymmetrical flow field-flow fractionation, ultrafiltration and inductively coupled plasma-mass spectrometry detection: A comparative approach.

Journal of Chromatography A 1129 (2006) 236-46

DENECKE, M. A.
Actinide speciation using X-ray absorption fine structure spectroscopy.

Coordination Chemistry Reviews 250 (2006) 730-54

DREW, M.G.B.; FOREMAN, M.R.S.; GEIST, A.; HUDSON, M.J.; MARKEN, F.; NORMAN, V.; WEIGL, M.

Synthesis, structure, and redox states of homoleptic d-block metal complexes with bis-1,2,4-triazin-3-yl-pyridine and 1,2,4-triazin-3-yl-bipyridine extractants.

Polyhedron 25 (2006) 888-900

EDELSTEIN, N.M.; KLENZE, R.; FANGHÄNEL, T.; HUBERT, S.
Optical properties of Cm(III) in crystals and solutions and their application to Cm(III) speciation.

Coordination Chemistry Reviews 250 (2006) 948-73

FANGHÄNEL, T.; GECKEIS, H.
MIGRATION 2005, The 10th international conference on the chemistry and migration of actinides and fission products in the geosphere.

Physics and Chemistry of the Earth 31 (2006) 497-498

GEIST, A.; HILL, C.; MODOLO, G.; FOREMAN, M.R.; WEIGL, M.; GOMPPER, K.; HUDSON, M.J., MADIC, C.

6,6'-Bis(5,5,8,8-tetramethyl-5,6,7,8-tetrahydro-benzo[1,2,4]triazin-3-yl) [2,2'] bipyridine, an effective extracting agent for the separation of americium(III) and curium(III) from the lanthanides.

Solvent Extraction and Ion Exchange 24 (2006) 463-83

- GOLUBEV, S.V.; BAUER, A.; POKROVSKY, O.S.
Effect of pH and organic ligands on the kinetics of smectite dissolution at 250 °C.
Geochimica et Cosmochimica Acta. 70 (2006) 4436-51
- GOMPPER, K
ACTINET- Ein EU-Excellenz-Netzwerk für Actinidenwissenschaften.
Atomwirtschaft 51-19 (2006) 626-31
- JUNG, E.C.; YUN, J.-I.; KIM, J.I.; PARK, Y.J.; PARK, K.K.; FANGHÄNEL, T.; KIM, W.H.
Size measurement of a nanoparticle by using the emission intensity of distribution of a laser-induced plasma.
Applied Physics B – Lasers and Optics 85 (2006) 625-29
- KIM, J.I.
Significance of actinide chemistry for the long-term safety of waste disposal.
Nuclear Engineering and Technology 38 (2006) 459-82
- KIM, J.-W.; HAN, J.J.; CHOI, J.-G.; KIM, D.-K.; JE, K.-C.; PARK, S.-H.; YUN, J.-I.; FANGHÄNEL, T.
Size analysis of CdSe/ZnS quantum dots in aqueous solution by using laser-induced breakdown detection.
Journal of the Korean Physical Society 49 (2006) 135-38
- KIM, S.S.; CHOI, J.W.; KANG, C.H.; CHO, W.J.; LOIDA, A.; MÜLLER, N.
Comparison of the amount of nuclides released from the spent fuel in contact with and without a compacted bentonite block.
Journal of Environmental Science and Health A 41 (2006) 1749-57
- KRETZSCHMAR, R.; SCHÄFER, T.
Metal retention and transport on colloidal particles in the environment.
Elements 1 (2005) 205-10
- KUNZE, S.
Beschichtungen für die Nuklearmedizin und –technik.
Welt der Farben 2 (2006) 12-15
- LEON, A.; FICHTNER, M.; ROTHE, J.
Bestimmung der lokalen Struktur von Dotiersubstanzen in nanoskaligen Wasserstoffspeichermaterialien mit Hilfe der Röntgenabsorptionsspektroskopie.
Nachrichten - Forschungszentrum Karlsruhe, 37 (2005) 197-203
- LEON, A.; KIRCHER, O.; FICHTNER, M.; ROTHE, J.; SCHILD, D.
Evolution of the local structure around Ti atoms in NaAlH₄ doped with TiCl₃ or Ti₁₃x6THF by ball milling using X-ray absorption and X-ray photoelectron spectroscopy.
Journal of Physical Chemistry B 110 (2006) 1192-200
- LINDQVIST-REIS, P.; WALTHER, C.; KLENZE, R.; EICHHÖFER, A.; FANGHÄNEL, T.
Large ground-state and excited-state crystal field splitting of 8-fold coordinate Cm³⁺ in [Y(H₂O)₈]Cl₃ 15-crown-5.
Journal of Physical Chemistry B 110 (2006) 5279-85
- LINDQVIST-REIS, P.; PERSSON, I.; SANDSTRÖM, M.
The hydration of the scandium(III) ion in aqueous solution and crystalline hydrates studied by XAFS spectroscopy, large-angle X-ray scattering and crystallography.
Dalton Transactions, (2006) 3868-78
- LÜTZENKIRCHEN, J.
Parsons Zobel plots: An independent way to determine surface complexation parameters?
Journal of Colloid and Interface Science 303 (2006) 214-23

LÜTZENKIRCHEN, J. [Edt.]

Surface Complexation Modelling.

Volume 11 (Interface Science and Technology), Academic Press (Oct. 25, 2006), pp 652

ISBN-10: 0123725720, ISBN-13: 978-0123725721

NABER, A.; PLASCHKE, M.; ROTHE, J.; HOFMANN, H.; FANGHÄNEL, TH.;

Scanning Transmission X-ray and Laser Scanning Luminescence Microscopy of the Carboxyl Group and Eu(III) Distribution in Humic Acid Aggregates.

Electron Spectroscopy and Related Phenomena 153 (2006) 71-74

NECK, V.

Comment on 'Hydrolysis of neptunium(V) at variable temperatures (10-85 °C)',

by L. Rao, T.G. Srinivasan, A.Yu. Garnov, P. Zanonato, P. Di Bernardo, and A. Bismondo.

Geochimica et Cosmochimica Acta 70 (2006) 4551-55

NECK, V.; ALTMAIER, M.; FANGHÄNEL, T.

Ion interaction (SIT) coefficients for the Th⁴⁺ ion and trace activity coefficients in NaClO₄, NaNO₃ and NaCl solution determined by solvent extraction with TBP.

Radiochim. Acta 94 (2006), 501-07

PIEPER, H.; BOSBACH, D.; PANAK, P.J.; RABUNG, T.; FANGHÄNEL, T.

Eu(III) coprecipitation with the trioctahedral clay mineral hectorite.

Clays and Clay Minerals 54 (2006) 45-53

POLLY, R.; WERNER, H.J.; DAHLE, P.; TAYLOR, P.R.

Application of Gaussian-type geminals in local second-order Møller-Plesset perturbation theory.

The Journal of Chemical Physics 124 (2006) 234107 (pp 11)

RABUNG, TH.; GECKEIS, H.; WANG, X.K.; ROTHE, J.; DENECKE, M.A.; KLENZE, R.;
FANGHÄNEL, TH.

Cm(III) sorption onto γ -Al₂O₃: New insight into sorption mechanisms by time-resolved laser fluorescence spectroscopy and extended X-ray absorption fine structure.

Radiochim Acta 94 (2006) 609-18

ROTHE, J.; DENECKE, M. A.; DARDENNE, K.; FANGHÄNEL, T.

The INE-Beamline for Actinide Research at ANKA.

Radiochimica Acta, 94 (2006) 691-96

STUMPF, S.; STUMPF, TH.; DARDENNE, K.; HENNIG, C.; KLENZE, R.; FOERSTENDORF, H.;
FANGHÄNEL, TH.

Sorption of Am(III) onto 6-line-ferrhydrite and its alteration products: Investigations by EXAFS.

Environmental Science and Technology 40 (2006)

STUMPF, T.; MARQUES FERNANDES, M.; WALTHER, C.; DARDENNE, K.; FANGHÄNEL, TH.

Structural characterization of Am incorporated into calcite: A TRLFS and EXAFS study.

J. Colloid Interface Sci. 302 (2006) 240-5

STUMPF, S.; STUMPF, T.; DARDENNE, K.; HENNIG, C.; FOERSTENDORF, H.; KLENZE, R.;
FANGHÄNEL, TH.

Sorption of Am(III) onto 6-line-Ferrhydrite and its Alteration Products: Investigations by EXAFS.

Environ. Sci. Technol. 40 (2006) 3522-8

STUMPF, S.; STUMPF, T.; WALTHER, C.; BOSBACH, D.; FANGHÄNEL, T.

Sorption of Cm(III) onto different Feldspar surfaces: a TRLFS study.

Radiochimica Acta 94 (2006) 243-8

SUTEERAPATARANON, S.; BOUBY, M.; GECKEIS, H.; FANGHÄNEL, T.; GRUDPAN, K.

Interaction of trace elements in acid mine drainage solution with humic acid.

Water Research 40 (2006) 2044-54

SZABO, G.; GUCZI, J.; REILLER, P.; GECKEIS, H.; BULMAN, R. A.
Investigation of complexation of thorium by humic acid using chemically immobilized humic acid on silica gel.
Radiochimica Acta 94 (2006) pp 553-57

WALTHER, C.; BÜCHNER, S.; FILELLA, M.; CHANUDET, V.
Probing particle size distributions in natural surface waters from 15 nm to 2 µm by a combination of LIBD and single-particle counting.
Journal of Colloid and Interface Science 301 (2006) 532-37

WEIGL, M.; GEIST, A.; MÜLLICH, U.; GOMPPER, K.
Kinetics of Americium(III) extraction and back extraction with BTP.
Solvent Extraction and Ion Exchange 24 (2006) 845-60

YIN, S.; XU, M.X.; YANG, L.; LIU, J.F.; RÖSNER, H.; HAHN, H.; GLEITER, H.; SCHILD, D.; DOYLE, S.; LIU, T.; HU, T.D.; TAKAYAMA-MUROMACHI, E.; JIANG, J.Z.
Absence of ferromagnetism in bulk polycrystalline Zn_{0.9}Co_{0.1}O.
Physical Review B 73 (2006) 224408/1-5

YUN, J.I.; KIM, M.A.; PANAK, P.J.; KIM, J.I.; FANGHÄNEL, T.
Formation of aquatic Th(IV) colloids and stabilization by interaction with Cm(III)/Eu(III).
Journal of Physical Chemistry B 110 (2006) 5416-22

Proceedings of Workshops and Conferences

CHO, H.R.; MARQUARDT, C.M.; NECK, V.; SEIBERT, A.; WALTHER, C.; YUN, J.I.; FANGHÄNEL, T.
Redox Behaviour of Plutonium(IV) in Acidic Solutions.
Proc. of the Conference Actinides 2005, Manchester, UK, July 4-8, 2005, in: Recent Advances in Actinide Science (Eds: R. Alvarez, N.D. Bryan, 1 May), The Royal Society of Chemistry, Spec. Publ. No. 305, RCS Publishing, Cambridge, UK, (2006) 602-604

DENECKE, M.A.; PANAK, P.; PLASCHKE, M.; ROTHE, J.; WEIGL, M.
Spectroscopic Actinide Speciation for Nuclear Waste Disposal.
Proc. of the Conference Actinides 2005, Manchester, UK, July 4-8, 2005, in: Recent Advances in Actinide Science (Eds: R. Alvarez, N.D. Bryan, 1 May), Royal Society of Chemistry, Spec. Publ. No. 305, RCS Publishing, Cambridge, UK, (2006) 673-79

DENECKE, M.A.
A new confocal µ-XRF set-up for measuring 3D elemental distributions with spatial resolution on the micrometer scale.
Proc. of the 1st Annual Workshop FUNMIG, Report CEA-R-6122 (Sep. 2006) 92-95

GECKEIS, H.
Research in actinide geochemistry: do we need speciation information at the molecular level?
In: Van Iseghem (Edt.) Scientific Basis for Nuclear Waste Management XXIX: MRS Symposium 2005, Gent, Belgium, Sep. 12-16, MRS Proceedings 932, Warrendale, PA, USA. (2006) 895-904

HROBARIK, P.; KOMOROVSKY, S.; MALKINA, O.L.; MALKIN, V.G.; REVIKINE, R.; KAUPP, M.; YAZYEV, O.V.; HELM, L.; SCHIMMELPFENNIG, B.
Paramagnetic NMR studies of lanthanide complexes with humic acids. Development of theoretical methods for a comprehensive extraction of structural and dynamical data from experimental spectra.
Proc. of the 1st Annual Workshop FUNMIG, Report CEA-R-6122 (Sep. 2006) 190-95

LAAKSOHARJU, M.; SMELLIE, J.; TULLBORG, E.-L.; MOLINERO, J.; GIMENO, M.; CEDERCREUTZ, J.; GURBAN, I.; BUCKAU, G.
Hydrological situation and geochemical processes in crystalline rock site investigations by real system analysis.
Proc. of the 1st Annual Workshop FUNMIG, Report CEA-R-6122 (Sep. 2006) 75-79

LINDQVIST-REIS, P.; KLENZE, R.; FANGHÄNEL, T.
Influence of temperature and ionic strength on the hydration of curium(III) in aqueous solution studied with TRLFS.

Proc. of the Conference Actinides 2005, Manchester, UK, July 4-8, 2005, in: Recent Advances in Actinide Science (Eds:R. Alvarez, N.D. Bryan, I May), Royal Society of Chemistry, Spec. Publ. No. 305, RCS Publishing, Cambridge, UK, (2006) 500-2

LOIDA, A.; KELM, M.; KIENZLER, B.; GECKEIS, H.; BAUER, A.
The effect of nearfield constraints on the corrosion behavior of high burnup spent fuel.
In: Van Iseghem (Edt.) Scientific Basis for Nuclear Waste Management XXIX: MRS Symposium 2005, Gent, Belgium, Sep. 12-16, MRS Proceedings 932, Warrendale, PA, USA. (2006) 473-80

LUCKSCHEITER, B.; NESOVIC, M.
HLW-glass dissolution and co-precipitation studies.
In: Van Iseghem (Edt.) Scientific Basis for Nuclear Waste Management XXIX: MRS Symposium 2005, Gent, Belgium, Sep. 12-16, MRS Proceedings 932, Warrendale, PA, USA. (2006) 361-68

KIENZLER, B.; BAUER, A.; FIEHN, B.
FZK-INE actinide diffusion experiment.
Proc. of the 1st Annual Workshop FUNMIG, Report CEA-R-6122 (Sep. 2006) 146-50

MARQUARDT, C.M.; SEIBERT, A..
Redox reactions of plutonium with hydroquinone as a redox model compound for humic substances.
Proc. of the 1st Annual Workshop FUNMIG, Report CEA-R-6122 (Sep. 2006) 201-04

NECK, V.; ALTMAIER, M.; FANGHÄNEL, T.
Solubility and Redox Reactions of Plutonium(IV) Hydrated Oxide in the Presence of Oxygen.
Proc. of the Conference Actinides 2005, Manchester, UK, July 4-8, 2005, in: Recent Advances in Actinide Science (Eds:R. Alvarez, N.D. Bryan, I May), Royal Society of Chemistry, Spec. Publ. No. 305, RCS Publishing, Cambridge, UK, (2006) 479-84

PLASCHKE, M.; ROTHE, J.; NABER, A.; FANGHÄNEL TH.;
Understanding humic acid metal ion interaction – a spectromicroscopy approach.
in: F. Frimmel, G. Abbt-Braun (Eds.), Humic Substances – Linking Structure to Functions, Proc. of the 13th Meeting of IHSS, Vol. 45-II (2006) 737

POINSSOT, C.; FERRY, C.; GRAMBOW, B.; KELM, M.; SPAHIU, K.; MARTINEZ, A.; JOHNSON, L.; CERA, E.; DE PABLO, J.; QUINONES, J.; WEGEN, D.; LEMMENS, K.; MCMENAMIN, T.
Mechanisms governing the release of radionuclides from spent nuclear fuel in geological repository: major outcomes of the European project SFS.
In: Van Iseghem (Edt.) Scientific Basis for Nuclear Waste Management XXIX: MRS Symposium 2005, Gent, Belgium, Sep. 12-16, MRS Proceedings 932, Warrendale, PA, USA. (2006) 421-32

REILLER, P.; BUCKAU, G.; KIENZLER, B.; DURO, L.; MARTELL, M. (Edts.)
Proceedings of the 1st Annual Workshop on the EC 6th FP Project Fundamental Processes of Radionuclide Migration (IP FUNMIG), Saclay, France, 28. Nov. 1. Dec. 2005
Report CEA-R-6122, ISSN 0429-3460 (Sep. 2006)

RÖMER, J.; KIENZLER, B.; SCHILD, D.
Sorption of actinides onto granite and altered material from Äspö HRL.
Proc. of the 1st Annual Workshop FUNMIG, Report CEA-R-6122 (Sep. 2006) 135-39

ROTHE, J.; PLASCHKE, M.; DENECKE, M. A.; FANGHÄNEL, TH.;
Interactions of humic acids with tetravalent cations – a spectromicroscopy approach.
in: F. Frimmel, G. Abbt-Braun (Eds.), Humic Substances – Linking Structure to Functions, Proc. of the 13th Meeting of IHSS, Vol. 45-II (2006) 777

SCHÄFER, T.; GECKEIS, H.; BOUBY, M.; MIHAI, S.; DELOS, A.; ALONSO, U.; MISSANA, T.
Bentonite colloid stability in natural and simulated granite groundwater.
Proc. of the 1st Annual Workshop FUNMIG, Report CEA-R-6122 (Sep. 2006) 100-04

SCHÄFER, T.; CLARET, F.; BUCKAU, G.
Smectite induced polymerization of organic matter.
Proc. of the 1st Annual Workshop FUNMIG, Report CEA-R-6122 (Sep. 2006) 119-23

SCHILD, D.; MARQUARDT, C.M.; SEIBERT, A.; FANGHÄNEL, TH.
Plutonium-humate complexation in natural groundwater by XPS.
Proc. of the Conference Actinides 2005, Manchester, UK, July 4-8, 2005, in: Recent Advances in Actinide Science (Eds:R. Alvarez, N.D. Bryan, I May), Royal Society of Chemistry, Spec. Publ. No. 305, RCS Publishing, Cambridge, UK, (2006) 107-109

SZABÓ, GY.; GUCZI, J.; REILLER, P.; GECKEIS, H.; BULMAN, R.A.
Investigation of complexation of thorium by humic acid using a composite of silica gel bearing chemically immobilized humic acid.
Proc. of the 1st Annual Workshop FUNMIG, Report CEA-R-6122 (Sep. 2006) 168-73

SZABÓ, GY.; GUCZI, J.; TELEGDI, J.; PASHALIDIS, I.; SZYMCZAK, W.; BUCKAU, G.
Further steps to characterization of immobilized humic acid on silicon wafer.
Proc. of the 1st Annual Workshop FUNMIG, Report CEA-R-6122 (Sep. 2006) 174-78

VAN ISEGHEM, P.; LEMMENS, K.; AERTSENS, M.; GIN, S.; RIBET, I.; GRAMBOW, B.; CROVISIER, J.L.; DEL NERO, M.; CURTI, E.; SCHWYN, B.; LUCKSCHEITER, B.; MCMENAMIN, T.
Chemical durability of high-level waste glass in repository environment: Main conclusions and remaining uncertainties from the GLASTAB and GLAMOR projects.
In: Van Iseghem (Edt.) Scientific Basis for Nuclear Waste Management XXIX: MRS Symposium 2005, Gent, Belgium, Sep. 12-16, MRS Proceedings 932, Warrendale, PA, USA. (2006) 293-304

FZK Reports, Project reports

BOHNERT E.; KELM M.; KIENZLER B.; MARQUARDT C.; METZ V., SCHILD D.
Flow-through studies on UO₂ dissolution as a result of alpha-radiolysis - experimental set-up and speciation analysis method.
NF-PRO deliverable 1.5.5.,. 27. (2006)

BRENDEBACH, B.; LUCKSCHEITER, B.; NESOVIC, M.; DENECKE, M.A.; ROTHE, J.; DARDENNE, K.
X-ray absorption spectroscopy (XAS) investigation of the leaching behavior of uranium containing high level waste glasses.
ANKA - Annual Report 2006, Forschungszentrum Karlsruhe, CD-ROM, 134-36

DARDENNE, K.; STUMPF, TH.; CURTIUS, H.; BRENDENBACH, B.
Eu L3 edge XAFS investigation on Eu-doped hydrotalcite.
ANKA - Annual Report 2006, Forschungszentrum Karlsruhe, CD-ROM, 137-38

FACIO, T.; KNEBEL, J.; TROMM, W.; GEIST, A.; GOMPPER, K.
Partitioning und Transmutation.
FZK-Nachrichten, Jahrgang 38, 1-2, 37-40 (2006)

FANGHÄNEL, TH.; ROTH, G.
Die Verglasung von hochradioaktiven Flüssigabfällen – ein Weg zu mehr Sicherheit in der nuklearen Entsorgung.
Forschungszentrum Karlsruhe Nachrichten, Jahrgang 38, 3, p. 166 - 171 (2006)

FLEISCH, J.; ROTH, G.; WEISENBURGER, S.
Verglasungseinrichtung Karlsruhe (VEK): Verglasung hochradioaktiver Abfalllösungen.
Forschungszentrum Karlsruhe Nachrichten, Jahrgang 38, 1-2, p. 33-36 (2006)

FLEISCH, J.; WEISHAUPT, M.; WEISENBURGER, S.; ROTH, G.;
HAWC-Entsorgung der WAK – eine mit der VEK zu lösende Aufgabe.
Forschungszentrum Karlsruhe Nachrichten, Jahrgang 38, 3, p. 172-176 (2006)

GECKEIS, H.; [Edt.]

Institute for Nuclear Waste Disposal. Annual report 2005.

Wissenschaftliche Berichte, FZKA-7249 (Aug. 2006)

GOMPPER, K.; KLENZE, R.; GECKEIS, H.; KIENZLER, B.; FANGHÄNEL, T.

Sicherheitsforschung zur Endlagerung.

Forschungszentrum Karlsruhe Nachrichten, Jahrgang 38, 1-2, p. 41-44 (2006)

LEON, A.; FICHTNER, M.; C.; ROTHE, J.

Local structure of dopants in nanoscale hydrogen storage materials using X-ray absorption spectroscopy.

Forschungszentrum Karlsruhe Nachrichten, Jahrgang 37,-4, (2005) pp 197-203

LEON, A.; FROMMEN, C.; ROTHE, J.; FICHTNER, M.

Influence of Ti-based dopants in NaAlH₄ on the performance for hydrogen storage application studied by fluorescence EXAFS.

ANKA - Annual Report 2006, Forschungszentrum Karlsruhe, CD-ROM, 102-04

LINDQVIST-REIS, P.; BRENDELBACH, B.; DARDENNE, K.; ROTHE, J.; KLENZE, R.; HAIRE, R.

Hydration of trivalent actinide ions: A combined study on the Cm³⁺ aqua ion at high ionic strength by laser-fluorescence spectroscopy and EXAFS.

ANKA - Annual Report 2006, Forschungszentrum Karlsruhe, CD-ROM, 141-43

LÜTZENKIRCHEN J.; KORTHAUS E.; METZ V.; KIENZLER B.

Experimentelles Programm zur Bestätigung der Ergebnisse von standortspezifischen Modellrechnungen für die Schachanlage Asse: Überprüfung der Gültigkeit thermodynamischer Rechnungen für die Einlagerungskammern bei Lösungsaustausch.

FZK-INE 007/06. Forschungszentrum Karlsruhe (2006)

KIENZLER, B.; VEJMEJKA, P.; RÖMER, J.; LUCKSCHEITER, B.; KISELY, T.; SOBALLA, E. ; WALSCHBURGER, C.; SEITHER, A.

Actinide migration experiment in the ÄSPÖ HRL in Sweden: analysis of retained uranium and technetium with core # 7. (Part V).

Wissenschaftliche Berichte, FZKA-7196 (Feb. 2006)

METZ V.; KORTHAUS E.; LÜTZENKIRCHEN J.; KIENZLER B.

Experimentelles Programm zur Bestätigung der Ergebnisse von standortspezifischen Modellrechnungen für die Schachanlage Asse: Berechnung des Radionuklidquellterms auf Grundlage der Verfüllkonzept G und MAW.

FZK-INE 008/05. Forschungszentrum Karlsruhe (2006)

NECK, V.; ALTMAIER, M.; METZ, V.

Kenntnisstand zu Redoxpotentialen und Löslichkeit von Plutonium bei Anwesenheit von korrodiertem Eisen. Stellungnahme (GSF-Bestellung 31/169553/06/T, FZK-INE Auftrag-Nr. 35013973).

FZK-INE 001/06, Forschungszentrum Karlsruhe (2006)

PAUL-BONCOUR, V.; THIEBAUT, S.; DARDENNE, K.; ROTHE, J.

EXAFS study of the aging of PdTx compounds.

ANKA - Annual Report 2006, Forschungszentrum Karlsruhe, CD-ROM, 144-45

PLASCHKE, M.; ROTHE, J.; DENECKE, M.A.

STXM/NEXAFS investigation of the humic acid/metal ion interaction.

4th Workshop on Speciation, Techniques, and Facilities for Radioactive Materials at Synchrotron Light Sources (Actinide-XAS-2006), Karlsruhe, Sep. 18-20, 2006 Book of Abstracts, p 47

SCHILD, D.; MARQUARDT, C.M.; SEIBERT, A.; FANGHÄNEL, TH.

Pu-humate complexation in natural groundwater by XPS.

Project Internal Deliverable, Integrated Project FUNMIG, Fundamental Processes of Radionuclide Migration, Project Number: FP6-516514 (July 2006)

SIMON, R.; MANGOLD, S.; GÖTTLICHER, J.; STEININGER, R.; DENECKE, M.; ROTHE, J.; BRENDEBACH, B.; NAGEL, P.; PELLEGRIN, E.; PINTA, C.; FUCHS, D.; SCHEERER, B.; SCHUPPLER, S.
Progress at the ANKA spectroscopy beamlines.

ANKA - Annual Report 2006, Forschungszentrum Karlsruhe, CD-ROM, 202-03

WALTER, M.; SOMERS, J.; DARDENNE, K.; ROTHE, J.; DENECKE, M.

Local atomic structure of Am in spinel ($MgAl_2O_4$) inert matrix fuel.

ANKA - Annual Report 2006, Forschungszentrum Karlsruhe, CD-ROM, 152-53

Invited oral presentations

D. BOSBACH, H. BRANDT, P. PANAK, T. FANGHÄNEL

Structural incorporation of trivalent actinides in clay minerals: TRLFS and EXAFS studies.

Seminar am Institut für Kernchemie, Universität Mainz, 21.9.2006

D. BOSBACH, M. MARQUES, F. HEBERLING, T. STUMPF, M. DENECKE, T. FANGHÄNEL

Actinide coprecipitation with calcite.

Jahrestagung der spanischen kristallographischen Gesellschaft, Oviedo, Spanien, 13.9.2006

BUCKAU, G.

Actinide speciation in the environment: Influence of natural organic matter.

NoE ACTINET Summer School, Saclay, France, 3-6 July 2006

BUCKAU, G.

Integrated Project Fundamental Processes of Radionuclide Migration (IP FUNMIG).

NF-PRO Annual Workshop, El Escorial, Spain, 14-16 Nov. 2006.

FLÖRSHEIMER, M.

Speciation of the functional groups of mineral/electrolyte interfaces in environmental geochemistry.

SFG Workshop of TOPAG Lasertechnik GmbH, Max-Planck-Institut für Kolloid- und

Grenzflächenforschung, Golm, Nov. 17, 2006

DENECKE, M. A.

X-ray spectroscopic investigations related to high level nuclear waste.

Diamond Light Source Ltd, Didcot Oxfordshire, GB, March 30, 2006

DENECKE, M. A.

Actinide speciation for nuclear waste disposal safety using X-ray absorption spectroscopy.

6th School on the Physics and Chemistry of Actinides, Mar 30- Apr.1, 2006

DENECKE; M.A.

Introduction to synchrotron-based radionuclide speciation investigations.

4th Swiss Geoscience Meeting, Bern, Switzerland; 24.-25. Nov. 2006

DENECKE; M.A.

Microanalysis of nuclear samples at a synchrotron.

Workshop on fundamentals of microbeam analysis organized by the European Microbeam Analysis Society (EMAS), Karlsruhe, 13.-16. Mai 2006

DENECKE; M.A.

XAFS spectroscopy in actinide research.

ACTINET Theoretical Users Lab Workshop, Lille, France, 16.-20. Mai 2006

FANGHÄNEL, T.; ALTMAIER, M.; CHO, H.R.; MARQUARDT, C.M.; NECK, V.; SEIBERT, A.;

WALTHER, C.; YUN, J.I.

Solubility and redox equilibria of plutonium.

Plutonium Futures - The Science 2006. A Topical Conference on Plutonium and Actinides, Asilomar, Pacific Grove, California, USA, July 9 - 13, 2006, Book of Abstracts (CD-Rom) pp 61-62

GECKEIS, H.; RABUNG, TH.

Interaction of actinides with iron oxides.

Workshop Fe-oxides in Nature and Industry, Copenhagen, 10. May, 2006

HAUSER, W.

A mobile laser-induced breakdown detection system: In-situ monitoring of colloid migration and stability of natural ground water colloids.

Seminar at China Institute of Atomic Energy, Radiochemistry Institute, Beijing, China, 10. April 2006

HAUSER, W.

Laser-induced photoacoustic spectroscopy with a highly sensitive sensor for trace speciation of aquatic actinides.

Seminar at China Institute of Atomic Energy, Radiochemistry Institute, Beijing, China, 10. April 2006

HAUSER, W.

Time-resolved laser-fluorescence spectroscopy (TRLFS) with optical fibre transmission of laser pulses

Seminar at China Institute of Atomic Energy, Radiochemistry Institute, Beijing, China, 10. April 2006

KIENZLER, B.

Spent fuel disposal concepts and criticality.

Seminar at Center for Nuclear Waste Regulatory Analyses (CNWRA), San Antonio, Texas, May, 2006

KHELASHVILI, G.; BEHRENS, S.; HINSCH, A.; HABICHT, W.; SCHILD, D.; EICHHOEFER, A.; SASTRAWAN, R.; BÖNNEMANN, H.

Physical characterization and electrochemical study of the Pt:SnO₂ electrocatalyst for printable dye solar cells.

E-MRS IUMRS ICEM 2006 Spring Meeting, Nice, France, May 29 – June 2, 2006

KIENZLER, B.

Safety research for nuclear waste disposal at INE.

Seminar at University of Nevada, Las Vegas, Nevada, USA

Department of Chemistry, 4.5.06

KIENZLER, B.,

Radionuklid Migration: Chemlab, FUNMIG, PET & Co.

Festkolloquium anlässlich der Verabschiedung von Dr. Richter

Institut für Interdisziplinäre Isotopenforschung Leipzig 20.10.2006

LOIDA, A.

Corrosion behavior of high burnup spent fuel in salt and clay environment.

Seminar at ONDRAF-NIRAS, SCK/CEN, Brussels, Belgium, 23.5.2006

MARQUARDT, C.M.

Long-term safety of final nuclear waste disposal - research and development on basis of a geochemical approach at the INE.

China Institute of Atomic Energy, Radiochemistry Institute, Beijing, China, 10. April 2006

NECK, V.

Löslichkeit und Redoxreaktionen von Pu(IV) in Gegenwart von Sauerstoff.

Universität Mainz, Institut für Kernchemie, 26. April 2006

PANAK, P. J.; WEIGL, M.; GEIST, A.; DENECKE, M. A.; KLENZE, R.; SCHIMMELPFENNIG, B.; FANGHÄNEL, TH.

Combined TRLFS, EXAFS and theoretical investigations on actinide/lanthanide complexed with partitioning relevant ligands.

4th Workshop on Speciation, Techniques, and Facilities for Radioactive Materials at Synchrotron Light Sources, Actinide XAS 2006, 18-20th Sep. 2006, Karlsruhe, Germany (2006)

Workshop proceedings NEA 6288, Nuclear Science 2007, p 21

PANAK, P. J.; WEIGL, M.; GEIST, A.; DENECKE, M. A.; KLENZE, R.; SCHIMMELPFENNIG, B.; FANGHÄNEL, TH.

Structural Investigations on Cm(III) and Eu(III) complexes with alkylated 2,6-Di(1,2,4-Triazin-3-yl) Pyridine (BTP).

ANKA Users` Meeting 2006, 9-10th Oct. 2006, Karlsruhe, Germany (2006).

ROTHER, J.; BRENDENBACH, B.; DARDENNE, K.; DENECKE, M.A.

The INE-Beamline for Actinide Research at ANKA.

ACTINIDE-XAS-2006 Workshop, Sep. 18-20, 2006, Karlsruhe, Germany

WALTHER, C

Untersuchungen zur Redoxchemie, Hydrolyse und Kolloidbildung des vierwertigen Plutoniums.

Radiochemisches Kolloquium Uni Heidelberg, 13.1.2006

C. WALTHER, P. LINDQVIST-REIS, TH. FANGHÄNEL, J.V. KRATZ

Exzitacions-Laserfluoreszenz: Ein wiederentdecktes Tool zur Strukturaufklärung von An(III) Verbindungen.

Workshop der Uni Mainz, Kernchemie, Oberwesel, 1.3.2006

YUN, J.-I.

Laser spectroscopic approaches to the fate of aquatic actinide colloids: Formation and stabilization.

Department of Chemistry, Yonsei University, Korea, 6 April, (2006)

Presentations at conferences and workshops

ALTMAYER, M.; NECK, V.; FANGHÄNEL, T.

Solubility of uranium(VI) in dilute to concentrated NaCl, MgCl₂ and CaCl₂ solutions.

12th International Symposium on Solubility Phenomena and Related Equilibrium Processes (ISSP 2006), TU Bergakademie Freiberg, Germany, July 23 – 28, 2006, Abstract Volume, p 29

BOSBACH, D.; MARQUES, M.; STUMPF, T.; DARDENNE, K.; FANGHÄNEL, T.

Trivalent actinide coprecipitation with calcite.

European Union of Geoscience conference, Wien, Österreich, 3.4.2006

CLARET, F.; SCHÄFER, T.; AMEKRAZ, B.; MOULIN, C.; REILLER, C.

Fractionation of natural organic matter on alpha-alumina.

13th Intern. Humic Substance Society (IHSS) Meeting, Karlsruhe, Germany, July 30 to Aug. 4, 2006.

Proceedings: Schriftenreihe des Lehrstuhls für Wasserchemie und der DVGW-Forschungsstelle am Engler-Bunte-Institut der Universität Karlsruhe (TH), Vol. 45-1, pp 221-4, ISSN 1612-118x.

DARDENNE, K.; BOSBACH, D.; DENECKE, M. A.; BRENDENBACH, B.

EXAFS investigation of the NaLn(MoO₄)₂ - Ca₂(MoO₄)₂ solid solution series local structure.

4th Workshop on Speciation, Techniques, and Facilities for Radioactive Materials at Synchrotron Light Sources (Actinide-XAS-2006), Karlsruhe, Sep. 18-20, 2006,

DARDENNE, K.; BOSBACH, D.; DENECKE, M. A.; BRENDENBACH, B.

EXAFS investigation of the NaLn(MoO₄)₂ - Ca₂(MoO₄)₂ solid solution series local structure.

5th ANKA Users Meeting, Karlsruhe, Oct. 9-10, 2006,

DEGUELDRE, C.; KASTORIANO, M.; DARDENNE, K.

Variable incident angle - x-ray absorption spectroscopy for the study of zircaloy corrosion layers.

JNM 2007 symposium N EMRS 2006, Nice, France, June 2006

DELOS, A.; SCHÄFER, T.; GECKEIS, H.; GUIMERÀ, J. CARRERA, J.

Colloid and colloid-borne radionuclide column migration experiments.

80th ACS Colloid and Surface Science Symposium, Boulder, Colorado, June 18-21 2006

Book of abstracts p 36

DELOS, A.; SCHÄFER, T.; GECKEIS, H.; WALTHER, C.; GUIMERA, J. CARRERA, J.
Colloid and colloid-borne radionuclide column migration experiments.
TRACER 4, Fourth International Conference on Tracers and Tracing Methods, Grenoble, France, Oct. 3-5, 2006,

EINSIEDL, F.; SCHÄFER, T.; NORTHRUP, P.
Evidence of bacterial sulfate reduction in oxic soils and groundwater systems determined by isotope analyses on groundwater sulfate, fulvic acid sulfur and S XANES spectroscopy.
European Geosciences Union (EGU), General Assembly 2006, Vienna, Austria, 02 – 07 April, 2006

FLÖRSHEIMER, M.; KRUSE, K; ABDELMONEM, A.; FANGHÄNEL, TH.
Symmetrie und Ordnung von Uranyl-Filmen auf Saphir-Oberflächen – detektiert durch Frequenzverdopplung.
4. Statusseminar des Virtuellen Instituts «Funktionelle Eigenschaften aquatischer Grenzflächen», INE, 22. Feb. 2006

FLÖRSHEIMER, M.; KRUSE, K; ABDELMONEM, A.; KLENZE, R.; KIM, J.-I.; FANGHÄNEL, TH.
Speciation of the functional groups at mineral surfaces in situ under water by sum frequency vibrational spectroscopy.
19th Meeting of the International Mineralogical Association (IMA 2006), Kobe (Japan), July, 23 – 28, 2006

FLÖRSHEIMER, M.; KRUSE, K; ABDELMONEM, A.; KLENZE, R.; KIM, J.-I.; FANGHÄNEL, TH.
Probing the chemical composition of mineral/electrolyte interfaces by sum frequency vibrational spectroscopy.
ACTINET Project Meeting , École Nationale Supérieure de Chimie de Paris (ENSPC), April 27, 2006

FROIDEVAL, A.; DEGUELDRE, C.; DARDENNE, K.
XAFS study of the niobium speciation in the corrosion layer of a zirconium based alloy.
SRMS-5 Conference, Chicago, July 30 - Aug. 2, 2006.

GECKEIS, H.; GUILLANEUX, D.; WISS, T.; COECK, M.; SCHEINOST, A.; GEIPEL, G.; SCHEIDEGGER, A.; METZ, V.; CHAIX, P.
European laboratories for actinide research: the ACTINET pooled facilities.
Fall Meeting 2006 of the Materials Research Society, Boston, Mass., Nov. 27 – Dec. 1, 2006
Book of Abstracts p 994

A. GEIST, M. A. DENECKE, P. J. PANAK, M. WEIGL, B. SCHIMMELPFENNIG, K. GOMPPER
On the Selectivity of BTP Extractants for Am(III) and Cm(III) over Lanthanides.
Actinide and Fission Product Partitioning & Transmutation.
Ninth Information Exchange Meeting, Nîmes, France, 25-29 Sept. 2006

A. GEIST, G. MODOLO, M. WEIGL, K. GOMPPER, R. ODOJ
Partitioning of minor actinides: Research at Jülich and Karlsruhe Research Centres.
Actinide and Fission Product Partitioning & Transmutation.
Ninth Information Exchange Meeting, Nîmes, France, 25-29 Sep. 2006

A. GEIST, D. MAGNUSSON, D. SERRANO-PURROY, B. CHRISTIANSEN, R. MALMBECK, K. GOMPPER
Towards a hot DIAMEX test in a hollow fibre module micro-plant.
Actinide and Fission Product Partitioning & Transmutation.
Ninth Information Exchange Meeting, Nîmes, France, 25-29 Sep. 2006

GOMPPER, K.; GEIST, A.; WEIGL, M.; FANGHÄNEL, T.
R&D on partitioning at Forschungszentrum Karlsruhe.
Jahrestagung Kerntechnik 2006, Aachen, 16.-18. Mai 2006, Berlin,
Abstract: INFORUM GmbH, CD-ROM (2006) 347-50

HARTMANN, E.; GECKEIS, H.; RABUNG, T.; KIENZLER, B.; FANGHÄNEL, T.
Sorption of Eu(III) and U(VI) onto natural clays.
84. Jahrestagung der Deutschen Mineralogischen Gesellschaft, Hannover, 25.-27. Sep. 2006 :
Abstract: Berichte der Deutschen Mineralogischen Gesellschaft, No.1, 2006, p 52

HEBERLING, F.; DENECKE, M.A.; BOSBACH, D.
Np(V) coprecipitation with calcite.
84. Jahrestagung der Deutschen Mineralogischen Gesellschaft, Hannover, 25.- 27. Sep. 2006
Abstract: Berichte der Deutschen Mineralogischen Gesellschaft, No.1, 2006, p 54

HENTSCHEL, D.; SEITHER, A.; GÖRTZEN, A.; FUß, M.; GECKEIS, H.; GOMPPER, K.
Prozessbegleitende chemische Analysen zur HAWC-Verglasung.
4. Workshop vom Verein für Kernverfahrenstechnik und Analytik Rossendorf e.V. (VKTA),
Dresden (Rossendorf), 19. - 20. June 2006,

KALMYKOV, S.; SCHÄFER, T.; CLARET, F.; TETERIN, Y.; KHASANOVA, A.; SHCHERBINA, N.;
PERMINOVA, I.
Neptunium speciation in the humic-acid- goethite system.
Actinides XAS 2006, 4th Workshop on Speciation, Techniques, and Facilities for Radioactive Materials
at Synchrotron Light Sources, Karlsruhe, Germany, Sep. 18 - 20, 2006
Workshop proceedings NEA 6288, Nuclear Science 2007, p 249

KHELASHVILI, G.; BEHRENS, S.; HINSCH, A.; HABICHT, W.; SCHILD, D.; EICHHOEFER, A.;
SASTRAWAN, R.; BÖNNEMANN, H.
Physical characterization and electrochemical study of the Pt:SnO₂ Electrocatalyst for printable dye
solar cells.
E-MRS IUMRS ICEM 2006 Spring Meeting, Nice, France, May 29 – June 2, 2006,

KIENZLER, B.
IP FUNMIG: The European far-field project.
Internat.High Level Radioactive Waste Management Conf. (IHLWM),
Las Vegas, Nev.; April 30 - May 4, 2006

KIENZLER, B.; LOIDA, A.; METZ, V.
Waste forms for a rock salt repository: concepts for future investigations.
Spring Meeting of the European Materials Research Society, Nice, F, May 29 -June 2, 2006

KIENZLER, B.; METZ, V.
IP FUNMIG: The European far-field project.
Fall Meeting 2006 of the Materials Research Society, Boston, Mass., Nov. 27 - Dec. 1, 2006
Book of Abstracts p 1009

KIENZLER, B.; VEJMEJKA, P.; METZ, V.; BAUER, A.; MAYER, H.
Langzeit-Verhalten von zementierten radioaktiven Abfällen in Salzlösungen.
GdCh Tagung Bauchemie, Karlsruhe, 5. - 6. Oct. 2006

KIENZLER, B.; VEJMEJKA, P.; RÖMER, J.; SCHILD, D.; JANSSON, M.
Experiences with Underground Laboratory Experiments.
2006 Internat.High Level Radioactive Waste Management Conf. (IHLWM), Las Vegas, Nevada,
April 30 – May 4, 2006

KIENZLER, B.; LOIDA, A.; MÜLLER, N.; METZ, V.
High level waste forms for repositories in rock salt or clay: Concepts for future investigations.
E-MRS Spring Meeting 2006, Nice, France, May 29 – June 2, 2006

LEON, A.; FROMMEN, C.; ROTHE, J.; SCHILD, D.; FICHTNER, M.
Influence of Ti-based dopants in NaAlH₄ on the performance for hydrogen storage application.
16th World Hydrogen Energy Conf. (WHEC 16), Lyon, France, June 13-16, 2006

LEWIN, E.; WILHELMSSON, O.; JANSSON, U.; STEUBER, M.; HALBRITTER, J.; ZIEBERT, C.; ULRICH, S.; SCHILD, D.

Discussion of a possible third carbon bonding state in PVD-deposited metal carbide / amorphous carbon nanocomposite thin films and its impact on mechanical and electrical properties.
European Materials Research Society Fall Meeting, Warszawa, Poland, Sep. 3-8, 2006

LINDQVIST-REIS, P.; WALTHER, C.; KLENZE, R.; FANGHÄNEL, T.

Characterization of 8- and 9-fold coordinate curium(III) in crystalline and aqueous solution by TRLFS.
6th International Conference on f-elements, 4-9th Sep. 2006, Wrocław, Poland,
Book of Abstracts DO 14

LOIDA, A.; MÜLLER, N.

Alteration behavior of spent fuel in salt brine under hydrogen overpressure and in presence of bromide
- Preliminary results.

International Spent Fuel Workshop, Uppsala, Sweden, May 15-16 (2006)

In: V.M. Oversby and L. Werme (Eds), International Spent Fuel Workshop, Uppsala, Sweden, p 3

LOIDA, A.; KIENZLER, B.; METZ, V.

Alteration behavior of high burnup spent fuel in salt brine under hydrogen overpressure and in presence of bromide.

MRS 2006, 30th International Symposium on the Scientific Basis of Nuclear Waste Management, Boston, Mass.; USA Nov 27- Dec 1, 2006, Book of Abstracts p 986

LÜTZENKIRCHEN, J.; LÖVGREN, L.; SJÖBERG, S.

Surface complexation of various arsenic compounds at the goethite-electrolyte interface.

Sixth International Symposium on Surface Heterogeneity Effects in Adsorption and Catalysis on Solids, ISSHAC-6, Zakopane, Polen, 28. Aug. bis 2. Sep., 2006,

Proceedings, p 173, ISBN 83-227-2570-1 (Abstract),

MARQUARDT, C.M.; SEIBERT, A.; FANGHÄNEL, TH.

Redox reactions of plutonium with hydroquinone and humic substances.

Plutonium Futures The Science 2006 - A Topical Conference on Plutonium and Actinides, Asilomar, Pacific Grove, California, USA, 9.-13. July 2006, Book of Abstracts (CD-Rom) pp 250-51

MARQUARDT, C.M.; SEIBERT, A..

Redox reactions of plutonium with hydroquinone as a redox model compound for humic substances.
1st Annual Workshop Proceedings 6TH EC FP - FUNMIG IP 2, Saclay (France) 28th Nov.- 1st. Dec. 2005

MARQUES FERNANDES, M.; STUMPF, T.; SCHMIDT, M.; BOSBACH, D.; FANGHÄNEL, T.

REE uptake by calcite in aqueous environment: spectroscopic identification of molecular sorption mechanisms.

84. Jahrestagung der Deutschen Mineralogischen Gesellschaft, Hannover, 25. - 27. Sep. 2006 :
Berichte der Deutschen Mineralogischen Gesellschaft, No.1, 2006, p 90

METZ V.; BOHNERT E.; KELM M.; SCHILD D.; KIENZLER B.; FANGHÄNEL T.

Effect of hydrogen and bromide on the yield of gamma-radiolysis products.

International Spent Fuel Workshop, Uppsala, Sweden, May 15-16 (2006)

In: V.M. Oversby and L. Werme (Eds), International Spent Fuel Workshop, Uppsala, Sweden, pp 1-2.

METZ, V.; BOHNERT, E.; KELM, M.; SCHILD, D.; REINHARDT, J.; KIENZLER, B.

Gamma-radiolysis of NaCl brine in the presence of UO₂: effects of hydrogen and bromide.

Fall Meeting 2006 of the Materials Research Society, Boston, Mass., Nov. 27 - Dec. 1, 2006
Book of Abstracts p 987

NECK, V.; ALTMAIER, M.; MARQUARDT, C.M.; SEIBERT, A.; YUN, J.I.; FANGHÄNEL, T.

Hydrous PuO_{2+x}(s): Solubility and thermodynamic data.

Plutonium Futures - The Science 2006. A Topical Conference on Plutonium and Actinides, Asilomar, Pacific Grove, California, USA, July 9 - 13, 2006, Book of Abstracts (CD-Rom) pp 180-81

NECK, V.; FANGHÄNEL, T.

Particle size effects on the solubility of M(III) and M(IV) oxyhydroxides.

12th International Symposium on Solubility Phenomena and Related Equilibrium Processes (ISSP 2006), TU Bergakademie Freiberg, Germany, July 23 – 28, 2006 Abstract Volume, p 30

PANAK, P. J.; WEIGL, M.; GEIST, A.; DENECKE, M. A.; KLENZE, R.; FANGHÄNEL, TH.,
Structural investigations on Cm(III) and Eu(III) complexes with alkylated 2,6-Di(1,2,4-Triazin-3-yl) Pyridine (BTP).

6th Intern. Conference on f-elements, Wrocław, Poland, 4-9th Sep. 2006, Book of Abstracts DO 17

PLASCHKE, M.; ROTHE, J.; DENECKE, M. A.;

STXM/NEXAFS investigation of the humic acid/metal ion interaction.

Actinide-XAS 2006, Forschungszentrum Karlsruhe, Germany, 18.-20. Sep. 2006

Workshop proceedings NEA 6288, Nuclear Science 2007, p 271

PLASCHKE, M.; ROTHE, J.; DENECKE, M. A.; FANGHÄNEL, TH.;

Understanding humic acid metal ion interaction – a spectromicroscopy approach. Nanospectroscopy using synchrotron radiation.

Workshop at PSI, Villigen, Schweiz, July 12 to 17, 2006

PLASCHKE, M.; ROTHE, J.; DENECKE, M. A.; SCHIMMELPFENNIG, B.; BALDEA, I.; NABER, A.; SCHIRMER, J.; FANGHÄNEL, TH.;

Understanding humic acid/metal ion interaction – a spectromicroscopy approach.

13. Koordinierungsgespräch FZK/INE - PSI/LES, 2. und 3. März 2006, Villigen, Schweiz

PLASCHKE, M.; ROTHE, J.; NABER, A.; FANGHÄNEL, TH.;

Understanding humic acid metal ion interaction – a spectromicroscopy approach

13th Meeting of IHSS, July 30 to Aug. 2 2006, Karlsruhe, Germany

PLASCHKE, M.; ROTHE, J.; SCHIMMELPFENNIG, B.; NABER, A.; BALDEA, I.; SCHIRMER, J.; FANGHÄNEL, TH.;

Understanding humic acid/metal ion interaction – a spectromicroscopy approach

Statusseminar des Virtuellen Instituts Funktionelle Eigenschaften aquatischer Grenzflächen, Forschungszentrum Karlsruhe, Germany, 22. Feb. 2006

RABUNG, TH, GECKEIS, H. SCHILD, D.; MITCHEL, S.; FANGHÄNEL, TH.

Cm(III) sorption onto aluminium oxides/hydroxides.

6th Intern. Conference on f-elements, Wrocław, Poland, 4-9 Sep. 2006, Book of Abstracts DO 20

REGENSPURG, S, SCHÄFER, T.; MALMSTRÖM, M.E.

Experimental determination of UO_2^{2+} sorption and reduction at mineral surfaces.

16th Annual V.M. Goldschmidt Conference 2006, Melbourne, Australia, 27 Aug. - 1 Sep. 2006

Geochimica Et Cosmochimica Acta 70, (2006) A523.

ROTH, G.; GRÜNEWALD, W.; FLEISCH, J.; WEISHAAPT, M.

Verglasungsanlage VEK - Technik und Massnahmen zur Herstellung qualifizierter HAW-Glasgebäude.

Jahrestagung Kerntechnik 2006, Aachen, 16.-18.Mai 2006 Berlin,

INFORUM GmbH, 2006, pp 343-46 CD-ROM

ROTHE, J.; BRENDENBACH, B.; DARDENNE, K.; DENECKE, M.A.

The INE-beamline for actinide research at ANKA.

4th Workshop on Speciation, Techniques, and Facilities for Radioactive Materials at Synchrotron Light Sources (Actinide-XAS-2006), Karlsruhe, Sep. 18-20, 2006

Workshop proceedings NEA 6288, Nuclear Science 2007, pp 135-140

ROTHE, J.; PLASCHKE, M.; DENECKE, M. A.;

Interactions of humic acids with tetravalent cations – a spectromicroscopy approach.

XAFS 13, Stanford University, Stanford, USA, July 9-14, 2006, Book of Abstracts p 284

ROTHER, J.; PLASCHKE, M.; DENECKE, M.A.

Understanding humic acid/Zr(IV) interaction - a spectromicroscopy approach.

4th Workshop on Speciation, Techniques, and Facilities for Radioactive Materials at Synchrotron Light Sources (Actinide-XAS-2006), Forschungszentrum Karlsruhe, Germany, Sep. 18-20, 2006
Workshop proceedings NEA 6288, Nuclear Science 2007, ??? Book of Abstracts S.50

ROTHER, J.; PLASCHKE, M.; DENECKE, M. A.; FANGHÄNEL, TH.;

Interactions of humic acids with tetravalent cations – a spectromicroscopy approach.

13th Meeting of IHSS, July 30 to Aug. 2 2006, Karlsruhe, Germany

SCHÄFER, T.

IP FUNMIG: The European far-field project and the influence of natural organic matter on the migration of radionuclides in the geosphere.

13th International Humic Substance Society Meeting, Karlsruhe, Germany, July 30 to Aug. 4, 2006
Proceedings: Schriftenreihe des Lehrstuhls für Wasserchemie und der DVGW-Forschungsstelle am Engler-Bunte-Institut der Universität Karlsruhe (TH), Vol. 45-2, pp 1109-12, ISSN 1612-118x.

SCHÄFER, T.; CLARET, F.

Organic matter clay association in natural and synthetic systems: What influences the organic matter preservation pathway?

13th International Humic Substance Society Meeting, Karlsruhe, Germany, July 30 to Aug. 4, 2006
Proceedings: Schriftenreihe des Lehrstuhls für Wasserchemie und der DVGW-Forschungsstelle am Engler-Bunte-Institut der Universität Karlsruhe (TH), Vol. 45-2, pp 565-68, ISSN 1612-118x.

STIPP, S.; SKOVBJERG, L.; CHRISTIANSEN, B.; HANSSON, E.; UTSUNOMIYA, S.; SCHILD, D.; GECKEIS, H.; EWING, R.

Green rust: structure, redox reaction mechanisms, transformation and colloidal behaviour.

Joint Assembly of AGU, GS, MAS, SEG and UGM, Baltimore, Md., May 23-26, 2006

Eos Trans. AGU, 87(36) (2006), Jt. Assem. Suppl., Abstract M34A-05

STUMPF, S.; BILLARD, I.; PANAK, P.J.

Solution chemistry of Cm(III) and Eu(III) in ionic liquids.

National Meeting of the American Chemical Society, Atlanta, Ga, March 26-30, 2006

Abstracts of Papers of the American Chemical Society 231(2006) p 394

STUMPF, T.; STUMPF, S.; MARQUES FERNANDES, M.; WALTHER, C.; BAUER, A.; FANGHÄNEL, TH.

Elucidation of geochemical reactions at the water-mineral interface on a molecular level by time resolved laser fluorescence spectroscopy with Cm(III).

19th General Meeting of the International Mineralogical Association, Kobe, Japan, July 23-28, 2006

VINOGRAD, V.R.; BOSBACH, D.; WINKLER, B.; FANGHÄNEL, T.

Subsolidus phase relations in $\text{Ca}_2\text{MoO}_8\text{-NaEuMoO}_8$ -powellite solid solution from static lattice energy calculations and Monte Carlo simulations.

84. Jahrestagung der Deutschen Mineralogischen Gesellschaft, Hannover, 25.- 27. Sep. 2006,

Berichte der Deutschen Mineralogischen Gesellschaft, No.1, 2006, p 149

WALTHER, C; BÜCHNER, S; FANGHÄNEL, TH

Measuring size distributions of aquatic colloids by Laser-Induced Breakdown Detection.

Laser induced plasma spectroscopy and applications, Montreal, Canada, Sep. 5-8, 2006

WALTHER;C ; FUSS;M, BÜCHNER S, ALTMAIER, M.; ROTHE J;E

Investigation on Th polyspecies in acidic solution by ESI TOF-MS.

3rd INE-CEA meeting, Saclay, France, Oct. 10-11, 2006

WALTHER;C ; FUSS;M, BÜCHNER S, KOLTSOV S, BERGMANN;T. ROTHE;J.

Mass-spectrometry for nuclear safety -investigation of actinide-oligomers and colloids by ESI TOF-MS.

17th Int. Mass Spectrometry Conference (IMSC) Prag, Czech Republic, Aug.27 –Sept.1, 2006

WALTHER, C.; CHO, H.R.; MARQUARDT, C.M.; NECK, V.; SEIBERT, A.; YUN, J.I.; FANGHÄNEL, T.
Disproportionation of Pu(IV) or a two step mechanism ? Redox behaviour of Pu(IV) in acidic solutions.
Plutonium Futures - The Science 2006. A Topical Conference on Plutonium and Actinides, Asilomar,
Pacific Grove, California, USA, July 9 - 13, 2006, Book of Abstracts (CD-Rom) pp 65-66

WALTHER, C.; ROTHE, J.; BÜCHNER, S.; CHO, H.-R.; FUSS, M.
Investigation of Zr(IV)-oligomers and colloids by ESI-TOF Mass Spectrometry and Zr K-XAFS.
ACTINIDE-XAS-2006 Workshop, Karlsruhe, Germany, Sep. 18-20, 2006
Workshop proceedings NEA 6288, Nuclear Science 2007, p 331

YUN, J.-I.; CHO, H.-R.; ALTMAIER, M.; NECK, V.; SEIBERT, A.; MARQUARDT, C.M.; WALTHER, C.;
FANGHÄNEL, TH.
Hydrolysis of Plutonium(IV) in 0.5 M HCl/NaCl.
Plutonium Futures-The Science 2006, Asilomar Conference Grounds, Pacific Grove, California, USA,
9–13 July, (2006), Book of Abstracts (CD-Rom) pp 448-49

